Strål
säkerhets
myndigheten
Swedish Radiation Safety Authority

Authors: Joel Geier
(Clearwater Hardrock Consulting, Corvallis, Oregon, U.S.A.)

K. E. Thatcher, R. K. Newson, S. J. Benbow
(Quintessa Ltd, Henley-on-Thames, U.K.)

Benoît Dessirier
(Dept. of Earth Sciences, Uppsala University, Sweden)

Research

2018:21

Research on Resaturation of Bentonite Buffer

Report number: 2018:21 **ISSN:** 2000-0456
Available at www.stralsakerhetsmyndigheten.se

SSM perspective

Background

Resaturation processes in the bentonite buffer in a KBS-3 type repository for spent nuclear fuel are complicated and are often illustrated, analysed and modelled multi-disciplinarily as coupled thermal (T), hydrological (H) and mechanical (M) processes with multi-phase flow, elastoplastic evolution in a swelling porous medium. Previous THM-modelling showed that the re-saturation time is strongly dependent on the hydraulic conditions in the near-field of the repository. Moreover, it is difficult to predict the degree of homogeneity during the processes of resaturation.

Some of the safety functions of bentonite buffer will not start working until the bentonite buffer becomes fully water saturated and the buffer material becomes homogenised. A slow resaturation process with uneven swelling of the bentonite buffer in a spent fuel repository is an important factor that may cause creep deformation and local corrosion of the copper canister during the early period of evolution of the repository. Creep deformation and local corrosion have been identified as decisive mechanisms for the long-term integrity of the canister.

Objective

Researches of the resaturation processes make it possible to better estimate the resaturation time and to better illustrate the homogeneity of the buffer material during the resaturation processes. Deep knowledge of both the estimate of resaturation time and the illustration of homogeneity are important for SSM's judgement of the long-term safety of spent fuel repository.

Results

This report consists of three parts: (1) Research on Resaturation of Bentonite Buffer – Hydrological Modelling; (2) Research on Resaturation of Bentonite Buffer – Modelling of Resaturation, and (3) Research on Resaturation of Bentonite Buffer – Coupling between Bentonite and Rock. The aim of the first part is mainly to supply boundary conditions of groundwater flow to the second part of coupled THM-modelling. The third part focuses on modelling of the coupled processes at the interface between bentonite and the bedrock.

The hydrological modelling reveals that

- Increase of groundwater pressure in the bedrock after closure of the repository could increase the transmissivity of horizontally oriented fractures by about a factor of 3.
- Shear displacements due to themomechanical or glacial induced stresses could give significant increases in fracture transmissivity.
- Excavation-induced fractures would be encountered only in the upper 0.5 to 1 m of a deposition hole.
- Thermally induced spalling could result in a spalled zone up to 10 cm deep and 30 cm wide extending vertically along the deposition hole.

The results of the saturation modelling are as follows

- Peak temperatures in the buffer were largely insensitive to the various fracture modelling options that were considered and were well within limits specified by SKB.

- Timescales for resaturation were found to be very sensitive to the choice of whether the bentonite pellet region was explicitly considered in the model.
- Timescales for resaturation were sensitive to the representation of the fracture intersection with the deposition hole, varying by more than a factor of four depending on whether the fracture was assumed to be planar, intersecting the deposition hole along the entire circumference, or whether it was assumed to be channelled, intersecting the deposition hole over a smaller area. In several cases, remote regions of the buffer did not achieve full saturation over the simulation timescales (up to 4 000 y).
- In THM calculations, gradients along the length of the canister of normal stresses to the canister surface were found to persist for the duration of the resaturation period and were greatest when resaturation was most rapid.
- As far as the alternative conceptual models are concerned, the threshold gradient model gives slower resaturation but no changes of spatial distribution of stress. The thermal osmosis model also has little effect on the results other than an increase in drying around the canister at early times. The micro-fabric evolution model significantly increases resaturation time but the stress gradients along the canister become lower.

The modelling of coupling between bentonite and rock gives the results that

- The pellet-filled slot acts as a fast pathway to distribute the water intake from the fracture onto the outer surface of the bentonite block, and thus amplifies the water intake from the fracture.
- A rough but fully connected fracture yields the same buffer resaturation time as a homogeneous parallel plate.
- Flow channelling in the fracture near the deposition hole can affect the buffer resaturation time significantly.

Need for further research

Regarding the modelling of the resaturation processes, further work is required to both improve the representation of resaturation of the pellets and also to enable a good representation of the mechanics of pellets in the modelling of the resaturation processes. It is also worth to further explore the uncertainties as to alternative conceptual models for hydraulics and mechanics of bentonite, especially over timescales longer than those used in experiments to date.

When studying the coupling effect between buffer and the bedrock, further work is also needed to consider scenarios with a strict constriction of the fracture trace lengths that can lead to water intake especially for situations with long resaturation times. It is also needed to investigate the potential for secondary flow pathways to form from the pressurized fracture to the deposition hole via the rock matrix.

Project information

Contact person SSM: Jinsong Liu

Reference: SSM 2017-2831 / 3030045-39
SSM 2017-2830 / 3030045-38
SSM 2017-3021 / 3030045-40

Strål
säkerhets
myndigheten
Swedish Radiation Safety Authority

Author: oel Geier
(Clearwater Hardrock Consulting, Corvallis, Oregon, U.S.A.)

K. E. Thatcher, R. K. Newson, S. J. Benbow
(Quintessa Ltd, Henley-on-Thames, U.K.)

Benoît Dessirier
(Dept. of Earth Sciences, Uppsala University, Sweden)

2018:21

Research on Resaturation of Bentonite Buffer

Date: September 2018
Report number: 2018:21 **ISSN:** 2000-0456
Available at www.stralsakerhetsmyndigheten.se

This report concerns a study which has been conducted for the Swedish Radiation Safety Authority, SSM. The conclusions and viewpoints presented in the report are those of the author/authors and do not necessarily coincide with those of the SSM.

SSM 2018:21

1

Author: Joel Geier
(Clearwater Hardrock Consulting, Corvallis, Oregon, U.S.A.)

Research on Resaturation of Bentonite Buffer – Hydrological Modelling

Project number: 3030045-39
Registration number: SSM2017-2831
Contact person at SSM: Jinsong Liu

Abstract

Analysis and recommendations are given for hydrogeological conceptual models and related hydromechanical factors that could affect boundary conditions for models of bentonite resaturation in a KBS-3 type repository located at the Forsmark site in Sweden.

The plausible range of transmissivity for fractures intersecting deposition holes at Forsmark is 10^{-12} m^2/s to 10^{-6} m^2/s. Taking into account practical constraints on the maximum inflow that could be tolerated during buffer emplacement, fractures with transmissivity higher than 10^{-7} m^2/s would most likely be avoided.

Increases in groundwater pressure in the bedrock after backfilling and closing a deposition tunnel could increase transmissivity of nominally horizontal fractures by about a factor of 3. Development of bentonite swelling pressure in the tunnel backfill has a comparatively minor effect. Glacial loading can be expected to decrease the transmissivity of horizontal fractures by about an order of magnitude.

Shear displacements caused by either thermomechanical or glacially induced stresses could produce more significant increases in transmissivity, but the specific effects and their likelihood would require detailed hydromechanical modelling beyond the scope of this study. Therefore it is recommended simply to consider a scenario in which transmissivity increases by 1.5 orders of magnitude at some future time.

Excavation-induced fractures should be encountered only in the upper 0.5 m to 1 m of a deposition hole. They can be associated with transmissivities as high as $6x10^{-5}$ m^2/s, but more typically in the range $1x10^{-8}$ m^2/s to $1x10^{-6}$ m^2/s.

Due to the dominance of matric suction relative to natural hydraulic potential gradients in the fracture network for most of the resaturation period, it should be sufficient to consider three idealized flow geometries: radially convergent flow in a homogeneous fracture plane, linear flow toward the deposition hole via a channel, and flow via an otherwise immobile zone connected to a linear channel.

Thermally induced spalling that develops after emplacement could result in a spalled zone up to 10 cm deep and 30 cm wide extending vertically along the hole. The permeability of this zone would likely be anisotropic, with hydraulic conductivity in the vertical direction at least an order of magnitude higher than that in the radial direction.

The most important cause of variation in the far-field pressure during the temperate period is local drawdown of the water table during repository operation, followed by recovery after closure. A simple step function increase in pressure after closure should be adequate to represent the main effect.

Content

1. Introduction

The purpose of this work is to provide expert analysis and guidance regarding hydrogeological and related hydromechanical factors affecting boundary conditions for models of bentonite resaturation in a KBS-3 type repository located at the Forsmark site in Sweden. The modelling of bentonite resaturation is being carried out by Quintessa Ltd. (Quintessa) under a separate contract with SSM. The consultant's role as proposed here is to support that work by providing calculations and expert judgment for specific hydrogeological factors that have been identified in discussions with Quintessa.

2. Scope

Preliminary considerations by Quintessa identified the following main needs in terms of types of information that are needed to specify realistic boundary conditions for the bentonite resaturation models:

- Expected ranges of fracture transmissivities for fractures intercepting deposition holes;
- Expected evolution of fracture transmissivities due to changes in rock stresses around repository openings in the operational phase and post-closure.
- Reasonable conceptual models for flow patterns in the fractures around the deposition hole (including uniform vs. channelized flow, with estimates of channel width distributions for the latter).
- Implications of an excavation damage zone (EDZ) including blast-induced fractures and stress-induced fractures, and their possible time-dependent behaviours.
- Expected patterns and implications of stress-induced spalling in deposition holes.
- Groundwater pressure (or hydraulic head) and flowrate conditions at the perimeters of deposition holes, which will form the buffer-fracture interface.
- Estimates of the expected time-dependent variation of these pressure/head and flowrate conditions over the operational period and long-term post-closure period.

These needs are addressed based on the available literature, supplementary calculations, and expert judgment as necessary.

3. Analysis

3.1 Expected ranges of fracture transmissivities for fractures intercepting deposition holes

A wide range of transmissivity values associated with fractures have been encountered by hydraulic testing at repository depth at Forsmark, ranging from below the detection limit of the equipment and methods used, up to 10^{-6} m^2/s or higher. However the range of transmissivity values likely to be encountered in flowing fractures that intersect deposition holes can be constrained by several considerations:

- Empirical relationships of fracture transmissivity to fracture size;
- Criteria for selecting deposition-hole positions that are designed to avoid intersections with nearly all of the largest fractures;
- Practical constraints on allowable inflows to deposition holes during the canister emplacement phase.

SKB has presented three different model variants for the relationship of fracture transmissivity to fracture size ("correlated," "semi-correlated," and "uncorrelated") for each of the two main rock domains (FFM01 and FFM03). All of these can be expressed (Geier, 2014) in the form:

$$T = ar^b 10^{\sigma N(0,1)}$$

where a, b, and σ are empirical parameters and $N(0,1)$ is a random value from the standard normal (Gaussian) distribution with zero mean and unit standard deviation. The values of these parameters for fracture domains FFM01 and FFM03, for the depth zone $z < -400$ m, are listed in Table 1.

The implications of these models for fracture transmissivity as a function of fracture radius are plotted in Figure 1. For the "uncorrelated" and "semi-correlated" models, upper and lower bounds are given corresponding to variability of two standard deviations around the mean (*i.e.*, sampled values of $N(0,1)$ ranging from -2 to +2).

The range of fracture sizes to be considered range from $r = 2$ m (roughly the smallest size for which a fracture could fully cut through a deposition hole and still have enough significant extension beyond the deposition hole to control flow) to $r = 50$ m (corresponding to a 100 m diameter fracture, roughly the upper bound of fracture size that could be missed with non-negligible frequency if SKB's proposed criteria for deposition holes are correctly implemented).

Within these bounds (as illustrated by the shaded band in Figure 1), the ranges of transmissivities indicated by SKB's three alternative model variants are approximately $1x10^{-12}$ m^2/s to $1.6x10^{-7}$ m^2/s for FFM01, and $1x10^{-9}$ m^2/s to $2.5x10^{-6}$ m^2/s for FFM03.

Table 1: Parameters of segment transmissivity models for Fracture Domains FFM01 and FFM03 in depth zones z < -400 m, based on Tables 6-75 and 6-77 of SKB TR-10-52 and using the formula $a = 10^{\mu}$ to convert from the values given in the case of the uncorrelated model. Parameter values in bold font are those listed in the specified tables in SKB TR-10-52. Parameter values in normal font are inferred based on the equations given above.

Fracture Domain	Case	a (m^2/s)	$\log_{10} a$	b (-)	σ (-)
FFM01	semi-correlated	**5.3×10^{-11}**	-10.3	**0.5**	**1.0**
	Correlated	**1.8×10^{-10}**	-9.7	**0.5**	0
	Uncorrelated	1.58×10^{-9}	**-8.8**	0	**1.0**
FFM03	semi-correlated	**1.8×10^{-8}**	-7.7	**0.3**	**0.5**
	Correlated	**7.1×10^{-9}**	-8.1	**0.6**	0
	Uncorrelated	6.3×10^{-8}	**-7.2**	0	**0.8**

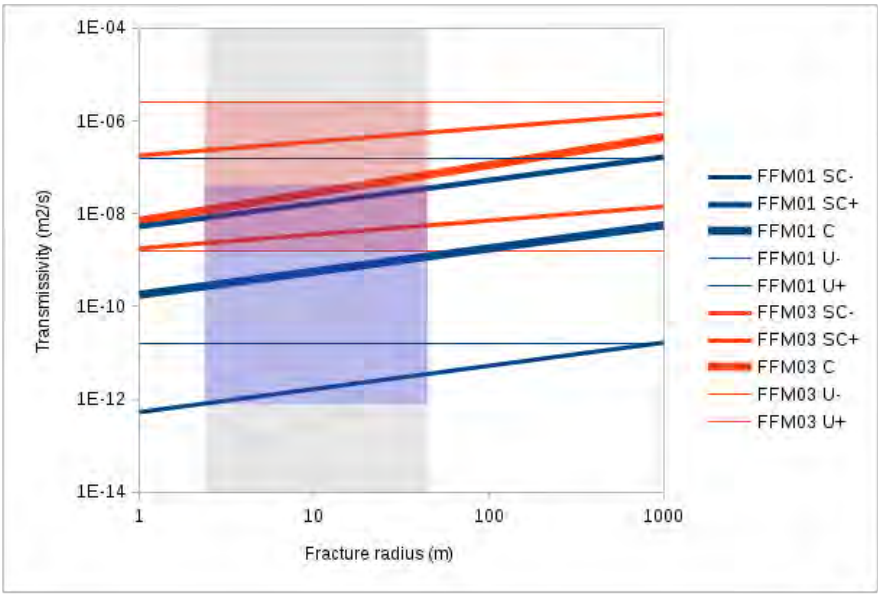

Figure 1: Fracture transmissivity ranges for the FFM01 (blue) and FFM03 (red) rock domains, based on ranges calculated for each of three model variants for the relationship of transmissivity to fracture size: C = correlated (thickest lines), SC = semi-correlated (medium-thickness lines) and U = uncorrelated (thin, horizontal lines). The shaded band highlights the range of fracture sizes from 2 m to 50 m that can most plausibly be encountered by deposition holes.

3.2 Expected evolution of fracture transmissivities due to changes in rock stresses around repository openings in the operational phase and post-closure

3.2.1 Empirical model for effect of stress on transmissivity

The effects of changing rock stresses on fracture transmissivities can be discussed in terms of changes in the components of stress relative to the plane of the fracture, namely the fracture normal stress σ_n and the shear stress τ_f (in the plane of the fracture).

Various empirical models relating fracture transmissivity to fracture normal stress have been proposed in the rock mechanics literature (Barton and Bandis, 1990). Recent modelling of hydromechanical effects for the Finnish repository programme (Hartley et al., 2016) adopted the following model for effective hydraulic aperture as a function of normal stress:

$$e_h = \left(\frac{A}{1 + \frac{\sigma'_n}{B}} \right) e_{h,0} + e_{res}$$

where A and B are empirical parameters, $\sigma'_n = \sigma_n - p$ is the effective normal stress, p is fluid pressure within the fracture, e_{res} is a "residual" aperture, and $e_{h,0}$ is a presumed value of e_h for unstressed conditions, i.e., for $\sigma'_n = 0$. The hydraulic aperture is related to fracture transmissivity T_f by the cubic law:

$$T_f = \frac{\rho_w g e_h^3}{12 \mu_w}$$

where μ_w is the dynamic viscosity and ρ_w is the density of water and g is gravitational acceleration.

For the Olkiluoto site, Hartley et al. (2016) used two different sets of values for the empirical parameters A and B, depending on a given fracture was considered to have undergone shear displacement:

$A_{preslip} = 1$	$B_{preslip} = 40$ MPa
$A_{slipped} = 3$	$B_{slipped} = 60$ MPa

The value of e_{res} was apparently taken as 1 μm.

The propensity of a fracture to slip was evaluated based on the Barton and Bandis (1990) criterion, according to which slip can occur when the shear stress τ_f exceeds a critical value in relation to the effective normal stress.

3.2.2 Effects of underground openings on stress and apertures

Rock stresses during the operational period are determined mainly by stress concentrations around the openings (tunnels and deposition holes), superposed on the prior in situ stresses.

According to SKB (2011), for the nominal repository depth the maximum horizontal stress is σ_H = 41 MPa, directed nominally NW-SE (parallel to the axis of the deposition tunnels), the minimum horizontal stress is σ_h = 23 MPa, and the vertical stress is σ_v = 13 MPa.

The modified stress field can be approximated by use of the Kirsch (1898) solution for stresses around a circular hole in an elastic solid:

$$\sigma_{rr} = \frac{\sigma_{xx} + \sigma_{yy}}{2}\left[1 - \left(\frac{a}{r}\right)^2\right] + \left[1 - 4\left(\frac{a}{r}\right)^2 + 3\left(\frac{a}{r}\right)^4\right]\left[\frac{\sigma_{xx} - \sigma_{yy}}{2}\cos 2\theta + \tau_{xy}\sin 2\theta\right]$$

$$\sigma_{\theta\theta} = \frac{\sigma_{xx} + \sigma_{yy}}{2}\left[1 + \left(\frac{a}{r}\right)^2\right] - \left[1 + 3\left(\frac{a}{r}\right)^4\right]\left[\frac{\sigma_{xx} - \sigma_{yy}}{2}\cos 2\theta + \tau_{xy}\sin 2\theta\right]$$

$$\tau_{r\theta} = \left[1 + 2\left(\frac{a}{r}\right)^2 - 3\left(\frac{a}{r}\right)^4\right]\left[\frac{\sigma_{yy} - \sigma_{xx}}{2}\sin 2\theta + \tau_{xy}\cos 2\theta\right]$$

where r is the radial distance from the center of the circular opening, θ is the angle from the x axis, and σ_{rr}, $\sigma_{\theta\theta}$, and $\tau_{r\theta}$ are respectively the radial and tangential compressive stresses and the shear stress.

The effects of a deposition tunnel on stresses impinging on a vertical deposition hole can be estimated from these equations by taking a = 2.5 m as a nominal diameter for the deposition tunnel, and setting $\sigma_{xx} = \sigma_h$ and $\sigma_{yy} = \sigma_v$ as the infinite-acting stresses, and considering the variation of tangential and radial stresses along the direction θ = 90° (i.e., perpendicular to the horizontal stress).

As shown in Figure 2, the main effect along the axis of the deposition hole is an increase in tangential (hoop) stress and decrease in radial (vertical) stress, mainly in the upper 2 m of the deposition hole. The corresponding effects in terms of hydraulic aperture and transmissivity for on fractures perpendicular to these stresses, along the deposition-hole axis, are also shown.

The increased hoop stress implies increased normal stress across vertical or steeply dipping fractures striking parallel to the tunnel. Thus hydraulic aperture and transmissivity will be reduced by this effect in vertical fractures, for portions close to the

tunnel floor. Conversely, the reduction in radial stress near the tunnel floor results in reduced normal stress across horizontal or gently dipping fractures, resulting in a dilation of aperture relative to the original aperture in situ, and increased transmissivity.

From these figures it can be seen that the main effects of stress redistribution around the tunnel are limited to the first 1.5 m below the tunnel floor. With SKB's design, this excavation-influenced zone is above the top of the canister. For fractures intersecting the portion of a deposition hole in which the canister is placed, the effects of this stress redistribution around the tunnel are practically negligible.

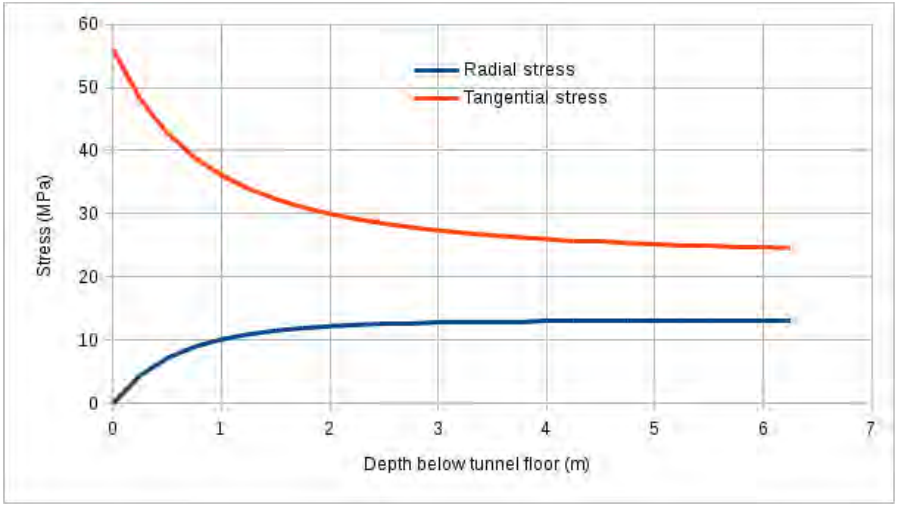

Figure 2: Effect of stress redistribution around a deposition tunnel, for radial and tangential stresses along a vertical section below the tunnel floor. The tunnel is approximated by a circular cylinder with diameter 5 m, assumed to be aligned with the far-field maximum horizontal stress σ_H so the far-field horizontal stress acting across the tunnel is σ_h = 23 MPa and the far-field vertical stress is σ_v = 13 MPa.

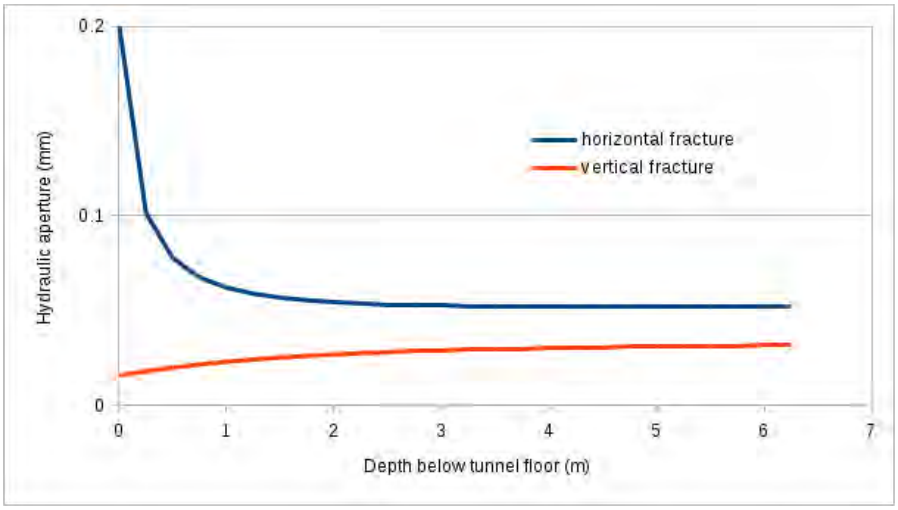

Figure 3: Expected effect of stress concentration on hydraulic aperture on vertical and horizontal fractures passing through a vertical line below a deposition tunnel floor. The fractures are assumed to have an aperture of 0.2 mm when unstressed (effective normal stress equal to zero), with closure controlled by the empirical model given in the text, with A = 1 and B = 40 MPa. Other assumptions and parameters are as in Figure 2.

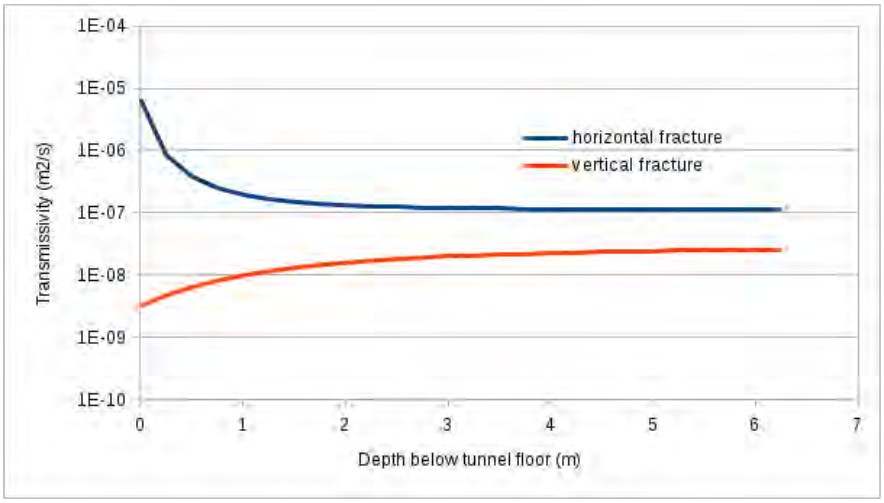

Figure 4: Expected effect of stress concentration on transmissivities of vertical and horizontal fractures passing through a vertical line below a deposition tunnel floor. Assumptions and parameters are as in Figures 2 and 3.

3.2.3 Effects of stress concentration around deposition hole

Similar calculations can be carried out to assess the influence of stress redistribution around a vertical deposition hole. For this situation the relevant far-field stresses are the horizontal stresses, σ_H and σ_h. It should be noted that this applies mainly to the part of the deposition hole below the top of the canister, as more complicated 3D stress-concentration effects affect the rock around the uppermost part of each hole.

The strongest effect is in the direction perpendicular to the direction of σ_H, *i.e.* along the direction of the deposition tunnels (in other words, on the side of the deposition hole that is tangential to the direction of σ_H). As shown in Figure 5, the calculated hoop stress at the wall of the deposition hole can reach 100 MPa, while the radial stress drops to zero at the free surface. This is based on the assumption of elastic behaviour for the mathematical solution used. Depending on the strength properties of the rock, spalling (as discussed in Section 3.5) could occur which would result in a modification of this stress profile.

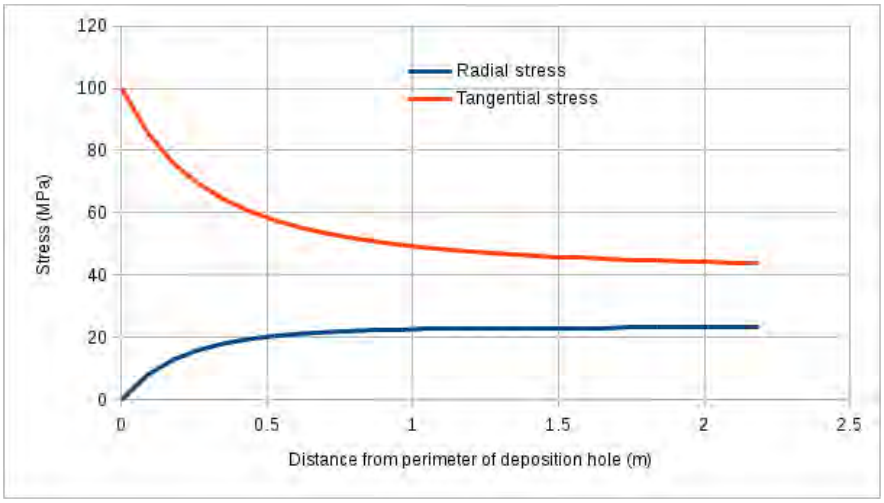

Figure 5: Effect of stress redistribution around a deposition hole of diameter 1.75 m, for radial and tangential stresses along a radial line perpendicular to the maximum horizontal stress σ_H. These curves are calculated based on the far-field maximum horizontal stress σ_H = 41 MPa and the far-field minimum horizontal stress σ_h = 23 MPa.

The hoop stress primarily affects subvertical fractures that make intersections close to radial with respect to the deposition-hole axis. The radial stress mainly affects subvertical fractures that are nearly tangential to the deposition hole.

The case of a vertical fracture that intersects, but is nearly tangential to the deposition hole, could be of interest as the most extreme case of a fracture affected by stress redistribution around a deposition hole. Such a fracture would have very low normal stress σ_n around its intersection with the hole, resulting in locally higher hydraulic aperture and transmissivity. However Figure 5 shows that the zone of low σ_n is limited to about half a meter distance from the deposition hole.

The stress concentrations along lines radial to the deposition hole in other directions are much less pronounced (Figure 6). The corresponding effects on hydraulic aperture and transmissivity for vertical fractures making radial intersections with the deposition hole are shown in Figures 7 and 8, respectively. The maximum effect in terms of transmissivity is a reduction by approximately an order of magnitude, and becomes negligible beyond a distance of about 0.5 m.

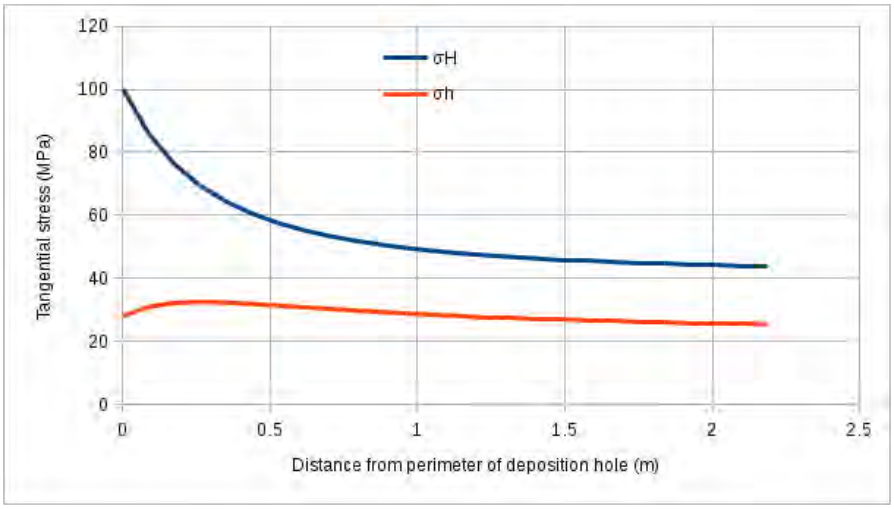

Figure 6: Effect of stress redistribution around a deposition hole of diameter 1.75 m, for tangential stresses along radial lines perpendicular to the maximum horizontal stress σ_H (blue) and perpendicular to the minimum horizontal stress (red). Parameters are the same as for Figure 5.

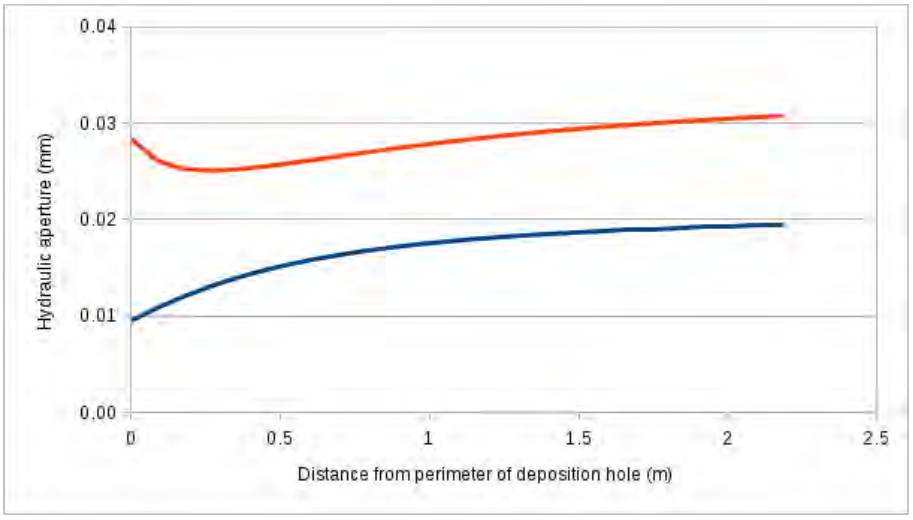

Figure 7: Expected effect of stress redistribution around a deposition hole on hydraulic aperture of vertical fractures making a radial intersection with the hole, for fractures perpendicular to the maximum horizontal stress σ_H (blue) and perpendicular to the minimum horizontal stress (red). Parameters are the same as for Figures 5 & 6.

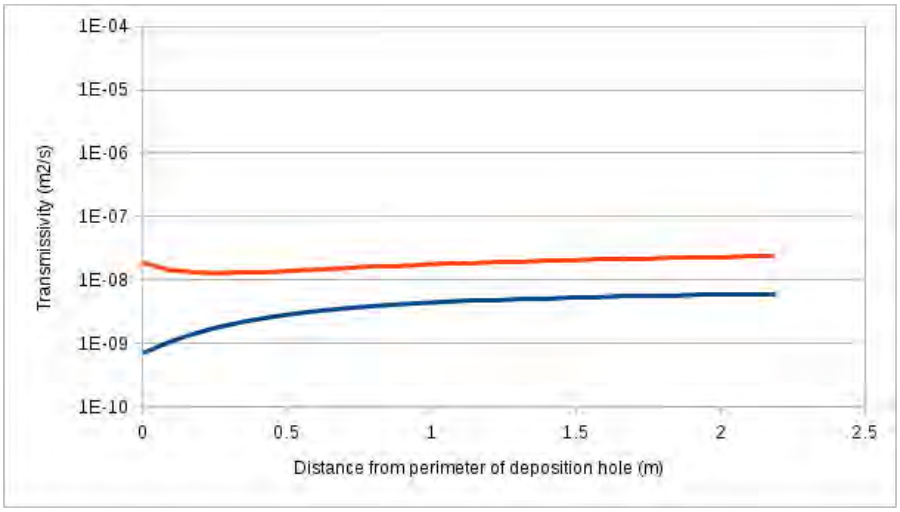

Figure 8: Expected effect of stress redistribution around a deposition hole on transmissivity of vertical fractures making a radial intersection with the hole, for fractures perpendicular to the maximum horizontal stress σ_H (blue) and perpendicular to the minimum horizontal stress (red). Parameters are the same as for Figures 5 & 6.

3.2.4 Post-closure evolution of stresses and influence on transmissivity

Stresses and effective stresses in the repository near field in the post-closure period are potentially affected by several processes, including:

- Restoration of near-hydrostatic pore pressures after pumping of water from repository openings ceases and the water table recovers;
- Development of swelling pressure in the buffer and backfill;
- Thermal stresses caused by the interaction between thermal expansion and rock elasticity as heat from the spent fuel is transmitted into the rock around the deposition holes; and
- Loading of the crust by an advancing ice sheet during the onset of glaciation, followed by glacial retreat.

The effects of these processes are considered in the following paragraphs.

Hydrostatic groundwater pressure at repository depth is roughly 5 MPa, which is small in relation to the maximum and minimum horizontal stresses, but more significant in relation to the vertical rock stress. Hence the main effect of increasing groundwater pressure is expected to be for horizontal fractures, for which the effective normal stress is reduced from 13 MPa under fully drained conditions to around 8 MPa upon return to hydrostatic pressure.

For a horizontal fracture with parameters as considered in Figure 4, a return to hydrostatic pressure increases the fracture transmissivity by roughly a factor of 3. For vertical fractures the effect of increasing groundwater pressure is generally less than

a factor of 1.7 (i.e., a 70% increase) at a distance of more than 1 m from the deposition hole. The effect diminishes closer to the deposition hole, where stress concentrations amplify the difference between rock stresses and fluid pressures.

More significant increases in fracture transmissivity could result if pore pressures in critically-stressed fractures decrease the ratio of effective normal stress to shear stress sufficiently for slip to occur. Empirical models of the effects of shear displacement on fracture transmissivity are not well bounded due to the difficulty of obtaining data on representative scales. The models considered by Hartley et al. (2016) indicated that hydraulic aperture in fractures that had undergone shear displacement could be more than three times larger than that for unsheared fractures, corresponding to a factor of 30 increase in transmissivity.

Effects of swelling pressure in the buffer and backfill are expected to be minor in relation to the ambient rock stresses, during the buffer saturation phase considered in this research project. According to the design specifications the swelling pressure developed in the fully saturated buffer should be at least 1 MPa to ensure tightness in the buffer and reduce microbial activity, but it must be less than 15 MPa to limit pressure on the canister and the rock. For the reference buffer materials, according to SKB's calculations the swelling pressure should be 7.8 MPa to 8 MPa, with a possible range in variation of 4.5 MPa to 13 MPa due to density variations (SKB 2011, p. 373). Thus at most, the swelling pressure is expected to be at least 10 MPa less than the minimum horizontal stress, and the main effect would be to decrease the stress-concentration effects as evaluated above. Furthermore swelling pressure develops as a consequence of saturation, and thus the full pressure would not be realized uniformly in a deposition hole, until the end stages of the processes considered in models of buffer resaturation.

The backfill is expected to have a lower swelling pressure than the buffer (SKB, 2011, p. 380). The effect of backfill swelling pressure p_s can be estimated by superposing the incremental stresses produced by applying a pressure on a circular opening in an unstressed medium (Timoshenko and Goodier, 1970):

$$\Delta\sigma_{rr} = \frac{a^2}{r} p_s$$

$$\Delta\sigma_{\theta\theta} = -\frac{a^2}{r} p_s$$

on those calculated from the Kirsch (1898) solution.

The main effect for fractures below the tunnel floor is a reduction in the contrast between horizontal and vertical fractures. Figure 9 shows the effects of a backfill swelling pressure p_s = 5 MPa on a fracture with the same hydromechanical parameters as considered in the foregoing examples. At a depth of 2 m below the tunnel floor, the transmissivity of a horizontal fracture is decreased by about 60%, due to the increased confinement radial to the tunnel, while the transmissivity of a vertical fracture is increased by about a factor of 2 due to the swelling pressure counteracting the tangential stress concentration produced by the horizontal far-field stress.

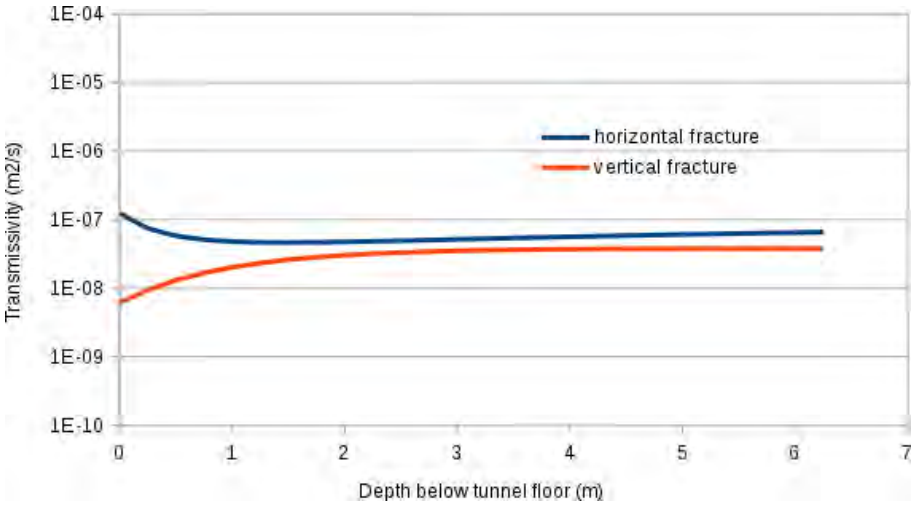

Figure 9: Expected effect of stress concentration counteracted by backfill swelling pressure of 5 MPa on transmissivities of vertical and horizontal fractures passing through a vertical line below a deposition tunnel floor. Other assumptions and parameters are as in Figures 2 and 3.

Glaciation brings the potential for a complicated series of events that affect both rock stresses and groundwater pressures at repository depth. The simplest situation to consider is during a glacial maximum, when the weight of 2 km of ice on the surface could increase the vertical component of rock stress by close to 20 MPa. The main effect is a reduction in the overall transmissivity of sub-horizontal fractures (Figure 10).

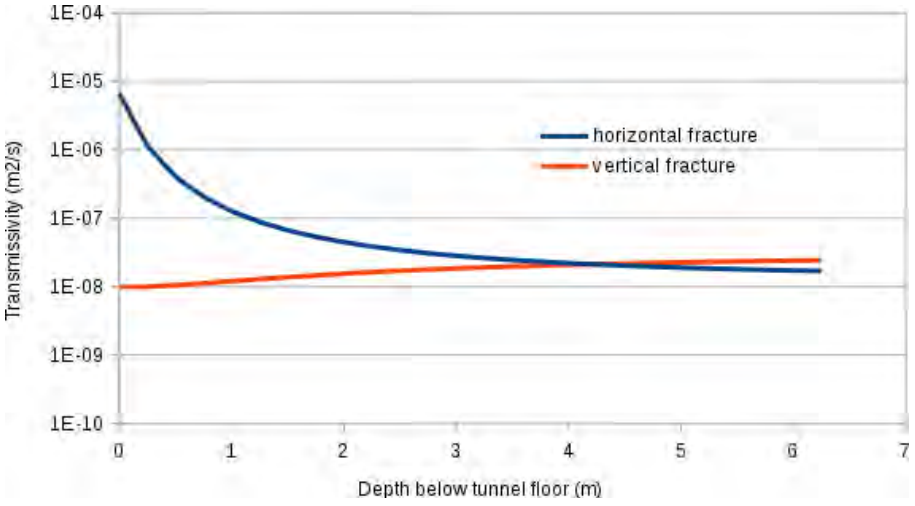

Figure 10: Expected effect of stress concentration on transmissivities of vertical and horizontal fractures passing through a vertical line below a deposition tunnel floor, when vertical stress is increased by 20 MPa to represent the effect of loading by a 2 km thick ice sheet over the repository. Other assumptions and parameters are as in Figures 2 and 3.

More complicated situations arise during periods of glacial advance and retreat. Quantitative assessment of the potential transmissivity changes during these periods would require detailed mechanical modelling taking into account alternative possibilities regarding the direction of glacial advance/retreat, beyond the scope of this

study. The most significant effects are likely to occur during glacial retreat when the combination of elevated pore pressures (due to glacial meltwater infiltration) and changing rock stress configurations could cause some fractures to become unstable and slip. Shear dilation produced by slip in this situation could very plausibly produce an order-of-magnitude increased in fracture transmissivity, based on the results of Hartley et al. (2016).

3.3 Implications of an excavation damage zone

A detailed study of the excavation damage zone (EDZ) for the drill-and-blast methods expected to be employed at Forsmark was carried out in the Äspö Hard Rock Laboratory, as described by Ericsson *et al.* (2014). Key findings of relevance for bentonite saturation included:

- The depth of the excavation-induced fractures beneath the floor is interpreted to be on average 0.3 m.
- Blast-induced fractures occur at low frequency, and are mainly associated with the ends of the holes drilled for each blast round.
- The connectivity between induced fractures is limited.
- Both blast-induced and stress-induced fractures will form sub-parallel to the tunnel contour (it should be noted, this finding by SKB is partly questioned by SSM's experts engaged in the DECOVALEX Project, who consider that blast-induced fractures are typically radial to the charged holes).
- Blast-induced fractures and increased apertures of natural fractures are the main source of high transmissivity values in injection tests down to a depth of 0.4 m or 0.5 m below the tunnel floor.
- The majority of injection tests with transmissivity greater than 10^{-8} m^2/s leaked to the tunnel floor. These flow paths are interpreted to be correlated with excavation-induced damage.

Based on these findings, excavation-induced fractures should typically be encountered only in the upper half meter of a deposition hole, though occasionally somewhat deeper (down to about 1 m depth). They can be associated with transmissivities as high as $6x10^{-5}$ m^2/s according to the data presented by Ericsson et al. (2014, Figure 9-4), but more typically in the range $1x10^{-8}$ m^2/s to $1x10^{-6}$ m^2/s.

3.4 Expected patterns and implications of stress-induced spalling in deposition holes

According to SKB's analysis, spalling should not occur around deposition holes at least prior to thermal effects caused by heat from the spent fuel, due to a rock strengths generally in excess of the expected stresses. According to SKB (2011, p. 113) the unconfined compressive strength (UCS) for intact rock in the proposed repository volume at Forsmark is generally high relative to the elastic stress concentration, with UCS > 200 MPa.

For two rock domains corresponding to the main fracture domain in the repository volume, FFM01, the SR-Site Data Report (SKB 2010, p. 289) mean values of 226 MPa and 214 MPa, with minimum and maximum values in the range 157 MPa to 289 MPa. The corresponding estimated ranges of spalling strength, evaluated as 57±5% of the mean UCS, are 129 ± 11 MPa and 122 ± 19 MPa. For the other fracture domain in the repository volume, FFM06, the corresponding estimated ranges of spalling strength are 37% to 75% higher.

From elastic analysis of the effects of a deposition hole on the local stress field, as given in Section 3.2 (Figure 6), it can be seen that stresses close to the deposition-hole wall, tangent to the direction of the maximum horizontal stress σ_H, can reach 100 MPa while the confining stress in the radial direction drops to zero.

A few in-situ measurements, regarded as low-confidence measurements by SKB, yielded estimates of σ_H up to 63 MPa (SKB, 2011, p. 124, Figure 4-15). This would yield elastic stress concentrations of up to 166 MPa around the deposition hole, which could be high enough to produce spalling prior to emplacement of canisters. According to SKB's design specifications, such spalling if detected would be removed by scaling, and the resulting irregular gap would be filled with bentonite pellets.

3.4.1 Likelihood and depth of thermally-induced spalling

After emplacement of the canister, thermally-induced increases in stress at the wall of the deposition hole, could lead to spalling. According to results of modelling by Hökmark *et al.* (2010), as summarized by SKB (2011, p. 335), the spalling strength is likely to be reached in all deposition holes during the thermal phase. Taking into account the superposed effects of stress concentration around the tunnel, the spalling in deposition holes could extend from the tunnel floor down to a depth of 7.3 to 7.9 m after 50 years (the range of depths is a function of parameter values assumed for thermal conductivity and spalling strength, considering the ranges of variability for the former and uncertainty for the latter).

An in-situ experiment at the Äspö Hard Rock Laboratory (Andersson, 2007) indicates that spalling could be suppressed by small pressures exerted by bentonite, but SKB (2011) note that these results are inconclusive. Such mitigation, if it occurs,

would presumably require that the bentonite be saturated sufficiently to develop swelling pressure. Thus for modelling holes in which resaturation occurs only after the development of thermal stresses, a reasonable assumption is that thermal spalling develops along the full depth of the deposition hole, during the first 50 years post-emplacement.

3.4.2 Geometry of spalled zones

In-situ data on the potential geometry of spalled zones around deposition holes comes mainly from a controlled-spalling experiment at the Äspö Hard Rock Laboratory (Andersson, 2007). In this experiment the tangential stress on one side of a 1.75 m diameter deposition hole was intentionally increased by boring a second hole approximately 1 m away, along the tunnel center line. The observed spalling varies by depth (Figure 11) and forms a nominally V-shaped notch with a notch opening angle of approximately 130 degrees (Figure 12).

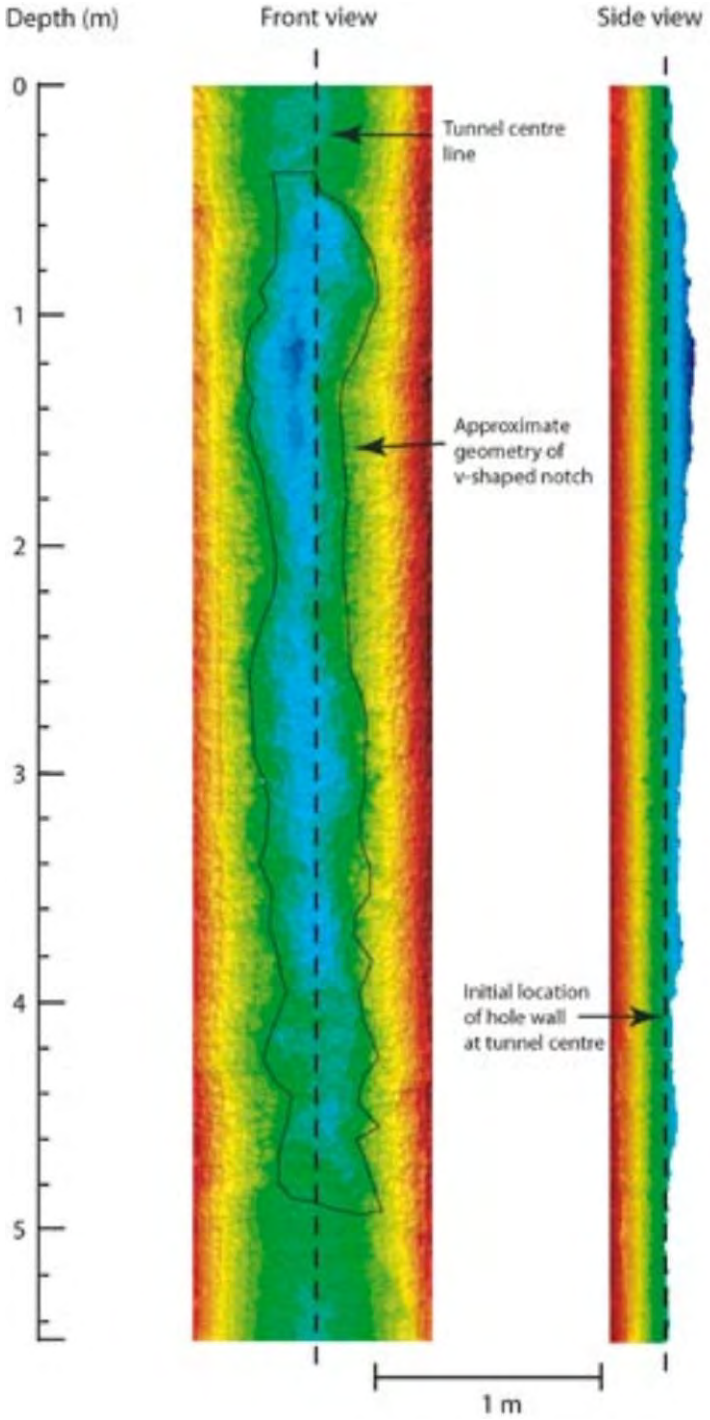

Figure 11: Depth of spalling failure observed in the APSE experiment (Andersson, 2007), as measured by laser scanning. The left-hand figure shows the variation in spalling depth as a function of depth and in relation to distance from the vertical line (shown as dashed) of closest proximity to the second hole. The right-hand figure shows an orthogonal profile along this line. Shades of blue indicate depth of spalled zone. Based on Figure 6-17 of Andersson et al. (2007).

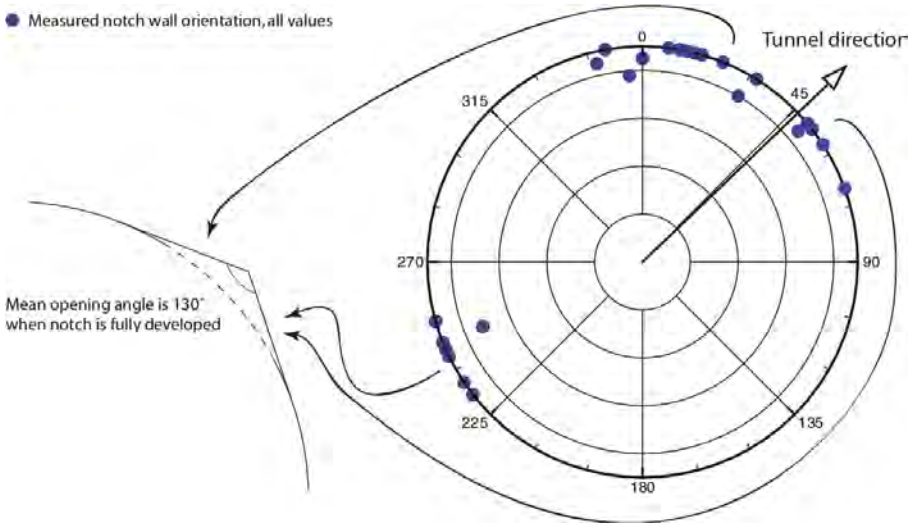

Figure 12: Variability of orientation of the walls of notch formed by spalling in the APSE experiment (Andersson, 2007), lower-hemisphere projection. The nominal opening angle where the notch is fully developed is approximately 130 degrees. Based on Figure 6-15 of Andersson et al. (2007).

Rock mechanics analyses of well bore breakouts (Zoback et al., 1985; Zheng et al., 1989) indicate that the geometry of spalled zones adjacent to a cylindrical opening is related to the ratio of the maximum and minimum horizontal stresses, σ_H/σ_h, as well as the parameters of the rock failure criterion that applies.

Figure 13 illustrates two idealizations and alternative parameterizations of breakout zone geometry in terms of radial depth r_b - r and half-angle φ_b, according to the notation used by Zoback et al. (1985), or as nominal depth d_{zone} and width w_{zone} according to the notation of Neretnieks (2006). In situ observations of wellbore breakouts tend to be irregular and intermediate between these idealizations as lunate or triangular.

A higher stress ratio leads to greater φ_b (or equivalently, width). For Forsmark σ_H/σ_h = (41 MPa) / (23 MPa) ≈ 1.8 which is low relative to ranges considered by Zoback et al. (1985). By comparison with the examples given by Zoback et al. (1985), the spalled zone half-angle should be no more than about φ_b = 10°. From graphical analysis of Figure 11, the maximum spalled zone width from APSE is approximately w_{zone} = 0.3 m which gives a similar value of φ_b.

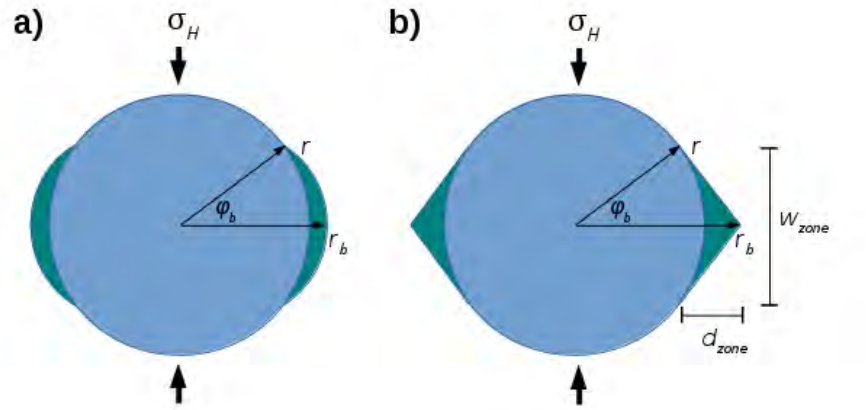

Figure 13: Idealized representations of spalled zones as nominally lunate (at left) or triangular (at right), extending from a borehole of radius *r* in the direction perpendicular to the maximum horizontal stress σ_H. The maximum distance from the center of the borehole to the deepest point in the spalled zone is r_b, and the half-angle spanned by each breakout zone is φ_b, following the notation of Zoback et al. (1985). In the drawing at right, the parameterization in terms of width w_{zone} and nominal depth d_{zone} as used by Neretnieks (2006) is also shown.

The depth of the spalled zone is controlled by the inelastic (post-failure) properties of the spalled material. Quantitative evaluation of this effect would be a complicated modelling task. An empirical relationship given by Martin et al. (1997) can be written in terms of the notation used here as:

$$\frac{r_b}{r} = (0.48 \pm 0.1) + 0.5\frac{\sigma_{\theta max}}{\sigma_{sm}}, \qquad \sigma_{\theta max} > \sigma_{sm}$$

where $\sigma_{\theta max}$ is the maximum tangential stress at the edge of the hole, and σ_{sm} is the spalling strength.

For SKB's rock stress model, $\sigma_{\theta max} < \sigma_{sm}$, so no spalling occurs prior to the thermal period. A worst-case analysis using the outlying stress measurement σ_H = 63 MPa (resulting in a stress concentration $\sigma_{\theta max}$ = 166 MPa), in combination with the minimum spalling strength (122 MPa – 19 MPa = 103 MPa) for FFM06 in the above empirical formula gives a notch depth $r_b - r \approx 25$ cm. This is no doubt excessive as it results from compounding the effects of extreme values. In the APSE experiment, the notch depth is 10 cm or less over most of the length of the deposition hole.

3.4.3 Hydraulic characteristics of spalled zones

No direct evidence is available for the hydraulic characteristics of spalled zones adjacent to deposition holes. Hence the best available indication of potential hydraulic properties comes from the observed geometry of fracturing within these zones.

The conceptual model for spalling based on observations from the APSE experiment is illustrated in Figure 14. As interpreted by Andersson (2007), the spalling process is considered to proceed by formation of slabs bounded by curved tensile fractures

that are approximately parallel to the wall of the deposition hole. These tensile fractures gradually grow shorter in width with distance from the wall, until the process is arrested as dilation of partly failed rock produces confining stresses in the radial direction. At the tip of the notch, horse-tail fractures may form as in Figure 15.

The continuity of spalling fractures in the vertical direction was not directly investigated in the APSE experiment. Photographs of the rock chips formed by spalling suggest that the length of these chips in the vertical direction is typically not more than twice their width in the tangential direction, and their thickness in the radial direction is typically less than one tenth of their width.

Based on these observations, it seems likely that if spalling occurs, it would result in a fractured zone with better connectivity in the vertical and tangential directions than in the radial direction. The anisotropy in effective permeability resulting from this geometry is likely at least a factor of 10.

Assuming a transmissivity of 10^{-8} m^2/s for each spalling fracture, and a spacing of 1 cm between fractures, leads to an estimated hydraulic conductivity of 10^{-6} m/s in the vertical direction. For an anisotropy ratio of 10, the corresponding value in the radial direction is 10^{-7} m/s.

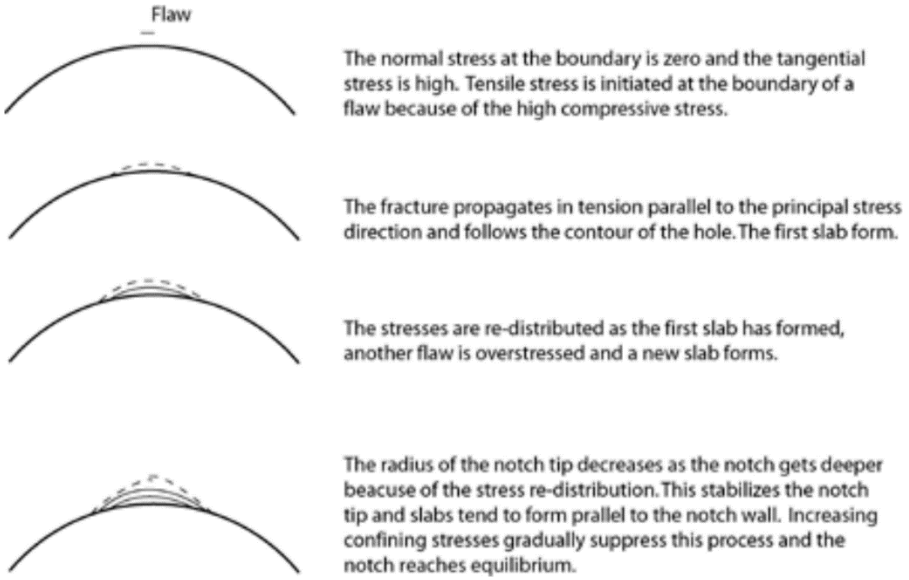

Figure 14: Conceptual model of spalling based on observations from the APSE experiment (Figure 11-11 of Andersson, 2007).

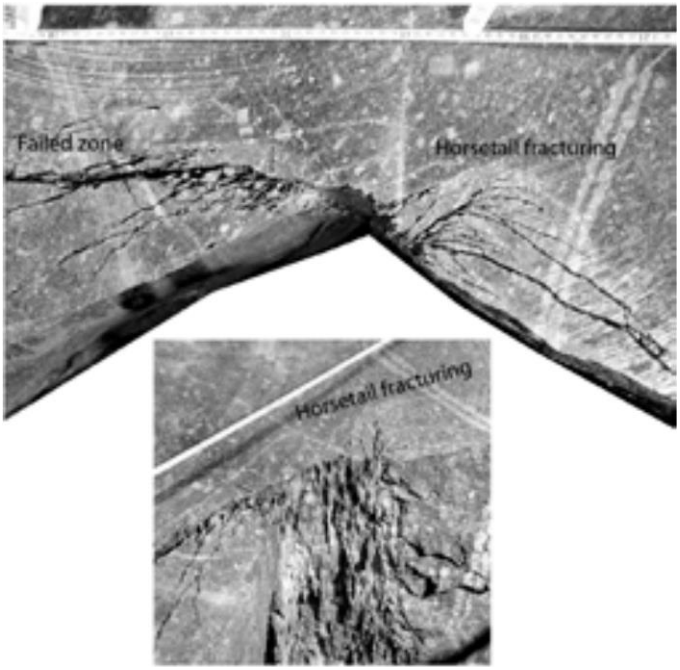

Figure 15: Photographs of fractures at tip of notch induced by spalling in the APSE experiment (Figure 10-14 of Andersson, 2007).

3.5 Flow patterns in the fractures around the deposition hole

Early in the resaturation period, the unsaturated or partly saturated bentonite exerts a strong matric suction on any water that comes into contact with it via a fracture. For low levels of saturation, the magnitude of the matric suction greatly exceeds the magnitude of local hydraulic potential gradients that can be expected in the natural fracture system. Hence initially flow should converge radially toward the deposition hole.

As the bentonite approaches saturation, the matric suction decreases, so do eventually the natural potential gradients. In this situation, the relatively low permeability of the clay-filled deposition hole makes it an impediment to flow through the fracture plane. The flow pattern for this situation could be calculated from classical solutions for 2-D flow around a low-permeability circular inclusion in an aquifer. However, such a situation need not be considered if the objective is to model just the period before the bentonite becomes fully saturated.

Flow channeling within a fracture may affect the details of the convergent flow field. The widths of channels within fractures is likely to be on the order of 10 cm for the scale of fractures considered, with a spacing between channels on the order of 1 m, based on comparison with detailed in-situ characterization of channeling in a single fracture in granite at the Stripa underground research facility (Abelin et al., 1990).

For purposes of modelling resaturation of the bentonite, two main flow geometries within an intersecting fracture can thus be considered: flow toward the deposition hole via a linear channel and radially convergent flow throughout the fracture plane (Figure 16). A variety of intermediate situations can be envisaged in heterogeneous fractures with varying degrees of flow channeling, but these two situations can be regarded as end members for bounding calculations and analysis of sensitivities.

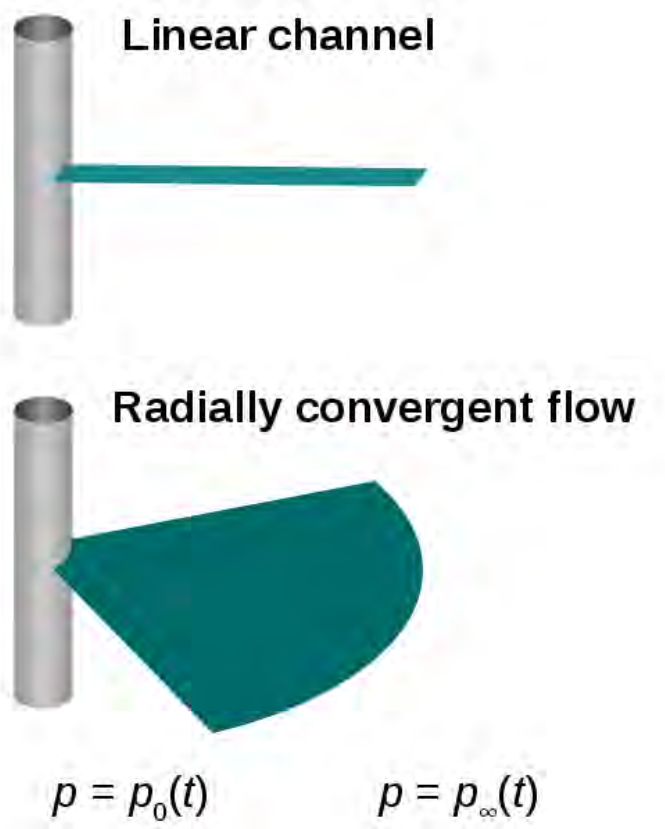

Figure 16: Idealized flow geometries and pressure boundary conditions for flow toward a deposition hole via (top) a single linear channel in a fracture or (bottom) radially converging flow in a fracture plane.

Analysis of tracer migration in the study by Abelin et al. (1990) indicated that channels within fractures may be connected to immobile zones within the fracture plane. The occurrence of such immobile zones connected to channels increases the probability that a deposition hole would connect to a channel, at least indirectly.

If the connection between channel and deposition hole is via one of these immobile zones, and the immobile zone has smaller aperture than the connected flow channel, then flow into the deposition hole may be restricted by the aperture of the immobile zone. This can be regarded as a reasonable scenario for contacting fractures that produce relatively high flow during the resaturation period, but are not detected during the open-hole period.

3.5.1 Groundwater pressure at the perimeters of deposition holes

At the boundary between the fracture or channel and the deposition hole, the initial condition is for pressure equal to atmospheric, *i.e.* $p_0(0) = 0$, due to drainage toward the opening. The subsequent development of pressure at this interface is a function of matrix suction developed by the bentonite (which depends on the degree of saturation) and is thus best handled by the bentonite resaturation model.

Groundwater pressures around underground openings in sparsely fractured granitic rock frequently exhibit high gradients, with pressures close to hydrostatic (i.e. $p = \rho_w g z$ where ρ_w is the density of water, g is gravitational acceleration and z is the depth of the repository below the regional groundwater table) within a few meters of the open tunnels. For a repository at 450 m depth, this implies far-field pressures of about 4.4 MPa early in the operational phase.

During the period of operations when the repository is open, the local water table is expected to be drawn down due to drainage into the repository tunnel system. Groundwater modelling of various grouting scenarios (Mårtensson and Gustafsson, 2010) indicate that the drawdowns at repository depth should be limited to about 20 m head (0.2 MPa pressure), except in high-transmissivity deformation zones that should be avoided by deposition tunnels, according to the repository design.

Thus the nominally undisturbed "far-field" pressure at the edge of the fracture or channel farthest from the hole, from the time of emplacement ($t = 0$) through the time of repository closure t_c is approximately:

$$p_\infty(t) \approx \rho_w g z - \delta p_\infty(t)$$

where the time-dependent drawdown $\delta p_\infty(t) \leq 0.2$ MPa. The magnitude of the initial drawdown $\delta p_\infty(0)$ for a given deposition hole may vary depending on its position within the repository, and whether that position is utilized early in the operational phase or late in the operational phase when the drawdown is more fully developed.

For $t > t_c$ the local groundwater levels continue to be depressed while the repository resaturates, drawing water into the pore space in the tunnels. Calculations by Svensson and Follin (2010) indicate that the time for resaturation of backfill in the tunnels is on the order of 3 years. Subsequently the groundwater levels recover to nominally undisturbed levels. Thus $\delta p_\infty(t>t_c)$ is nominally constant for the first few years, then decreasing asymptotically to zero.

For the remainder of the temperate period, the far-field pressure should remain relatively constant, except for the changes in the effective value of z, due for example sea level rise induced by anthropogenic climate change, brackish water intrusion, and longer-term post-glacial isostatic rebound.

Figure 17 gives an illustrative plot of possible combined effects of these processes for the first 1000 years after buffer placement. Note that the timing and magnitude of the effects of different processes may vary depending on factors such as time of emplacement prior to repository closure, rate of inflow to the backfilled filled tunnels during the resaturation period, and rate of global sea level rise in response to climate change. However these effects are small in relation to the effects of drawdown recovery following repository closure. For the sake of simplicity, the main effect could

be represented as a step function with far-field pressure p_∞ increasing from about 4.2 MPa to 4.4 MPa after repository closure.

The onset of a glacial period could initially bring somewhat lower far-field pressures due to reduced groundwater infiltration during periglacial conditions, followed by increases proportional to the thickness of ice cover.

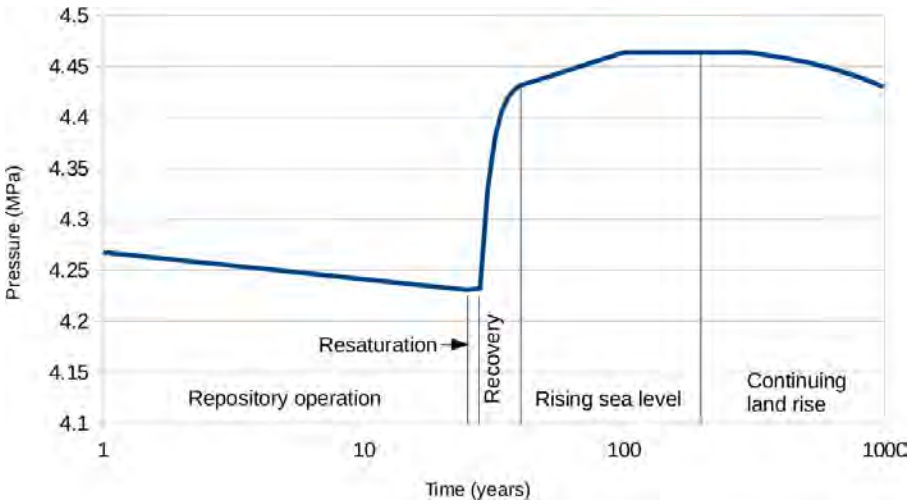

Figure 17: Illustrative plot of possible evolution of far-field pressure at repository depth, for a fracture affecting an emplacement hole that is utilized 25 years prior to repository closure, with a three-year resaturation period following closure, then local groundwater recovery from the draw-down due to the repository, followed by a period of rising sea level due to global climate change, followed by a period where groundwater levels are affected by continuing land rise caused by post-glacial isostatic rebound.

4. Recommendations

Expected ranges of fracture transmissivities

The plausible range of transmissivity for fractures intersecting deposition holes, based on consideration of SKB's DFN model in combination with constraints on fracture size, is from 10^{-12} m^2/s to 10^{-6} m^2/s.

This range could be constrained further by considering the maximum inflow that could be tolerated for a deposition hole. SKB (2011, p. 298) has indicated that a maximum inflow criterion for rejecting deposition holes might be considered in order to improve performance, but thus far no maximum value has been specified. Based on practical needs for emplacement of the buffer, it seems likely that fractures with transmissivity higher than 10^{-7} m^2/s would be avoided.

Expected evolution of fracture transmissivities due to changes in rock stresses

For a nominally horizontal fracture intersecting a deposition hole at the depth of the canister, increasing pore pressure after backfilling and closing a deposition tunnel can increase transmissivity by about a factor of 3, compared with fully-drained conditions. Development of bentonite swelling pressure in the tunnel backfill has a comparatively minor effect. Glacial loading can be expected to decrease the transmissivity of horizontal fractures by about an order of magnitude.

Bentonite swelling pressure in the buffer could potentially increase the transmissivity of a vertical fracture intersecting the deposition hole, within 1-2 m of the hole, but this would likely be negated by extrusion of bentonite gel into the fracture.

More significant changes could result from shear displacements caused by either thermomechanical or glacially induced stresses. Increases in transmissivity by as much as a factor of 30 are plausible based on laboratory evidence. The potential for slip to occur is dependent on the specific fracture mechanical properties and geometrical configuration, and would require use of sophisticated 3D rock mechanics models to evaluate. For the present research project, a more practical approach may be simply to treat this as a scenario in which fracture transmissivity increases by 1.5 orders of magnitude at some future time.

Implications of excavation damage zone

Excavation-induced fractures should be encountered only in the upper 0.5 m to 1 m of a deposition hole. They can be associated with transmissivities as high as $6x10^{-5}$ m^2/s, but more typically in the range $1x10^{-8}$ m^2/s to $1x10^{-6}$ m^2/s.

Conceptual models for flow patterns in fractures around the deposition hole

Due to the dominance of matric suction relative to natural hydraulic potential gradients in the fracture network, a reasonable simplification would be to assume that flow is directed toward the deposition hole for most of the resaturation period. Three main flow geometries are suggested:

- Radially convergent flow within a homogeneous fracture plane,
- Linear flow toward the deposition hole via a channel, and
- Flow to one side of a deposition hole via an otherwise immobile zone connected to a linear channel.

Channel widths on the order of 10 cm, with a mean spacing between channels on the order of 1 m to 2 m, can be regarded as representative for the geology and fracture scales considered. A reasonable approach for choosing a channel transmissivity would be to multiply the fracture transmissivity by the ratio of the assumed channel spacing to the channel width (e.g. for 10 cm wide channels on a 2 m spacing in fracture with a transmissivity of 10^{-8} m^2/s, the corresponding channel transmissivity would be $2x10^{-7}$ m^2/s).

Expected patterns and implications of stress-induced spalling

Spalling of deposition holes is very unlikely to occur prior to emplacement of bentonite and subsequent development of thermally induced stresses. If spalling does develop while a deposition hole is still open, it would likely be detected and then either addressed by corrective procedures (scaling the spalled material, then filling the gap with bentonite pellets), or by abandoning the hole. For modelling of the bentonite resaturation process, the former case would simply mean a modification of the geometry of the rock/bentonite boundary.

Thermally induced spalling that develops after emplacement could result in a spalled zone extending vertically along the hole. Based on results from the APSE experiment at Äspö, a spalled zone up to 10 cm deep and 30 cm wide could be envisaged.

Based on the observed geometry of rock chips/flakes formed by spalling, the permeability of this zone would likely be anisotropic, with hydraulic conductivity in the vertical direction at least an order of magnitude higher than that in the radial direction. Direct measurements of spalled zone hydraulic conductivity are lacking. For scoping the potential significance of this case, directional hydraulic conductivity values of 10^{-6} m/s in the vertical direction and 10^{-7} m/s in the radial direction are suggested.

Groundwater pressure and flowrate boundary conditions

Flowrate and pressure conditions at the fracture/bentonite interface are expected to be dominated by matric suction, during most of the resaturation period. Rather than imposing boundary conditions at this interface, it would be preferable to impose a far-field pressure boundary condition on the outer boundary of the planar fracture or channel that intersects the deposition hole.

The most important cause of variation in the far-field pressure during the temperate period is local drawdown of the water table during repository operation, followed by

recovery after closure. Other effects (e.g. relative sea level change due to climate change and post-glacial isostatic rebound) are comparatively minor. Therefore a simple step function representation is recommended:

$$p_{\infty}(\mathrm{t}) = 4.2\ \mathrm{MPa} + (0.2\ \mathrm{MPa})\ H(t\text{-}t_c)$$

where $H(t)$ is the Heaviside step function equal to 0 for $t<0$ and equal to 1 for $t\geq 0$.

5. References

Abelin H., Birgersson L., Widén H., Ågren T., Moreno L., and Neretnieks I. (1990). Channeling Experiment. Stripa Project Technical Report 90-13. Swedish Nuclear Fuel and Waste Management Co.

Andersson J. C. (2007). Äspö Hard Rock Laboratory: Äspö Pillar Stability Experiment, Final report. Rock mass response to coupled mechanical thermal loading. SKB Technical Report TR-07-01. Swedish Nuclear Fuel and Waste Management Co.

Barton N. R., Bandis S. C. (1990). Review of predictive capabilities of JRC-JCS model in engineering practice. In: Barton N. and Stephansson, O. (eds.). Rock Joints; Proceedings of the International Symposium on Rock Joints. Loen, Norway. P. 603- 610. Rotterdam: Balkema.

Ericsson L-O., Thörn J., Christiansson R., Lehtimäki T., Ittner H., Hansson K., Butron C., Sigurdsson O., Kinnbom P. (2015). A demonstration project on controlling and verifying the excavation-damaged zone. Experience from the Äspö Hard Rock Laboratory. SKB Report R-14-30. Swedish Nuclear Fuel and Waste Management Co.

Geier J. (2014). Assessment of flows to deposition holes. Main Review Phase. SSM technical note 2014:05. Swedish Radiation Safety Authority.

Hartley L., Baxter S., Williams, T. (2016). Geomechanical Coupled Flow in Fractures during Temperate and Glacial Conditions. Posiva Working Report 2016-08. Posiva Oy.

Hökmark H., Lönnqvist M., Fälth B. (2010). THM-issues in repository rock. Thermal, mechanical, thermo-mechanical and hydromechanical evolution of the rock at the Forsmark and Laxemar sites. SKB Technical Report TR-10-23. Swedish Nuclear Fuel and Waste Management Co.

Kirsch E.G. (1898). Die Theorie der Elastizität und die Bedürfnisse der Festigkeitslehre, Zeitschrift des Vereines deutscher Ingenieure, 42, pp. 797-807.

Martin C. D., Read R. S., Martino J. B. (1997). Observations of brittle failure around a circular test tunnel. Int. J. Rock Mech. Min. Sci. 34 (7), pp.1065–1073.

Mårtensson E., Gustafsson L.-G. (2010). Hydrological and hydrogeological effects of an open repository in Forsmark. Final MIKE SHE flow modelling results for the Environmental Impact Assessment. SKB Report R-10-18. Swedish Nuclear Fuel and Waste Management Co.

Neretnieks I. (2006). Flow and solute transport in a zone damaged due to spalling. SKB Report R-06-91. Swedish Nuclear Fuel and Waste Management Co.

SKB (2010). Data report for the safety assessment SR-Site. SKB Technical Report TR-10-52. Swedish Nuclear Fuel and Waste Management Co.

SKB (2011). Long-term safety for the final repository for spent nuclear fuel at Forsmark. Main report of the SR-Site project. SKB Technical Report TR-11-01. Swedish Nuclear Fuel and Waste Management Co.

Svensson U., Follin S. (2010). Groundwater flow modelling of the excavation and operational phases – Forsmark. SKB Report R-09-19. Swedish Nuclear Fuel and Waste Management Co.

Timoshenko S. P., Goodier J. N. (1970). Theory of Elasticity, 3rd Edition. McGraw-Hill, New York, 567 pp.

Zheng Z., Kemeny J., Cook N. G. W. (1989), Analysis of borehole breakouts. Journal of Geophysical Research, v. 94B, no. 6, June 10, p. 7171-7182.

Zoback M. D., Moos D., Mastin L., Anderson R. N. (1985). Well bore breakouts and in situ stress. Journal of Geophysical Research, v. 90B, no. 7, June 10, p. 5523-5530.

Authors: K. E. Thatcher, R. K. Newson, S. J. Benbow
(Quintessa Ltd, Henley-on-Thames, U.K.)

2

Research on Resaturation of Bentonite Buffer – Modelling of Resaturation

Project number: 3030045-38
Registration number: SSM2017-2830
Contact person at SSM: Jinsong Liu

Summary

This report is a research contribution to facilitate the Swedish Radiation Safety Authority's (SSM's) multistep review of the SR-Site safety assessment, which has been undertaken by the Swedish Nuclear Fuel and Waste Management Co. (SKB). The first-step safety assessment was undertaken to support SKB's licence application to construct and operate a final repository for spent nuclear fuel (SF) at Forsmark in the municipality of Östhammar, Sweden.

The work undertaken in the research concerns the modelling of resaturation processes in the bentonite buffer in the KBS-3 repository for spent nuclear fuel. Resaturation of the buffer is a multi-phase flow process that occurs as a consequence of coupled Thermal (T), Hydrological (H) and Mechanical (M) processes in the Engineered Barrier System (EBS) and in the near field. Resaturation and subsequent swelling and homogenisation of the buffer underpins several of the safety functions that are intended to ensure as-designed performance of the EBS. In particular, the following safety functions assume at least partly that the buffer will be water-saturated and homogenised:

- Buff1: Limit advective transport;
- Buff2: Reduce microbial activity;
- Buff4: Resist transformation; and
- Buff6: Limit pressure on canister and rock.

SKB's TH and THM modelling of buffer resaturation and swelling/homogenisation is described in SKB (2011, Section 10.3.8 and 10.3.9) and Åkesson et al. (2010). The resaturation scenarios considered by SKB largely assume that resaturation in the buffer arises from a uniformly flowing fracture that intersects the buffer horizontally, leading to axisymmetric patterns of resaturation. The results of the modelling suggest that resaturation time is strongly dependent on the hydraulic conditions in the near-field of the repository

The review by Black (2012) of hydrogeological models for Forsmark analysed the results of packer test experiments at the site and concluded that fracture flows in the host rock are likely to occur in channels rather than in homogeneously flowing fractures. In this case the fracture system may be better represented by a sparse channel network. Geier (2014) noted that the hyper-convergent flow effects that arise in such sparse channel networks could affect flow rates towards deposition holes during the resaturation period.

Depending on channel sizes and their frequency, channelled flows in the near-field would be likely to intersect deposition holes in the repository non-uniformly, leading to alternative resaturation scenarios to the uniform channel intersection cases considered by SKB. Such scenarios might be expected to lead to axially non-uniform patterns of resaturation and homogenisation in the buffer due to the more localised ingress of fracture porewater into the buffer.

Heterogeneous wetting patterns in the buffer could lead to uneven swelling pressures exerted on the copper canister surface. The duration of the resaturation period is uncertain (Börgesson et al., 2013), possibly taking 1 000's of years in some cases, and theoretical complete (100% fully saturated) resaturation of the buffer is not likely in any case. Uneven swelling pressures could therefore persist around the canister for long periods. Any uneven mechanical loading on the copper canister could potentially lead to sustained creep of the copper overpack in all slowly resaturating deposition holes and enhance the vulnerability of the canister to creep-ductility failure (Segle, 2015). In the worst case, this could lead to a common mode failure for the copper canister at time periods shorter than those due to chemical corrosion by HS^- diffusion from the fracture waters, which is the primary common failure mode considered in SKB (2011). (It is noted however that the buffer would not be eroded by this time, compared to the assumptions of the chemical corrosion failure mode.)

Since the modelling in Åkesson et al. (2010) was undertaken, some alternative conceptual models of hydraulic processes in bentonite have been proposed. The review by Åkesson (2013) of modelling tasks undertaken within the FEBEX project summarises three such alternatives: the threshold gradient, thermo-osmosis and micro-fabric evolution conceptual models, and provides an initial evaluation of each.

The purpose of the modelling undertaken in this work is to provide a preliminary investigation of the issues outlined above and assess their impact upon buffer resaturation. Specifically, it:

- Investigates the potential for channelling of flows in fractures to induce non-uniform resaturation of the buffer,
- Assesses sensitivity to fracture transmissivity and fracture channel size distributions, and
- Considers alternative conceptual models for hydraulic processes in the buffer.

For the scenarios that are considered, the model outputs provide information on

- Potential timescales for resaturation and homogenisation of the buffer and the degree to which each occurs,
- The eventual distribution of saturation and swelling pressure throughout the buffer,
- Mechanical loading patterns on the canister surface in relation to the potential for the development of copper creep,
- Impacts of heterogeneous buffer evolution on thermal evolution and peak temperatures in the buffer

A summary of the implications of the modelling results on SKB's expected evolution of the EBS is given below:

- Peak temperatures in the buffer were largely insensitive to the various fracture modelling options that were considered and were well within limits specified by SKB.
- Timescales for resaturation were found to be very sensitive to the choice of whether the bentonite pellet region was explicitly considered in the model. When pellets were omitted (to simplify some calculations, but possibly representative of non-ideal emplacement), resaturation timescales could be increased by an order of magnitude, well beyond the range of timescales predicted in similar modelling by SKB.
- Timescales for resaturation were sensitive to the representation of the fracture intersection with the deposition hole, varying by more than a factor of four depending on whether the fracture was assumed to be planar, intersecting the deposition hole along the entire circumference, or whether it was assumed to be channelled, intersecting the deposition hole over a smaller area. In several cases, remote regions of the buffer did not achieve full saturation over the simulation timescales (up to 4 000 y).
- In THM calculations, gradients along the length of the canister of normal stresses to the canister surface were found to persist for the duration of the resaturation period and were greatest when resaturation was most rapid. In TH calculations, where stresses were not calculated directly, water pressures were found to vary similarly, suggesting that gradients in the normal stress would also be present.

An investigation of the potential effect of the evolving stress/pressure gradient along the canister surface on the shape and durability of the copper overpack, and in particular whether there would be any effect on copper creep, is beyond the scope of the current work.

Contents

1. Introduction

This report is a contribution to Swedish Radiation Safety Authority's (SSM's) Review of the SR-Site safety assessment, which has been undertaken by Swedish Nuclear Fuel and Waste Management Co. (SKB). This safety assessment was undertaken to support SKB's licence application to construct and operate a final repository for spent nuclear fuel (SF) at Forsmark in the municipality of Östhammar, Sweden.

The work undertaken in this report concerns the modelling of resaturation processes in the bentonite buffer in the KBS-3 repository for spent nuclear fuel. Resaturation of the buffer is a multi-phase flow process that occurs as a consequence of coupled Thermal (T), Hydrological (H) and Mechanical (M) processes in the Engineered Barrier System (EBS) and in the near field. Resaturation and subsequent swelling and homogenisation of the buffer underpins several of the safety functions that are intended to ensure as-designed performance of the EBS. In particular, the following safety functions assume at least partly that the buffer will be homogenised:

- Buff1: Limit advective transport;
- Buff2: Reduce microbial activity;
- Buff4: Resist transformation; and
- Buff6: Limit pressure on canister and rock.

SKB's TH and THM modelling of buffer resaturation and swelling/homogenisation is described in SKB (2011, Section 10.3.8 and 10.3.9) and Åkesson et al. (2010). The resaturation scenarios considered by SKB largely assume that resaturation in the buffer arises from a uniformly flowing fracture that intersects the buffer horizontally, leading to uniform inflow around the circumference of the deposition hole, and axisymmetric resaturation. The results of the modelling suggest that resaturation time is strongly dependent on the hydraulic conditions in the near-field of the repository.

The review by Black (2012) of hydrogeological models for Forsmark analysed the results of packer test experiments at the site, and concluded that fracture flows in the host rock are likely to occur in channels rather than in homogeneously flowing fractures. In this case the fracture system may be better represented by a sparse channel network. Geier (2014) noted that the hyper-convergent flow effects that arise in such sparse channel networks could affect flow rates towards deposition holes during the resaturation period.

Depending on channel sizes and their frequency, channelled flows in the near-field would be likely to intersect deposition holes in the repository non-uniformly, leading to alternative resaturation scenarios to the uniform channel intersection cases considered by SKB. Such scenarios might be expected to lead to axially non-uniform patterns of resaturation and homogenisation in the buffer due to the more localised ingress of fracture porewater into the buffer.

Heterogeneous wetting patterns in the buffer could lead to uneven swelling pressures exerted on the copper canister surface. The duration of the resaturation period is uncertain (Börgesson et al., 2013), possibly taking 1 000's of years in some cases, and theoretical complete (100% fully saturated) resaturation of the buffer is not likely in any case. Uneven swelling pressures could therefore persist around the canister for long periods[1]. Any uneven mechanical loading on the copper canister could potentially lead to sustained creep of the copper overpack in all slowly resaturating deposition holes and enhance the vulnerability of the canister to creep-ductility failure (Segle, 2015). In the worst case, this could lead to a common mode failure for the copper canister at time periods shorter than those due to chemical corrosion by HS^- diffusion from the fracture waters, which is the primary common failure mode considered in SKB (2011). (It is noted however that the buffer would not be eroded by this time, compared to the assumptions of the chemical corrosion failure mode.)

Since the modelling in Åkesson et al. (2010) was undertaken, some alternative conceptual models of hydraulic processes in bentonite have been proposed. The review by Åkesson (2013) of modelling tasks undertaken within the FEBEX project summarises three such alternatives: the threshold gradient, thermo-osmosis and micro-fabric evolution conceptual models, and provides an initial evaluation of each.

The purpose of the modelling undertaken in this work is to provide a preliminary investigation of the issues outlined above and assess their impact upon buffer resaturation. Specifically, it:

- Investigates some possible patterns and rates of buffer resaturation for realistic fracture flow geometries and transmissivities,
- Analyses the effect of alternative conceptual models for hydraulic processes in the buffer,
- Evaluates plausible loading patterns on the canister, and
- Considers the effect on resaturation behaviour of the use of alternative bentonite materials.

Some of the scenarios that are to be considered are expected to lead to 3D patterns of resaturation in the buffer, as opposed to the 2D axisymmetric patterns that arise when a uniformly flowing fracture intersection is assumed. Numerical convergence was not achieved for 3D THM calculations, so a mixture of 3D TH calculations and 2D THM calculations have been used, with a common reference base case that allows inter-comparison of results. A similar approach is taken in Åkesson et al. (2010).

The report is structured as follows. In Section 2, an overview of the scenarios that are considered is given and the context in which modelling results will be evaluated is described. Section 3 provides details of the numerical

[1] It is noted that SKB suggest that water saturation is not an ideal indicator for pressure in the buffer and that the buffer attains a specified pressure for a range of degrees of water saturation (Supplementary material in addition to SR-Site modeling report TR-10-11 as requested by SSM – SKB document ID 1415873).

models that have been implemented and their parameterisation, including details of the alternative bentonite hydrology models. Section 4 gives the detailed conceptual and mathematical models for the difference scenarios. Results of the modelling are presented in Section 5 and are synthesised and discussed in Section 6. Finally, conclusions on how the outcomes of the modelling might affect evolution of the KBS-3 EBS and the relevance of the results and observations for SR-Site are given in Section 7.

2. Modelling Context

The KBS-3 concept proposes the disposal of spent nuclear fuel in copper canisters with a cast iron insert. The canisters are surrounded by a bentonite clay buffer within deposition holes that are located along tunnels that are filled with a bentonite clay backfill. The tunnels are located at a depth of approximately 500 m in groundwater saturated granitic rock (Figure 2-1). The buffer is initially emplaced using compacted bentonite blocks (solid above and below the canister, and ring-shaped around the canister) and the gap between the blocks and the rock surface is filled with pellets, as shown in Figure 2-2. The initially emplaced compacted bentonite blocks will be partially water saturated and are expected to resaturate and homogenise as water is taken up by the buffer from fractures intersecting the deposition hole and tunnel, whereupon they will attain a sufficient degree of homogenisation to achieve their desired safety functions. The following safety functions of the buffer assume, at least partly, that the buffer will be homogenised (SKB (2011), Section 8.3.2):

- Buff1: Limit advective transport;
- Buff2: Reduce microbial activity;
- Buff4: Resist transformation; and
- Buff6: Limit pressure on canister and rock

Resaturation and swelling/homogenisation of the buffer are discussed in SKB (2011) Sections 10.3.8 and 10.3.9 respectively.

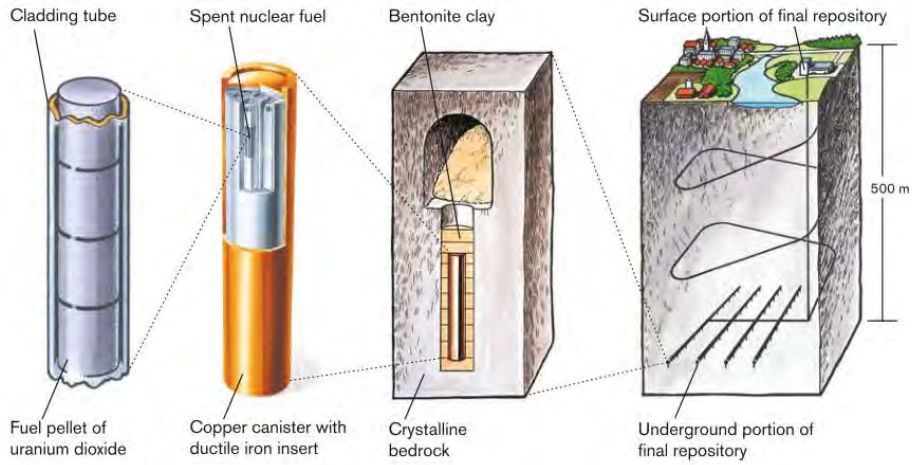

Figure 2-1: KBS-3 concept for disposal of spent nuclear fuel (from SKB, 2011).

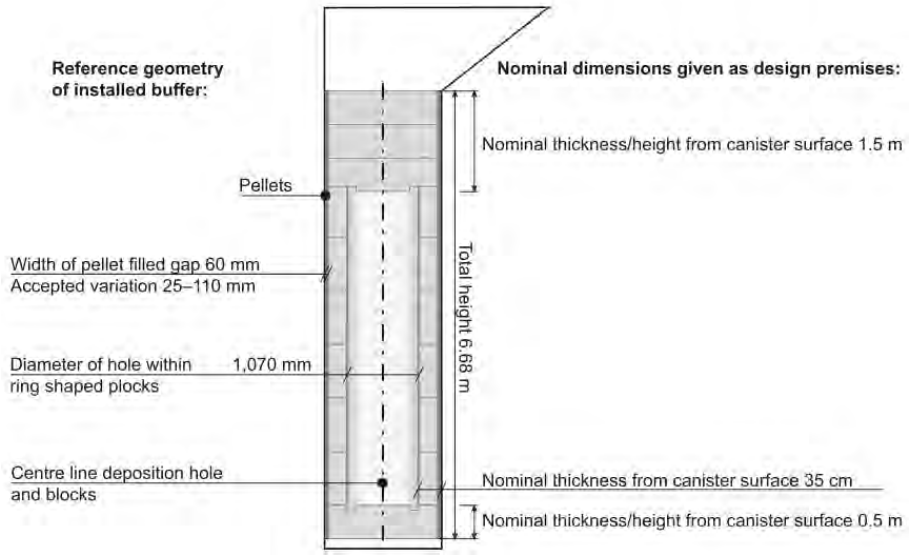

Figure 2-2: Reference geometry of the installed buffer (from SKB, 2011).

The scenarios that will be modelled consider the resaturation of the bentonite block and pellet region in the buffer from fractures that intersect the deposition hole. The tunnel region is not included in the analysis. An overview of buffer resaturation / homogenisation modelling of this scenario that was used to support the SR-Site safety case is provided in Section 2.1 of this report (a more comprehensive review is made in Benbow et al., 2012). The modelling simulations all considered the case of a uniformly flowing fracture, although subsequent modelling (Börgesson et al., 2013) did go on to consider point sources of resaturation. In Section 2.2 of this report, a brief overview of the justification for considering alternative non-uniform (channelled) flows in the fractures is given, and possible ranges of channel transmissivities, separations and widths are presented. Since the modelling in Åkesson et al. (2010) was undertaken, some alternative conceptual models of hydraulic processes in bentonite have been proposed that could potentially reduce the rates of water uptake in the buffer from fractures. These are introduced in Section 2.3. Based on these alternative flow and hydraulic models, scenarios that are considered in this work are presented in Section 2.4. Key outputs of the modelling that will be used to compare the various cases that are considered, with reference to SKB's safety functions for the buffer, are given in Section 2.5.

2.1. Summary of SKB Analysis

Buffer resaturation and homogenisation are analysed separately in Åkesson et al. (2010). The analysis of resaturation times is undertaken using 2D axisymmetric TH models and two scenarios are considered: one in which the resaturating fracture intersects the tunnel wall (T) and one in which the fracture intersects the deposition hole at the canister mid-height (CMH). Swelling of the bentonite as it resaturates will act to redistribute the bentonite within the deposition hole to fill voids and equalise density differences be-

tween the blocks and pellet filling. Bentonite thermal, hydrological and mechanical material properties will therefore evolve throughout the buffer. Since mechanical processes are not considered in the TH modelling, two edge cases for the bentonite properties are considered; which are assumed to bound any outputs that would have arisen if the system were modelled as THM: it is assumed that the material properties either remain fixed at their initial state, or in a perfectly homogenised state (characterised by identical void ratio throughout the buffer).

The axisymmetric geometry assumed in the 2D TH modelling is shown in Figure 2-3. The model includes a representative volume of tunnel backfill, with different material properties to the buffer. Scenarios in which it is assumed that the resaturating fracture intersects the tunnel wall are assumed to intersect the boundary of this region.

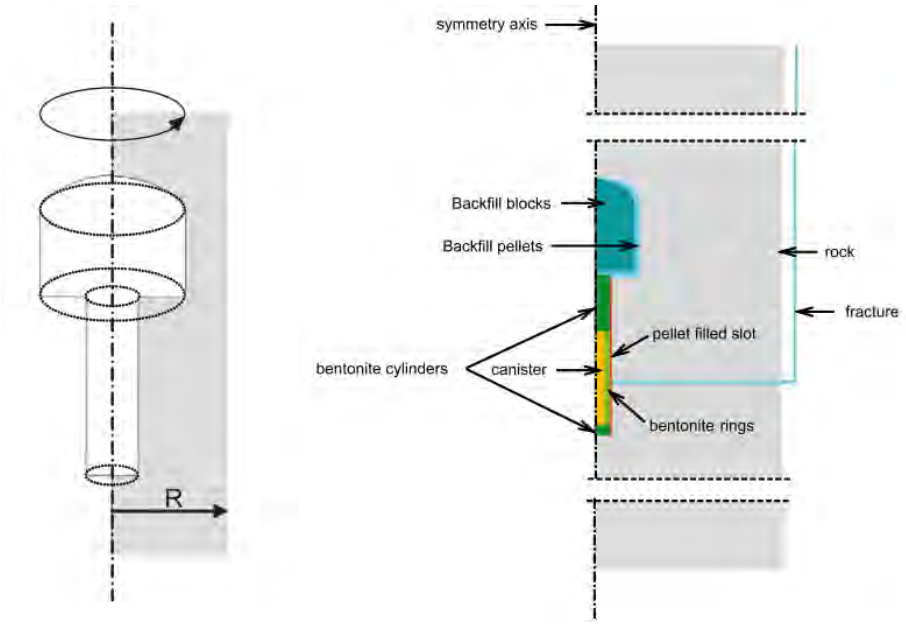

Figure 2-3: Axisymmetric buffer model geometry (left) assumed in the TH modelling in Åkesson et al. (2010) and the corresponding tunnel cross-section (right). (from Åkesson et al., 2010).

To validate the omission of mechanical processes in the analysis, the TH models are applied to a separate analysis of the Canister Retrieval Test (CRT). This was a full-scale test that simulated a deposition hole with a heated canister and buffer material consistent with the reference KBS-3 design. The experiment was a test of retrievability of the canister rather than aiming to realistically simulate resaturation of the buffer under repository conditions, and so the buffer was artificially wetted along the rock surface rather than from discrete fractures intersecting the deposition hole. The buffer was instrumented to capture data for use in homogenisation modelling studies undertaken in the Task Force for Engineered Barrier Systems (TF-EBS). The TH models used to simulate resaturation were applied to the rapid saturation CRT data and results were compared with a 1-D THM model of the CRT system. Generally, the results suggest that the TH model

with initial state material properties provides a better match to the rapid resaturation time data from the CRT THM model (e.g. Figure 2-4). However, separate SKB analysis showed that the TH model with homogenised buffer properties gave rise to a faster buffer resaturation than the initial state property model in the case of a slow wetting process.

The comparison between the TH and THM models therefore provides some confidence that for rapid wetting cases, where saturation is achieved on the order of 1-2 years (Figure 2-4), the 1-D TH models provide a reasonable approximation to evolution that would be predicted by a 1-D THM model.

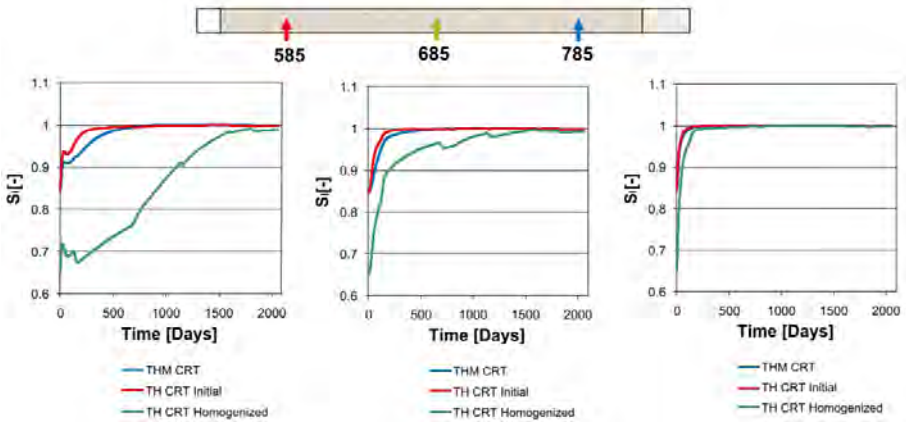

Figure 2-4: Water saturation evolution at three different radii (585, 685 and 785 mm) (from Åkesson et al., 2010).

The times predicted by the 2D TH models for resaturation of the various scenarios considered in Åkesson et al. (2010) are shown in Figure 2-5. The resaturation time is taken to be the time at which the saturation of liquid water is >0.99 throughout the entire buffer. For the CMH case, upon which the independent modelling discussed in the remainder of the report will focus, resaturation times ranging from 7 to 40 years are predicted, depending on the rock conductivity and bentonite material properties that are assumed. This encompasses a range up to ten times longer than the time for resaturation in the CRT test, upon which the models were benchmarked.

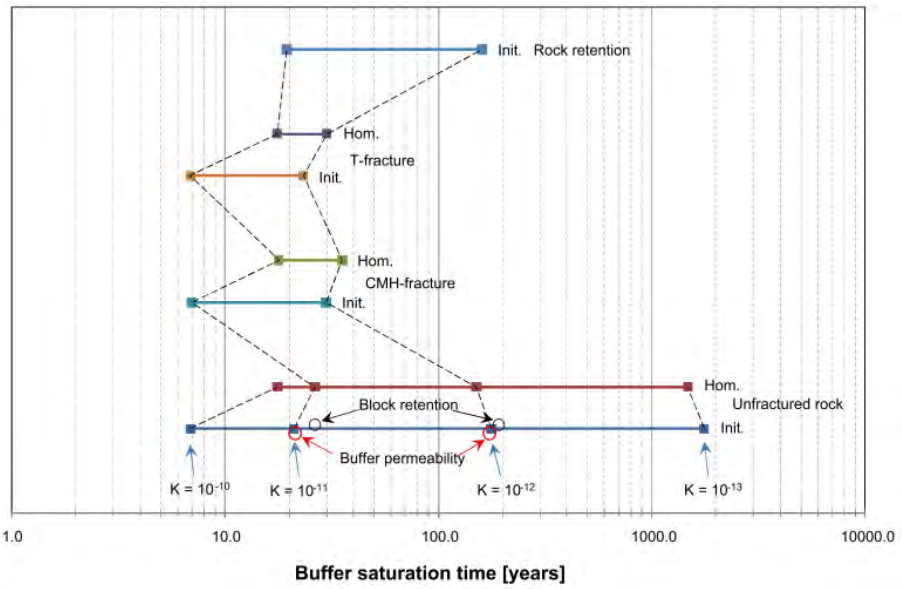

Figure 2-5: Compilation of buffer resaturation times for the range of resaturation scenarios considered in the SKB 2D TH modelling (from Åkesson et al., 2010). The results cover a range of rock conductivities (indicated by the dashed lines) assuming initial state or homogenised material properties.

In response to requests for more information from SSM, SKB undertook further 3D HM modelling to investigate rates of resaturation in dry deposition holes with point inflows (Börgesson et al., 2013). This subsequent modelling suggested that significant resaturation in such cases could take several 1 000s of years and that > 0.99 saturation throughout the buffer was not necessarily achieved in this time. The modelling in Åkesson et al. (2010) also considered cases in which resaturation was from the rock matrix only. In these cases, resaturation times of up to 1 500 y were seen in the lowest rock hydraulic conductivity cases that were assumed (Figure 2-5). In Börgesson et al. (2013) it is argued that this provides an upper bound on the longest time scales for resaturation because resaturation from the rock matrix is expected in all cases, so that the slowest point inflows will be overtaken by the homogeneous wetting from the rock that occurs simultaneously. The analysis suggests that uneven wetting of the buffer will only arise if the point inflow rate (into an empty deposition hole) is greater than $5\ 10^{-6}$ L/min. Further, the analysis also suggests that for point inflow rates greater than 10^{-3} L/min, the pellet region will be filled, leading to a uniform resaturation in the bentonite rings. SKB therefore suggest that uneven wetting should only occur for point inflows with rates between these values and states that around 1 in 14 deposition holes are expected to have inflows in this range. SKB noted that the hydraulic model for the dry pellet infilling in these models was not verified or calibrated.

2.2. Alternative Fracture Flow Models

The review by Black (2012) of hydrogeological models for Forsmark analysed the results of packer test experiments at the site and concluded that fracture flows in the host rock are likely to occur in channels rather than in homogeneously flowing fractures. Geier (2018) estimates flowing channels within a fracture could have widths on the order of 10 cm and spacings on the order of 1-2 m. The dimensions mean that a possible scenario is that a single channel intersects a deposition hole but that it does not intersect the full circumference of the deposition hole, leading to a non-axisymmetric pattern of resaturation. Geier (2018) also suggests that a reasonable approach to estimating channel transmissivity is to multiply the fracture transmissivity by the ratio of channel spacing to channel width. This effectively focusses the flow into the channels so that the rate of water flow through the fracture plane is preserved.

2.3. Alternative Conceptual Models of Bentonite Hydraulic Processes

Since the modelling in Åkesson et al. (2010) was undertaken, some alternative conceptual models of hydraulic processes in bentonite have been proposed. The review by Åkesson (2013) of modelling tasks undertaken within the FEBEX project summarises three such alternatives:

- The threshold gradient conceptual model, which assumes there is a critical hydraulic gradient below which flow does not occur; there is also a higher hydraulic gradient above which Darcy's Law is valid. This model would suggest that water flows in bentonite cease whilst hydraulic gradients remain, and the bentonite doesn't reach full saturation.
- The thermo-osmosis conceptual model, which assumes that a temperature gradient can cause liquid fluid flow from hotter towards colder regions in the bentonite. This model suggests that whilst a thermal gradient exists, the bentonite may not fully resaturate.
- The micro-fabric evolution conceptual model, which assumes that most water that enters bentonite is held within micro-pores and causes swelling which reduces the hydraulic conductivity. This model would suggest a slower water uptake, but that the bentonite does eventually resaturate fully.

2.4. Scenarios Considered

The modelling undertaken in this study seeks to explore some of the uncertainties that are present in the earlier modelling in Åkesson et al. (2010) and Börgesson et al. (2013). Specifically, it attempts to:

- Investigate some possible patterns and rates of buffer resaturation for realistic fracture flow geometries and transmissivities,

- Analyse the effect of alternative conceptual models for hydraulic processes in the buffer,
- Evaluate plausible loading patterns on the canister, and
- Consider the effect on resaturation behaviour of the use of alternative bentonite materials.

A comprehensive investigation of all possible combinations of these uncertainties is not possible in the current project, so a limited number of illustrative variations on a common base case have been considered. More information on the precise details of the various cases run are given in Section 4.

All of the scenarios that are considered assume the case of a dry deposition hole in which all resaturation is from a single fracture that intersects the deposition hole perpendicular to the canister axis at the canister mid-height. No resaturation from the tunnel is assumed. Therefore, all of the cases that are investigated are variants of the CMH scenario considered in SKB (2010). For simplicity, the tunnel volume is not considered in the simulations. Adding the tunnel would act to further prolong the resaturation time as water would be lost from the buffer to the tunnel backfill.

The initial scenario considered will be that of a uniformly flowing fracture intersecting the deposition hole, as sketched in Figure 2-6. If it is assumed that there is a negligible drop in fracture porewater pressure around the buffer, which would imply that the fracture is sufficiently transmissive to rapidly resupply the fracture with water lost to the buffer during the resaturation period, the rates of water uptake will be identical along the length of the intersection and the case can be approximated by the 2D axisymmetric geometry shown in Figure 2-7. The flow in the fracture need not be modelled explicitly. Instead it can be approximated by a boundary condition that accounts for the fracture transmissivity, given a reference porewater pressure and location in the fracture (Section 3.5).

The uniformly flowing fracture scenario is analogous to the 2D CMH scenario considered in Åkesson et al. (2010).

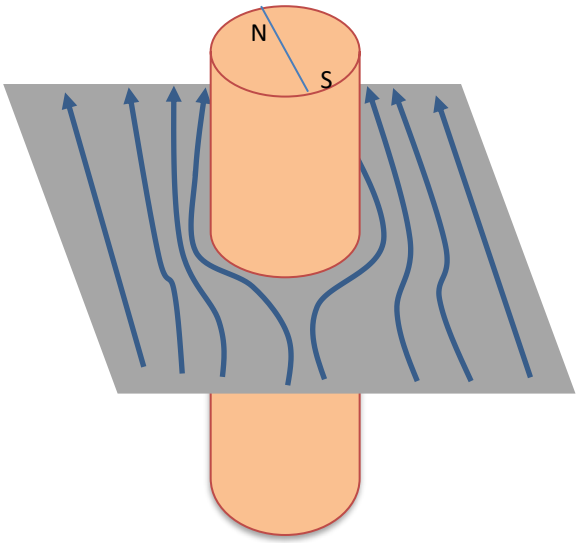

Figure 2-6: Uniformly flowing fracture scenario. (Flow arrows show expected flow direction after buffer resaturation. During resaturation, flows will be towards the buffer).

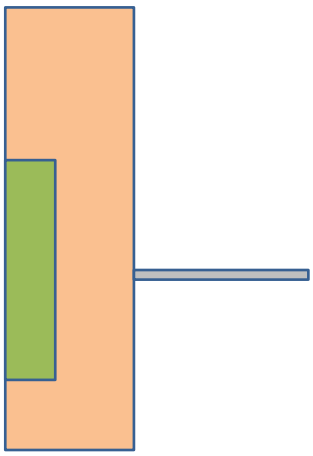

Figure 2-7: 2D axisymmetric geometry used to model the uniform flowing fracture case.

When it is assumed that impermeable fault breccia, or other infilling material, is present in the fracture, heterogeneous flow channels will develop. If the average width of the channels is much greater than the deposition hole diameter, then the flow geometry would continue to resemble that depicted in the uniformly flowing fracture scenario (Figure 2-6), although the focussing of flows towards the deposition hole may be more limited due to the narrower catchment area. Due to the large suction of the unsaturated bentonite, it is likely that water uptake by the buffer would continue to be uniform along the length of the fracture intersection, and so the only difference to the uniform fracture case may be that the fracture appears less transmissive due to the reduction in catchment area. Therefore, this scenario is likely to be bounded by considering a range of fracture transmissivities in the uniformly flowing fracture scenario.

When smaller flow channels that are narrower than the deposition hole diameter are present (which is likely, see Section 2.2), there is a possibility the deposition holes will be located to interrupt the channel pathway, as sketched in Figure 2-8. In this case, flows along the channel are disconnected and water inflows to the buffer are from line sources on the buffer surface.

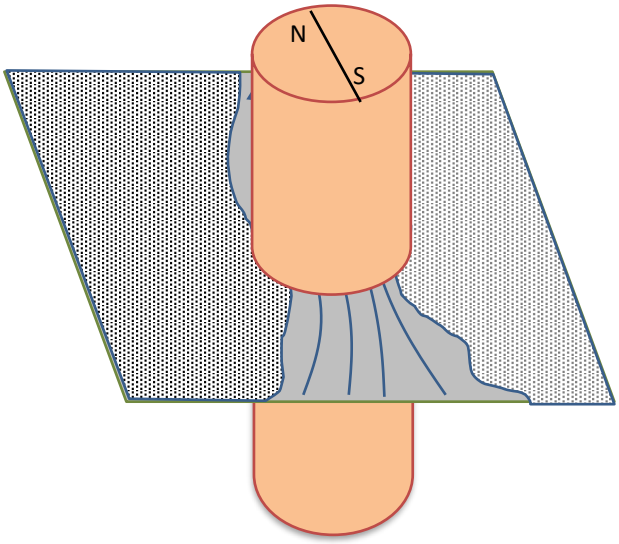

Figure 2-8: Disconnected channelled flow scenario.

This disconnected channel flow scenario is not axisymmetric. Patterns of resaturation will evolve three dimensionally, spreading vertically and circumferentially in the buffer from the intersection with the fracture. The scenario therefore requires to be modelled in 3D. If it is assumed that upstream/downstream rates of resaturation are similar (meaning that there is still a supply of water to both north and south sides of the buffer, as depicted in Figure 2-8), then the system can be approximated with a 3D quadrant geometry (e.g. the NE quadrant, with a water supply near the north corner). If it is assumed that the disconnection of the channel prevents the supply of water to one side of the buffer, then a semi-circular 3D geometry (e.g. east half) can be used to model the system, with a water supply near only one of the north or south corners.

In common with the uniformly flowing fracture case, rates of resaturation in the disconnected channelled flow scenario will be dependent upon the fracture transmissivity, but will also depend on the width of the channel since this will control the degree to which the flow of water must spread circumferentially. For very narrow channels, the resaturation will be similar to that from a point source (as was considered in Börgesson et al., 2013).

If the channel separation is sufficiently large, there is a chance of a grazing channel intersection with the buffer, as shown in Figure 2-9. The likelihood

of such a system arising would depend on the distributions of channel separations and widths. Geier (2018) suggests channels could be 10 cm wide and 1-2 m apart and so it is possible that channels will graze the deposition hole. Since the buffer intersects with the edge of the channel, there is also a chance that the intersection could be with a stagnant region within the channel, which could further limit rates of water uptake. Compared to the disconnected channel scenario (Figure 2-8), longer resaturation times are anticipated, since water must migrate 180° around the canister (although the case is similar to the disconnected channelled fracture case if it is assumed that the disconnection cuts-off the supply of water to one side of the buffer).

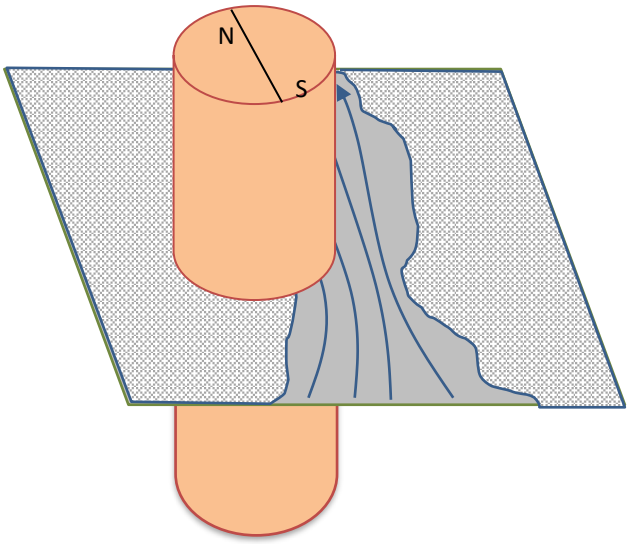

Figure 2-9: Grazing channelled flow scenario.

If symmetry is assumed, a 3D semi-circular geometry can be used to approximate the system (e.g. be made by assuming symmetry along the east-west axis in Figure 2-9). If the intersection between the channel and the buffer is small, the system can be simulated by a point source (like that considered in Börgesson et al., 2013).

For each of the three fracture geometry scenarios, the resaturation behaviour from fractures of varying transmissivities will be investigated. Additionally, the effect of the alternative conceptual models for hydraulic processes in the buffer (Section 2.3 of this report), and the possible use of alternative bentonite materials, will be considered.

2.5. Key Outputs

The outputs of the modelling can be related directly to safety function indicator criteria specified for the buffer safety functions (Table 2-1). The safety criteria as written in SKB (2011) assume that the buffer is sufficiently homogenised that the criteria are met everywhere. One aspect of the modelling is to investigate the extent to which it may be possible to satisfy the criteria within a region of the buffer (e.g. a saturated region), whilst failing to meet the criteria in another (e.g. a partially saturated region). The duration of any

such inconsistency will determine whether there are likely to be any potential implications on the intended performance of the buffer.

Table 2-1: Summary of safety functions, safety function indicators and associated criteria for the buffer (SKB, 2011).

Safety Function	Safety Function Indicator	Safety Function Indicator Criterion
Buff1: Limit advective transport	• Hydraulic conductivity • Swelling pressure	• $< 10^{-12}$ m/s • > 1 MPa
Buff2: Reduce microbial activity	Density	High
Buff4: Resist transformation	Temperature	$< 100°C$
Buff5: Prevent canister sinking	Swelling pressure	> 0.2 MPa
Buff6: Limit pressure on canister and rock	• Swelling pressure • Temperature	• < 15 MPa • $> -4°C$

In addition to the outputs to test adherence to the safety function criteria, model outputs will be reported to allow the mechanical influence of the bentonite swelling on the copper overpack to be considered. Stress gradients along the canister length that could potentially contribute to copper creep processes (Segle, 2015) can be reported directly from THM models. From TH models, the gradient of suction along the canister surface can be reported as a proxy measure. The duration of any such gradient will be a key factor in determining whether any gradients that develop could potentially affect performance.

The rate of water uptake is not directly needed to analyse the safety function criteria or the potential for creep on the canister surface, but may be interesting in distinguishing the effect of the alternative bentonite hydraulic models.

The key outputs that from the modelling include both transient quantities that evolve as the buffer resaturates and quantities associated with the steady state that is ultimately reached.

Outputs will include:

- Time to reach steady state / saturated state;
- The change in saturation at key locations (Figure 2-10) throughout the buffer as a function of time;
- The peak temperature in the buffer as a function of time;
- The suction along the canister (TH calculations);
- The radial stress acting along the canister (THM calculations);
- The bentonite density throughout the buffer at steady state (THM calculations).
- The rate of uptake of water as a function of time.

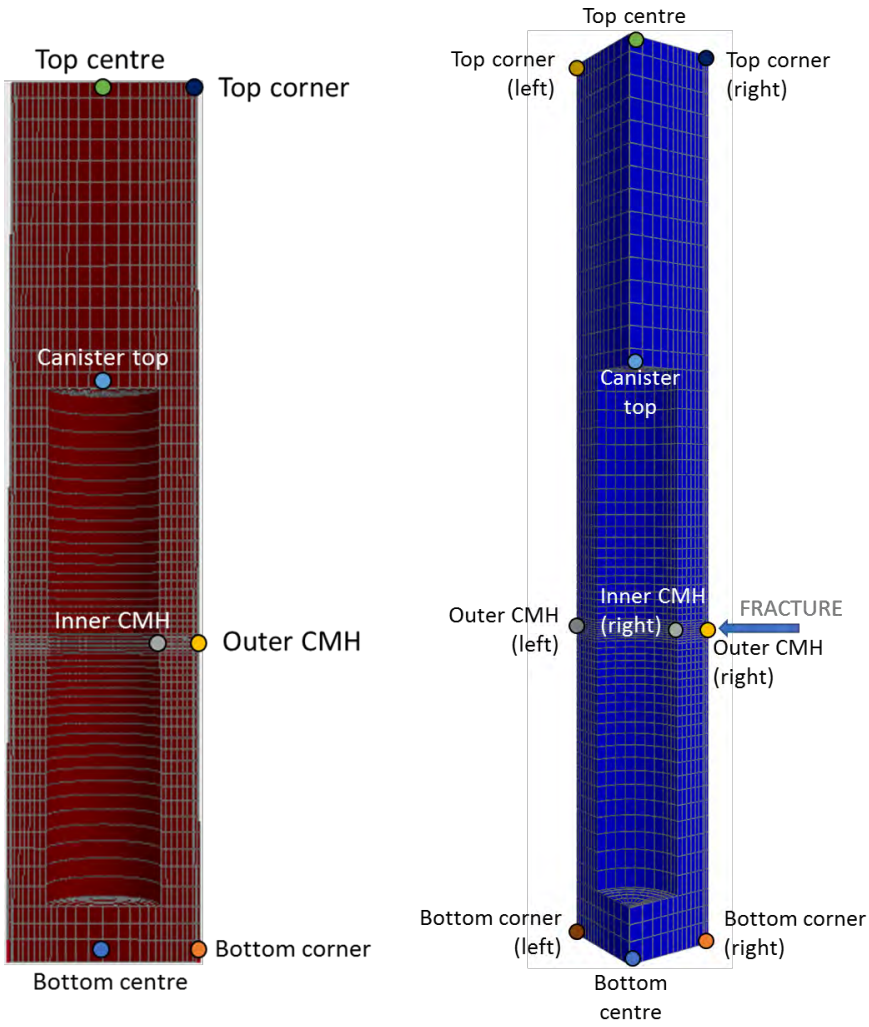

Figure 2-10: Output locations for saturation and water pressure results for the uniform flowing fracture cases (left) and the disconnected channel flow cases (right).

3. Model Descriptions

3.1. Processes Considered

Bentonite emplaced within a deposition hole is affected by thermal, hydraulic, mechanical and chemical processes. Chemical processes are expected to occur as the bentonite equilibrates with the inflowing groundwater, which can potentially impact upon bentonite physical properties, but these are not considered in this work. Thermal processes arise due to the heat generated by radioactive decay from the local waste canister and from the waste canisters in the wider disposal facility. Hydraulic processes arise due to water flowing into the bentonite from the surrounding granite. Mechanical processes arise due to heating of the bentonite and water within the bentonite and also due to bentonite swelling as it resaturates. The relationships between the thermal, hydraulic and mechanical processes occurring within the bentonite are shown in Figure 3-1.

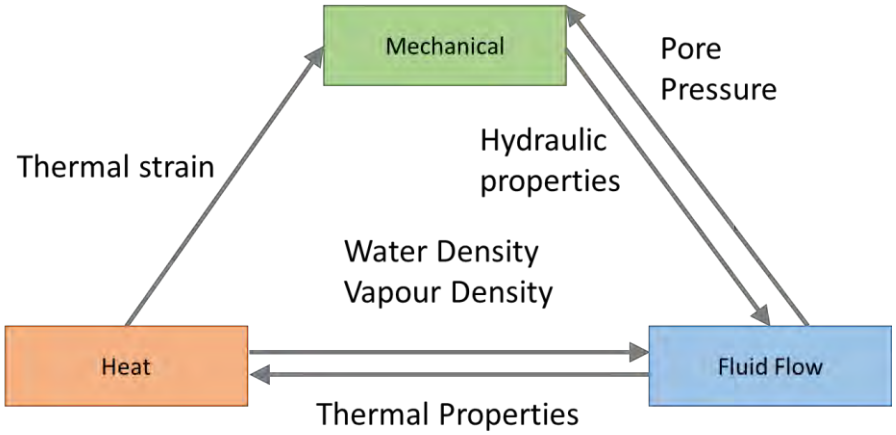

Figure 3-1: Conceptual diagrams of process couplings.

Heat moves around the system by thermal conduction (convection is assumed to be insignificant due to the low permeability of the bentonite). The thermal diffusivity of the bentonite is dependent upon the saturation of the bentonite and hence the thermal problem is coupled to the hydraulic problem through the thermal properties of the bentonite.

The fundamental physics / chemistry of the driving forces for water flow through bentonite are currently not well understood, but a reasonable approximation to observed behaviour is to assume that liquid flow is driven by gradients in water pressure and that vapour flow is driven by gradients in vapour density (alternative conceptual models are considered – see Section 2.3). Water pressure depends upon water density, and both water density and vapour density depend on temperature, hence the hydraulic problem is coupled to the thermal problem through the density. Water flow also depends

upon the hydraulic properties of the bentonite, and in this model, the hydraulic conductivity and porosity depend on strain in the bentonite, hence coupling the mechanical deformation to the hydraulic problem.

The mechanical behaviour of bentonite is generally represented using equations to describe the elastic and plastic response of bentonite to stresses. There is no single accepted model of the mechanical behaviour of bentonite. Many models are based on the Modified Cam Clay model (Roscoe and Burland 1968) and the Barcelona Basic Model (Alonso et al. 1990) and customised to individual requirements. The model used in this work is based on the MCC model (Thatcher et al 2016) and represents swelling of bentonite as the water content of the bentonite increases as well as volumetric changes due to heating.

There is significant computational overhead in solving the coupled system of equations as described above, so to improve efficiency and allow a wider variety of cases to be considered, some simpler models have been considered alongside the fully coupled THM models. These simpler models include only thermal and hydraulic processes (TH) as shown in Figure 3-2. The implications of this modelling decision will be discussed in Section 6.

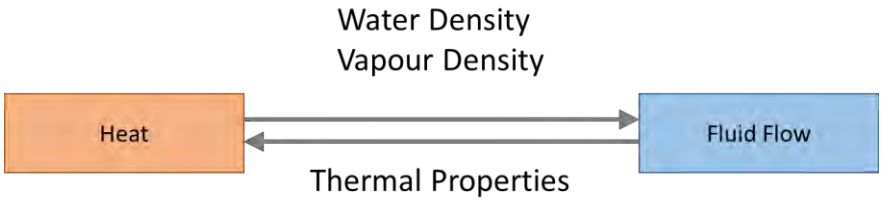

Figure 3-2: Conceptual diagram of process couplings for TH models.

3.2. Mathematical Model

The mathematical model described below has been implemented in QPAC (Quintessa, 2013), Quintessa's in house modelling software.

3.2.1. Thermal

The conservation of heat and movement of heat through the system is represented by thermal conduction through the diffusion equation:

$$\rho_{bulk} c_p \frac{dT}{dt} - \nabla \cdot (\lambda \nabla T) = 0$$

where T is temperature [K], t is time [y], ρ_{bulk} is bulk density [kg/m^3], c_p is specific heat capacity [J/kg/K] and λ is thermal conductivity [W/m/K].

Bulk density is coupled to the mass based water content through the equation:

$$\rho_{bulk} = \rho_g (1 - \varphi)(1 + \omega)$$

where ρ_g is grain density [kg/m^3], φ is porosity [-] and ω is mass based water content [-] and thermal conductivity is related to water saturation by the following equations (Åkesson et al., 2010):

$$\lambda = \begin{cases} {\lambda_{sat}}^{\theta^{0.5}} {\lambda_{dry}}^{(1-\theta)^2} & \text{for bentonite blocks} \\ \lambda_{sat}\theta & \text{for bentonite pellets} \end{cases}$$

where λ_{sat} is saturated thermal conductivity [W/m/K], λ_{dry} is thermal conductivity of dry bentonite [W/m/K] and θ is saturation [-].

There are two sources of heat in the model, one is the canister boundary conditions (see Section 3.5), and the other is a source due to canisters in surrounding deposition holes. This second heat source has been added into the temperature calculation such that:

$$T = T_{local} + T_{background}$$

and $T_{background}$ is taken from Åkesson et al. (2010), see Figure 3-4.

3.2.2. Hydraulic

Water flow through the system is represented by Richards' equation, which combined with conservation of mass gives the equation:

$$\frac{d}{dt}(\varphi\rho_w\theta) = \nabla.\left(\frac{\rho_w k}{\mu}\nabla(P + \rho_w g z)\right)$$

where ρ_w is density of water [kg/m^3], k is permeability [m^2], μ is the viscosity of water [Pa.s], P is water pressure [MPa], g is acceleration due to gravity [m/s^2] and z is height [m].

Permeability is composed of an intrinsic permeability (k_i[m^2]), which depends on porosity via the Kozeny-Carman equation, and a relative permeability (k_r[-]) that depends on saturation as follows:

$$k = k_i k_r$$

$$k_i = k_0 \cdot \frac{\varphi^3}{(1-\varphi)^2}\frac{(1-\varphi_0)^2}{{\varphi_0}^3}$$

$$k_r = \theta^3$$

where k_0 is the initial permeability [m^2] which corresponds to the initial porosity, φ_0 [-].

Water pressure is calculated as the difference between gas pressure (held constant at 0.1 [MPa]) and suction. For the TH model, suction is defined by a van Genuchten curve

$$\Psi = P_0\left(\theta^{-1/\xi} - 1\right)^{1-\xi}$$

where Ψ is suction [MPa], P_0 [MPa] and ξ [-] are constants. For the THM model, suction is related both to water content and to stress, as explained in Section 3.2.4.

3.2.3. Mechanical

The mechanical problem is expressed in terms of conservation of momentum, which is otherwise referred to as the Navier equation (Howell et al. 2009):

$$\rho_{bulk}\frac{\partial^2 \bar{u}}{\partial t^2} = \nabla\bar{\bar{\sigma}} - \rho_{bulk} g$$

where $\bar{u}$ is the displacement vector [m], $\bar{\bar{\sigma}}$ is the stress tensor [MPa]. The stress vector assumes a pseudo steady state and is given by:

$$\bar{\sigma} = \bar{\bar{S}}(\bar{\varepsilon} - \bar{\gamma}) - P$$

where $\bar{\bar{S}}$ is the elastic stiffness matrix [MPa], $\bar{\varepsilon}$ is the strain vector [-] and $\bar{\gamma}$ are additional strains [-], e.g plastic strain and swelling strain. P is water pressure, but in this work, water pressure is nearly always negative as the bentonite is in suction, so P is set equal to zero.

For this application, an isotropic elastic stiffness matrix is used whereby

$$\bar{\bar{S}} = \begin{bmatrix} \Lambda+2\tau & \Lambda & \Lambda & 0 & 0 & 0 \\ \Lambda & \Lambda+2\tau & \Lambda & 0 & 0 & 0 \\ \Lambda & \Lambda & \Lambda+2\tau & 0 & 0 & 0 \\ 0 & 0 & 0 & 2\tau & 0 & 0 \\ 0 & 0 & 0 & 0 & 2\tau & 0 \\ 0 & 0 & 0 & 0 & 0 & 2\tau \end{bmatrix}$$

Where $\Lambda = n * E/(1+n) * (1-2n)$ and $\tau = E/(2(1+n))$, E [MPa] is Young's Modulus and n [-] is Poisson's ratio. Poisson's ratio is a constant and Young's Modulus is dependent on the average effective stress (κ_0 and κ_1 are constants):

$$E = \kappa_0 + \kappa_1\left[\frac{1}{3}(\sigma'_{ii} + \sigma'_{jj} + \sigma'_{kk})\right]$$

For bentonite subjected to heating, it is assumed that there are three additional sources of strain: thermal expansion, swelling strains due to changes in water content of the bentonite; and plastic strains due to plastic failure of the bentonite. Swelling strains are discussed later as they are coupled to the hydraulics.

Thermal strains are given by:

$$\varepsilon^T_{nn} = \alpha_T(T - T_0)$$

where α_T is the linear coefficient of thermal expansion and T_0 is the initial temperature.

Plastic strains are calculated according to the MCC model (Roscoe and Burland 1968). The plastic yield surface is given by:

$$\left[\frac{q}{M}\right]^2 + p'\,(p' - p_c) = 0$$

whilst the virgin consolidation line in the MCC model, which describes how the yield surface changes with stress, has the equation:

$$v = \Gamma - \lambda \ln p'$$

where v [-] is the specific volume ($v = 1 + e$, where e [-] is the void ratio), p' [MPa] is the effective confining stress, q [MPa] is deviatoric stress, p_c [MPa] is the pre-consolidation pressure (which is a point on the virgin consolidation line) and M, Γ and λ are all constant parameters. The plastic strain is calculated as the derivative of the plastic yield surface.

3.2.4. Coupling

Coupling between the hydraulic and mechanical models is expressed through the dependence of porosity on strain, through the dependence of suction on stress, through swelling dependent upon water content and through the observation that suction, swelling pressure and plastic failure can all be expressed as a function of dry density with only two independent parameters (Thatcher et al, 2016). This model has been named the Internal Limit Model (or ILM).

Porosity as a function of strain is given by:

$$\varphi = 1 - \frac{V_0(1 - \varphi_0)}{V}$$

where V_0 is the initial compartment volume [m^3] and V is the current compartment volume [m^3].

Suction as a function of stress is given by the equation (Dueck, 2005):

$$\Psi = \Psi^{free} - 1/3(\sigma_{ii} + \sigma_{jj} + \sigma_{kk})$$

where Ψ^{free} is the unconfined suction for a given dry density of bentonite.

Swelling strain is calculated in the three principal directions as follows:

$$\varepsilon_{nn}^{swell} = \frac{a}{3}\,\frac{(\omega_{nn} - \omega_0)m_s}{\rho_w V_{comp}}$$

where ω_0 is the initial water content (kg/kg), ω_{nn} is the water content in direction nn, m_s is the mass of solids (kg), ρ_w is the density of water (kg/m^3), V_{comp} is the compartmental volume (m^3) and a is a swelling efficiency term which reflects that not all additional water will cause a volume increase, some will just fill void space in the sample. Directional water content is not a standard idea, but has been used in this model, based on the conceptual idea that bentonite grains aligned in different orientations relative to the stress field will be able to take up different amounts of water.

Unconfined suction is defined by a curve following the method of Thatcher et al (2016). The curve has the form

$$p = \alpha * exp(\beta \rho_{dry})$$

where p is energy density (interpreted as stress or suction) [MPa], ρ_{dry} is dry density [kg/m3] and α [MPa] and β [m^3/kg] are fitting parameters. For unconfined suction,

$$\Psi^{free} = p$$

but this same curve is also used in the model to define the virgin consolidation pressure:

$$p_c = p.$$

The parameters α and β can be determined by fitting the exponential equation to commonly available data such as swelling pressure versus dry density, the virgin consolidation line in oedometer tests or water retention data.

3.3. Geometry and Discretisation

The model has been set up to represent the bentonite within a deposition hole in the KBS-3V repository concept. Within the bentonite, thermo-hydraulic or thermo-hydro-mechanical equations are solved. The host rock around the bentonite is also represented in the model, but only thermal equations are solved there, since the rock is assumed to be rigid and have no water flow except in the location of the fracture, which is represented by a boundary condition.

This is a smaller modelling domain than that considered by Åkesson et al. (2010) who included water flow in the host rock in their model along with bentonite in the tunnel above the deposition hole. These elements have not been included in the current model since this modelling study is specifically focussed on resaturation from a single fracture in the deposition hole, and reducing the geometric complexity improves computational efficiency allowing more model runs to be carried out to examine the specific question.

In the Åkesson et al. (2010) work, there were three different types of bentonite within the deposition hole, bentonite rings around the waste canister, bentonite cylinders above and below the waste canister and bentonite pellets between the bentonite blocks and the host rock. In the current modelling, no distinction has been made between the bentonite rings and the bentonite cylinder, again to reduce complexity and allow the focus to be on the relevant question.

The geometry of the system as represented in the model is shown in Figure 3-3 and Table 3-1. THM equations are solved in a domain that represents the inside of the deposition hole, but in order to use appropriate thermal boundary conditions, thermal equations are also solved on a much larger domain representing the host rock.

The model has been implemented in QPAC. The grid discretisation has been tested for convergence.

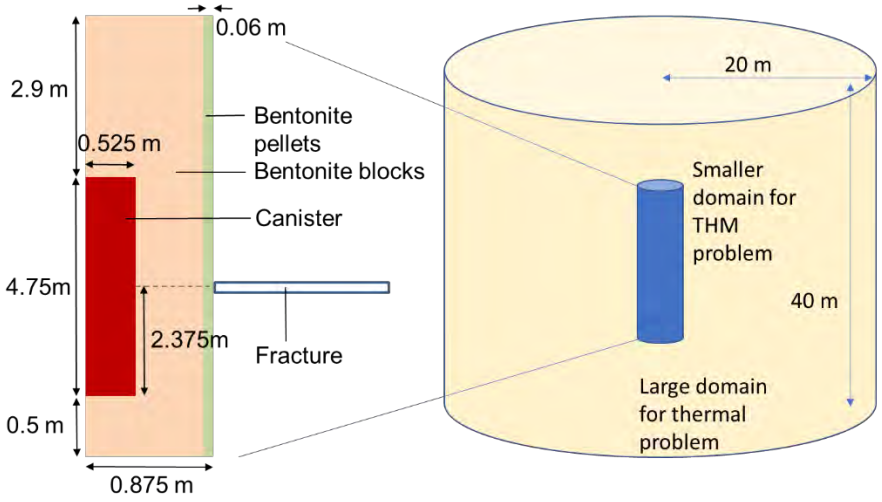

Figure 3-3: Geometry taken from Åkesson et al. (2010) and showing the relationship between the domain in which THM equations are solved and the domain in which T equations are solved.

Table 3-1: Geometry parameters (Åkesson et al., 2010).

Canister radius	0.525 m
Canister length	4.75 m
Deposition hole radius	0.875 m
Length of bentonite buffer	8.15 m
Thickness of bentonite beneath canister	0.5 m
Outer radius of bentonite blocks	0.815 m
Radial width of bentonite pellets	0.06 m
Location of fracture (distance from base of buffer)	2.875 m

3.4. Initial Conditions

The initial temperature of the system is set at 15°C.

The initial water content of the bentonite is 0.17 in both the pellets and the bentonite blocks and from this and porosity, the initial saturation and initial water pressure are calculated.

For the THM model, the initial dry density of blocks is 1779 kg/m^3 and pellets are not represented as model convergence was not achieved for THM models with pellets.

3.5. Boundary Conditions

The heat from the radioactive decay in the canister is represented as a specified heat flux on the inner boundary of the bentonite buffer. The heat power (W) varies with time according to the following decay law:

$$P(t) = P_0 \sum_{i=1}^{i=7} a_i exp\left(\frac{-t}{t_i}\right)$$

where P_0 is the initial canister power, equal to 1700 W (Åkesson et al., 2010). The parameters a_i (-) and t_i (y) depend on the isotopes which are present. These are given in Table 3-2. Power is applied to the surface area of canister (including ends).

Table 3-2: Parameters used to specify the heat power of the canister (Åkesson et al., 2010).

i	t_i	a_i
1	20	0.060
2	50	0.705
3	200	-0.055
4	500	0.250
5	2 000	0.025
6	5 000	-0.009
7	20 000	0.024

The remaining temperature boundaries (at the outer edge of the host rock – see Figure 3-3) are assumed to be at a constant temperature of 15°C.

Hydraulic boundaries are all no flow boundaries apart from at the location of the fracture. The fracture is represented by a flux boundary condition, where the flux is dependent upon the fracture transmissivity and a nominal head gradient in the fracture:

$$q = 2\pi r F \frac{P - P_0}{dg}$$

where r is the radius of the deposition hole [m], F is the fracture transmissivity [m^2/y], P_0 is a reference pressure equal to hydrostatic pressure (4.4 [MPa]) and d is a reference distance equal to 10 [m]. Geier (2018) estimated that around a deposition hole water pressure in fractures would be hydrostatic within a few meters. When representing channelled fractures, the transmissivity of the channel is scaled such that the overall fracture plane transmissivity does not change (see Section 4.5).

The mechanical boundary conditions are all roller boundaries (zero displacement normal to the boundary), except at the top and bottom of the canister

where a small amount of displacement (< 1mm) is allowed before the boundary condition becomes very stiff.

3.6. Parameter values

Material properties are given in Table 3-3. Note that in the rock, only thermal equations are solved. For the THM calculations, only blocks are assumed to be present. In the THM calculations an alternative porosity is used for the bentonite blocks to represent the average porosity of the blocks and pellets in the deposition hole. This assures that the stresses calculated by the model are reasonable.

Table 3-3: Parameters for representing materials.

Parameter	Value			Reference
	Blocks	Pellets	Rock	
Thermal Properties				
Specific heat capacity [J kg^{-1} K^{-1}]	800	800	770	Åkesson et al., 2011 Tables 3-1, 3-3
Grain density [kg m^{-3}]	2780	2780	2277	Åkesson et al., 2011 Tables 3-1, 3-3

Thermal conductivity [W m^{-1} K^{-1}]	Dry 0.33 Wet 1.3	Dry 0 Wet 1.3	2.8	Åkesson et al., 2011 Table 3-3 (pellets), Figure 3-20 (Blocks)
Hydraulic Properties				
Intrinsic Permeability [m^2]	1.2 x 10^{-21}	5.2 x 10^{-19}	N/A	Åkesson et al., 2011 Table 3-1 & 16-3 (cylinder)
Porosity [-]	0.36 (0.44 for THM)	0.61	N/A	Åkesson et al., 2011 Table 3-1
Suction – van Genuchten parameters (TH)	P_0 67.2 [MPa] λ 0.48 [-]	P_0 0.508 [MPa] λ 0.26 [-]	N/A	Åkesson et al., 2011 Table 3-1 & 16-3 (cylinder)
Vapour Diffusivity [m^2/s]	2 x 10^{-6}	2 x 10^{-6}	N/A	Claesson and Sällfors, 2004
Mechanical Properties				
Bulk modulus at zero stress [MPa]	50	N/A	N/A	From fit to oedometer data
Bulk modulus scaling factor	30	N/A	N/A	From fit to oedometer data
Poisson Ratio [-]	0.2	N/A	N/A	Table 7-1 in Åkesson et al., 2011
Coefficient of thermal expansion [K-1]	6.7E-5	N/A	N/A	Tang et al., 2008
Plastic rate [MPa^{-1} y^{-1}]	1 x 10^{-3}	N/A	N/A	Thatcher et al., 2016
M	1.25	N/A	N/A	From fit to oedometer data
ILM				
Alpha	3.69E-4	N/A	N/A	See below
Beta	6.25	N/A	N/A	See below

The heat source from surrounding canisters is represented as a time dependent temperature effect at the local deposition hole (Figure 3-4).

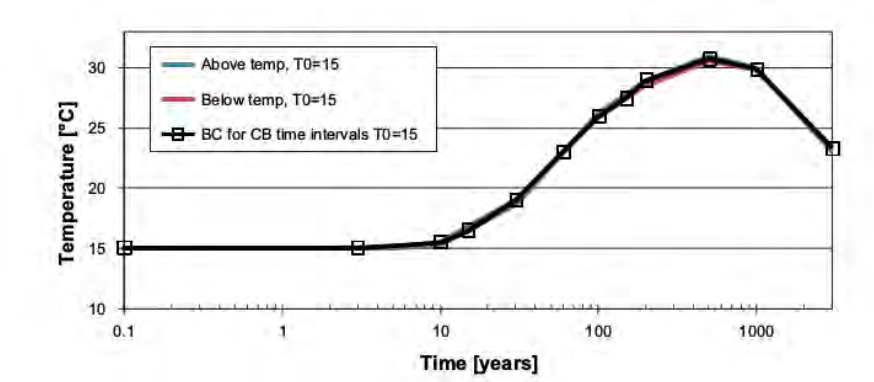

Figure 3-4: Temperature profile at a local waste canister reflecting heating from surrounding waste canisters (Åkesson et al., 2010). The temperature increase above 15°C is used as the background temperature increase in the model.

Parameters alpha and beta for the ILM model can be derived by fitting an exponential curve to any one dataset of information either on swelling pressure versus dry density, plastic failure in an oedometer test or water retention data. Here alpha and beta have been calibrated to swelling data (Villar, 2005: Figure 3-5).

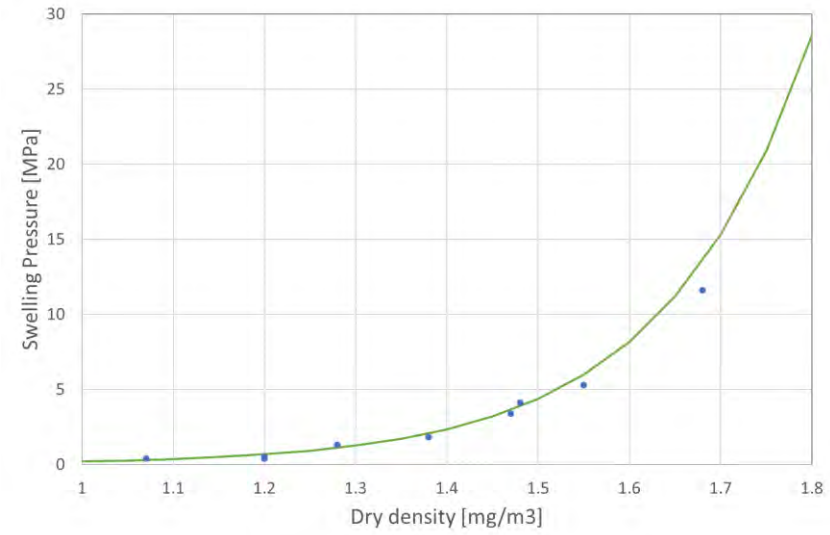

Figure 3-5: ILM curve calibrated to swelling pressure data Villar (2005).

4. Simulation Cases

The simulation cases that have been considered are listed in Table 4-1 with further details of the models given in subsequent sections.

Table 4-1: Simulation cases considered: UFF – Uniformly Flowing Fracture; DCF – Disconnected Channel Fracture; GCF – Grazing Channel Fracture; DF – Darcy Flow; TG – Threshold Gradient; TO – Thermo Osmosis; MF – Micro-Fabric Evolution; HI – High Inflow; LI – Low Inflow; TH – Thermo-Hydraulic; THM – Thermo-Hydro-Mechanical.

Name	Model components
Case_0	**Base cases testing impact of pellets and including mechanics in the model**
Case_0a	UFF_DF_HI_TH
Case_0b	UFF_DF_HI_TH_NoPellet
Case_0c	UFF_DF_HI_THM_NoPellet
Case_1	**Flow rate in the fracture**
Case_1a	UFF_DF_LI_TH
Case_1b	UFF_DF_LI_THM_NoPellet
Case_2	**Threshold gradient flow model**
Case_2a	UFF_TG_HI_TH
Case_2b	UFF_TG_HI_THM_NoPellet
Case_3	**Thermo-osmosis model**
Case_3a	UFF_TO_HI_TH
Case_3b	UFF_TO_HI_THM_NoPellet
Case_4	**Micro-fabric evolution model**
Case_4a	UFF_MF_HI_TH
Case_4b	UFF_MF_HI_THM_NoPellet
Case_5	**Disconnected channel fracture**
Case_5a	DCF_DF_HI_TH_NoPellet
Case_6	**Disconnected channel fracture flow rate**
Case_6a	DCF_DF_LI_TH_NoPellet
Case_7	**Glancing channel fracture**
Case_7a	GCF_DF_HI_TH_wide_NoPellet
Case_7b	GCF_DF_HI_TH_point_NoPellet
Case_8	**Glancing channel fracture flow rate**
Case_8a	GCF_DF_LI_TH_wide_NoPellet

Case_8b	GCF_DF_LI_TH_point_NoPellet
Case_9	**Alternative bentonite**
Case_9a	UFF_DF_HI_TH_NoPellets_FEBEX
Case_9b	UFF_DF_HI_THM_NoPellets_FEBEX

4.1. Case 1 - Flow rate in the fracture

There are a range of possible water inflow rates from the intersecting fracture. Case 1 aims to investigate the impact of varying this fracture flow rate on the resaturation of the bentonite. In the model, this is done by varying the fracture transmissivity (see Section 3.5).

The range of realistic fracture flow rates can be constrained by considering the fracture size, the criteria for siting deposition holes away from large fractures, and practical constraints on allowable inflows to deposition holes during canister emplacement. According to (Geier, 2018), the range of fracture transmissivities which correspond to fractures of a suitable size is approximately 1×10^{-12} m^2/s to
2.5×10^{-6} m^2/s. This can be further constrained by assuming that fractures with transmissivity higher than 10^{-7} m^2/s will have too high an inflow rate for practical emplacement of the buffer.

Upon implementation of the model, it was discovered that the permeability of the bentonite limits the maximum flow rate for fractures with high transmissivities (SKB refer to this as "chocking of inflow", Börgesson et al, 2013). Because of this effect, there is no difference in inflow for cases with fracture transmissivities higher than 1×10^{-10} m^2/s. Therefore, the minimum and maximum possible fracture flow rates correspond to fracture transmissivities of 1×10^{-12} m^2/s and 1×10^{-10} m^2/s.

The maximum fracture transmissivity has been used in Case 0 as a reference value. To test the impact of flow rates and provide bounds on the resaturation behaviour of the bentonite, the lower fracture transmissivity of 1×10^{-12} m^2/s has been used in variant Case 1.

This was implemented in both a TH and THM model for comparison (Case 1a and 1b respectively).

4.2. Case 2 - Threshold gradient flow model

The threshold gradient flow model is an alternative conceptual model for the hydraulic behaviour of the bentonite (Åkesson, 2013).

Darcy's law (a linear relationship between flux and hydraulic gradient) is generally only valid for low Reynolds numbers up to a critical pressure or hydraulic gradient. In the threshold gradient model, an additional lower limit

for the applicability of Darcy's law is proposed. This 'threshold gradient' must be exceeded before flow can be initiated.

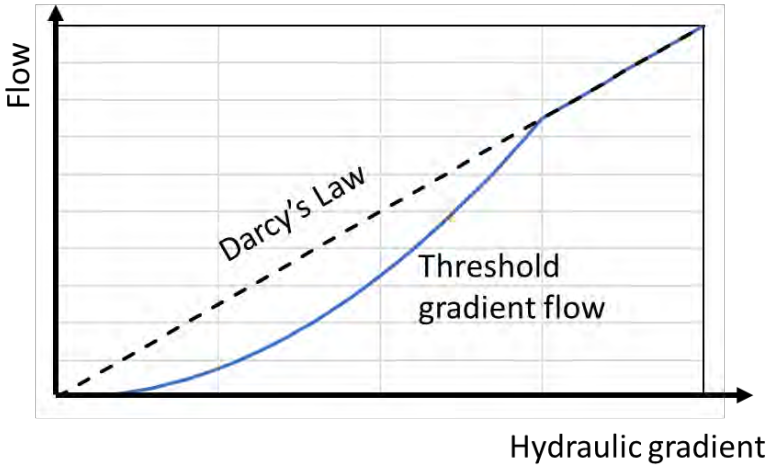

Figure 4-1: Threshold gradient concept.

For this variant model (Case 2), a threshold head gradient of 50 and a critical head gradient of 1500 were chosen. Below the threshold gradient, no flow is permitted. Above the critical gradient, the Darcy flow in the model is calculated as before. For simplicity, a linear scaling factor is used for gradients between the two limits.

Both TH and THM versions of this variant case were run for comparison (Case 2a and 2b).

4.3. Case 3 - Thermo-osmosis model

The thermo-osmosis model is another alternative hydraulic conceptual model that was tested. Thermo-osmosis is the fluid flow in a porous medium which is driven by a temperature gradient (Åkesson, 2013). To represent this effect in the QPAC model, an extra term must be added to the Darcy flow:

$$q = -\frac{k}{\mu}(\nabla P - \rho g \nabla z) - \boldsymbol{c\nabla T}$$

where c ($m^2/K/s$) is a constant. Here c is assumed to be equal to 2.73 x 10^{-13} $m^2/K/s$ (Åkesson, 2013) – this value is for FEBEX bentonite but is suitable to illustrate the effect of the thermo-osmosis process.

Both TH and THM versions of this variant case were run for comparison (Case 3a and 3b).

4.4. Case 4 - Micro-fabric evolution model

The micro-fabric evolution model is an alternative conceptual model based on a double porosity model of bentonite (Åkesson, 2013). The micro-fabric

evolution model attempts to represent physically the reduction in the effective hydraulic conductivity of the bentonite as the bentonite saturates. It assumes that most of the water that enters the bentonite is adsorbed into the micro-pores. The particles then swell and, since the bentonite is constrained, this reduces the size of the macro-pores and hence reduces the volume available for flow.

This process was represented in QPAC by multiplying the intrinsic permeability of the bentonite by a suction-dependent scaling factor. At high suctions of 17 MPa and above (corresponding to unsaturated bentonite), the intrinsic permeability is unaffected. At suctions less than 2 MPa, the intrinsic permeability is reduced to 15% of its original value (Åkesson, 2013). The scaling factor is linearly increased between these two points.

Both TH and THM versions of this variant case were run for comparison (Case 4a and 4b).

4.5. Case 5 - Disconnected channel fracture

The fracture geometry used in the base case assumes a uniformly flowing fracture which intersects the full width of the buffer. In reality, fracture flows in the host rock at Forsmark are likely to occur heterogeneously in channels (Black, 2012). One potential interaction between the buffer and a channelled fracture would be a disconnected fracture intersecting the middle of the buffer (see Figure 2-8). To be comparable with the base case, this fracture is also assumed to be at the canister mid-height, and to have the same aperture.

Using this geometry, the system is no longer axisymmetric as the fracture flow is not uniform around the buffer. A 3D QPAC model with angular discretisation is therefore required. However, assuming the upstream and downstream rates of resaturation are similar, symmetry arguments can be used to approximate the system with a 3D quadrant geometry (see Figure 4-2).

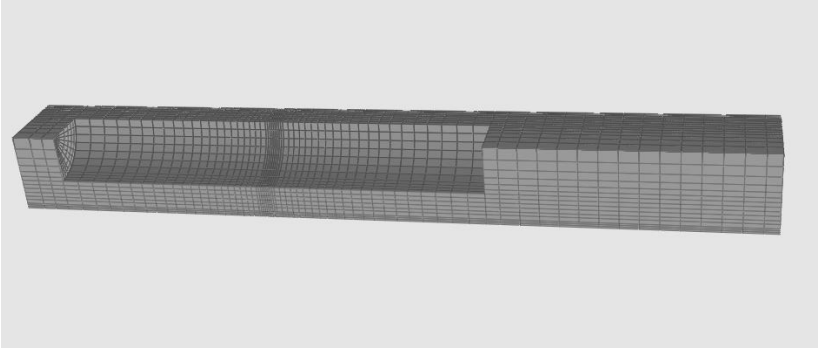

Figure 4-2: Image from QPAC showing the 3D quadrant geometry of the disconnected channel fracture model.

A likely channel width is around 10 cm and channel spacing is of the order of 1-2 m (Geier, 2018). The channel transmissivity can be calculated by multiplying the fracture transmissivity by the ratio of the assumed channel spacing to the channel width. In the QPAC model, the channel intersection is represented by a 5° wide compartment along the symmetry boundary, corresponding to a channel width of 15.2 cm. A channel separation of 2 m is assumed. With this spacing, only one fracture would be expected to intersect the buffer. This means that the channel transmissivity is approximately 13 times higher than the whole-fracture transmissivity.

4.6. Case 6 - Disconnected channel fracture flow rate

As with the uniformly flowing fracture, there is a range of potential channelled fracture transmissivities and hence a range of possible inflow rates. Using the same realistic fracture transmissivity range, and applying the scaling factor for channelled flow described in the previous section, gives a range of channelled fracture transmissivities from 1.3×10^{-11} to 1.3×10^{-9} m^2/s.

The maximum transmissivity was used in Case 5 as a reference value. The minimum transmissivity is tested in Case 6 for comparison.

4.7. Case 7 - Glancing channelled fracture

In variant Cases 7-8, another alternative fracture geometry is tested. In these cases, the channelled fracture intersects with the edge of the buffer rather than being completely disconnected by the buffer (see Figure 2-9). The other properties of the channelled fracture (including transmissivity and vertical thickness) are identical.

Using symmetry, a 3D semi-circular geometry can be used to approximate the system (Figure 4-3).

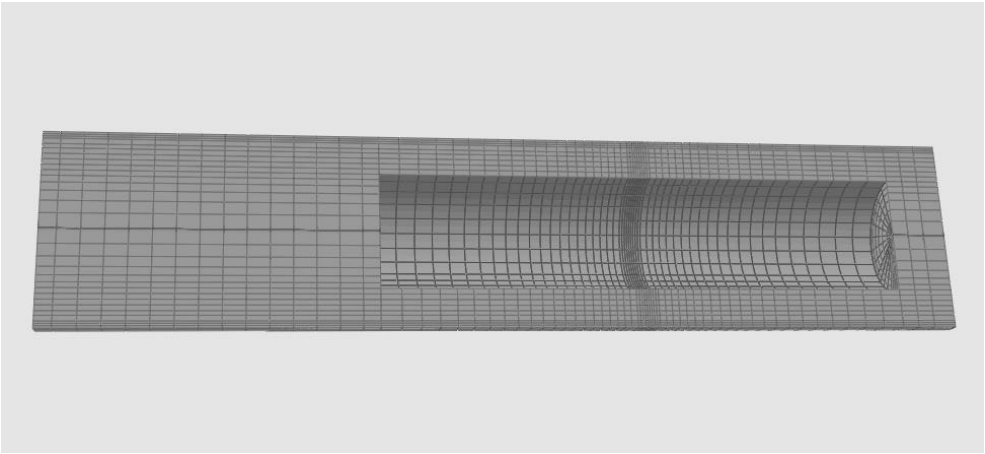

Figure 4-3: Water pressure gradient along the canister through time for Case 0b (base TH model without pellets).

In Case 7a, the channel intersection with the buffer is assumed to be represented by a 5° arc on the buffer surface to be consistent with the disconnected channelled fracture in Cases 5-6. In Case 7b a smaller channel intersection of 1° is modelled to approximate a point source (like that considered in Börgesson et al., 2013).

4.8. Case 8 - Glancing channelled fracture flow rate

For the wider glancing channelled fracture, the range of possible channel transmissivities (and hence possible flow rates) is the same as for the disconnected channelled fracture. The maximum transmissivity of 1.3 x 10^{-9} m^2/s is used in Case 7 and the minimum transmissivity of 1.3 x 10^{-11} m^2/s is used in Case 8 for comparison.

For the smaller 'point source' fracture, the channelled transmissivity is higher using the scaling factor described in Section 4.5. The maximum transmissivity is therefore 6.5 x 10^{-9} m^2/s and the minimum transmissivity is 6.5 x 10^{-11} m^2/s.

4.9. Case 9 - Alternative bentonite

The previous cases use MX-80 bentonite. In Case 9, the extent to which the behaviour is dependent on the type of bentonite is investigated. This was done by using a different bentonite – FEBEX (or Serrata) bentonite. FEBEX bentonite has a different chemistry to MX-80 bentonite, including a higher smectite content, which affects its properties. This alternative bentonite was chosen because data for FEBEX bentonite is widely available and the model used in this report has previously been tested successfully for this material.

Implementing this model required changes to many of the material parameters. The FEBEX bentonite parameters used are listed in Table 4-2. These are taken from Thatcher (2017). The MX-80 parameters from Table 3-3 are re-listed here for comparison. The initial conditions in terms of density and water content of the bentonite are kept the same to enable direct comparison of the two bentonites.

The thermal conductivity of FEBEX bentonite is given as:

$$\lambda_{FEBEX} = 1.3^{\theta^{0.5}} \cdot 0.7^{(1-\theta)^2}$$

Its intrinsic permeability has a different porosity dependence from that of MX-80 and is calculated as:

$$k_i = k_0 \exp(30\varphi - 0.4)$$

This variant case is implemented with both TH and THM processes (Case 9a and 9b). Pellets are omitted in both models to avoid the need for FEBEX pellet data and to directly compare the behaviour of the different bulk bentonites.

Table 4-2: List of FEBEX material parameters, with MX-80 parameters shown for comparison.

Parameter	Value	
	MX-80	**FEBEX**
Specific heat capacity [J kg^{-1} K^{-1}]	800	1100
Grain density [kg m^{-3}]	2780	2780
Initial permeability k_0 [m^2]	1.2 x 10^{-21}	2.5 x 10^{-21}
Reference Porosity φ_0 [-]	0.36	0.36
Suction – van Genuchten parameters (TH)	$P_{0,}$ 67.2 [MPa]	$P_{0,}$ 43.5 [MPa]
	λ, 0.48 [-]	λ, 0.38 [-]
Vapour Diffusivity [m^2 s^{-1}]	2 x 10^{-6}	2.5 x 10^{-6}
Bulk modulus at zero stress [MPa]	50	100
Bulk modulus scaling factor [-]	30	30
Poisson's Ratio [-]	0.2	0.27
Coefficient of thermal expansion [K^{-1}]	6.7E-5	6.7E-5
Plastic rate [MPa^{-1} y^{-1}]	1 x 10^{-3}	1 x 10^{-2}
M	1.25	1.25
Alpha [MPa]*	3.69E-4	-7.895[MPa/C] T + 1674 [MPa]
Beta*	6.25	-7 [-]

*For FEBEX the ILM relationship used was written in terms of void ratio rather than dry density as used in this report, so these parameters are not directly comparable.

5. Results

5.1. Case 0 – Base cases

The base case models are designed to be points of comparison against which alternative models of water inflow and alternative hydraulic models can be tested.

5.1.1. Case 0a – TH model with pellets

Peak temperatures are found in the bentonite close to the surface of the canister (a discretisation size into the bentonite of 5 cm is used adjacent to the canister), and at two heights either side of the mid-line of the canister (Figure 5-1). The bentonite is slightly cooler at the canister midline because resaturation from the fracture increases saturation and hence thermal conductivity of the bentonite around the middle of the canister. This increases heat flow and lowers peak temperature by 2°C at the canister mid height. The peak temperature of the bentonite close to the canister is 69°C, with a highest temperature of 66.5°C at the canister mid height (Figure 5-2).

Heating of the bentonite is rapid, with peak temperature occurring within two years and then the temperature decreases slowly over the following 10s of years (Figure 5-3). The temperature remains around 30°C above the initial temperature after 140 years, with around 12°C of this due to heating from surrounding canisters.

Initially, the bentonite blocks have a much higher saturation (0.84 [-]) than the bentonite pellets (0.30 [-]). As water enters the deposition hole, the pellets next to the fracture become saturated very rapidly and water moves into the bentonite blocks (Figure 5-4). The saturation front then spreads vertically upwards and downward through the pellets and blocks but slightly faster in the blocks. The last part of the system to reach saturation at around 300 years is the pellets at the top of the deposition hole (Figure 5-5). Water pressure results show that initially pellets and adjacent blocks equilibrate in terms of suction pressure with water flowing from the pellets into the blocks (Figure 5-6), once equilibrated, resaturation of pellets and nearby blocks occurs at a similar rate. Figure 5-7 shows how water pressure increases at the canister mid height first followed by spreading towards the ends of the canister.

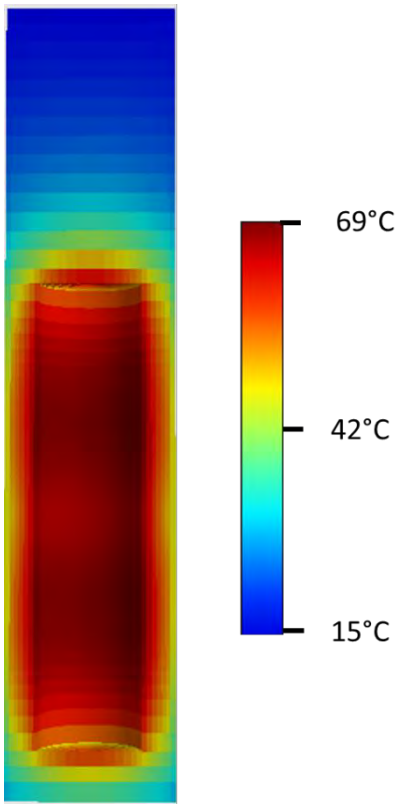

Figure 5-1: Temperature distribution in bentonite after 2 years of heating for Case 0a.

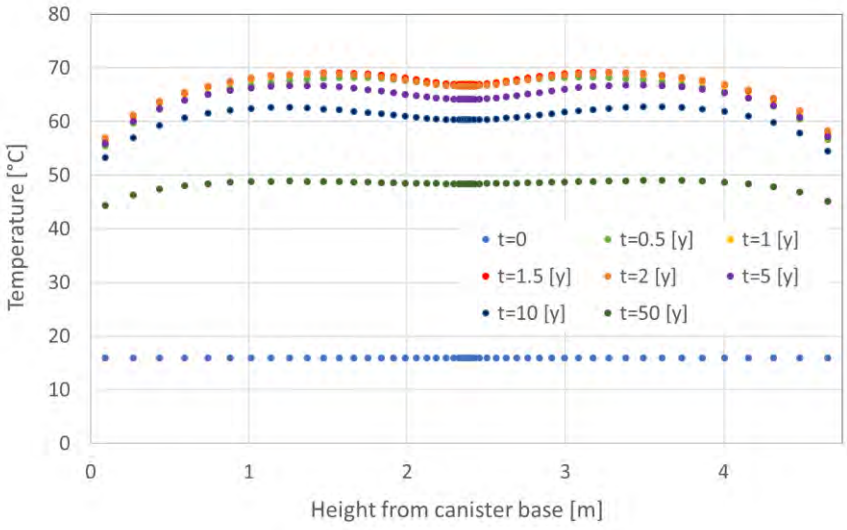

Figure 5-2: Temperature in the 5 cm of bentonite next to the canister along the length of the canister at different times for Case 0a.

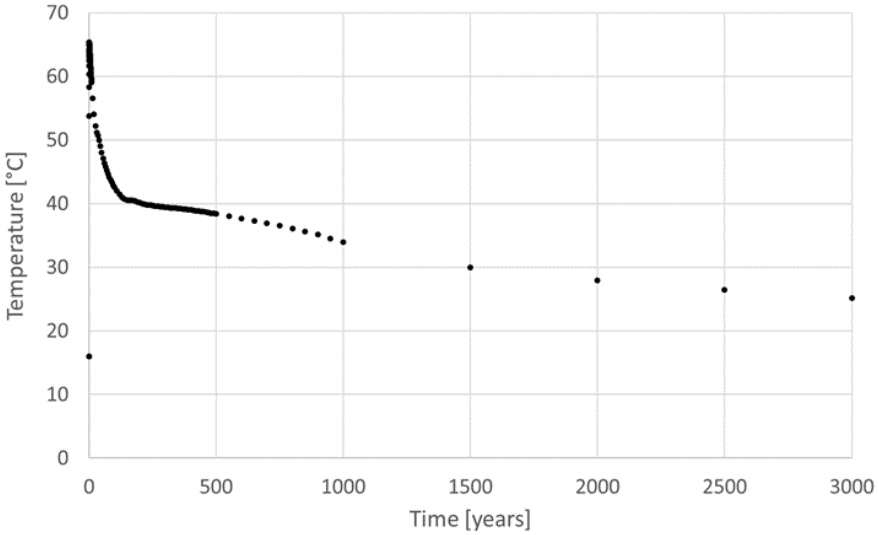

Figure 5-3: Temperature in the 5 cm of bentonite next to the canister at canister mid height through time for Case 0a.

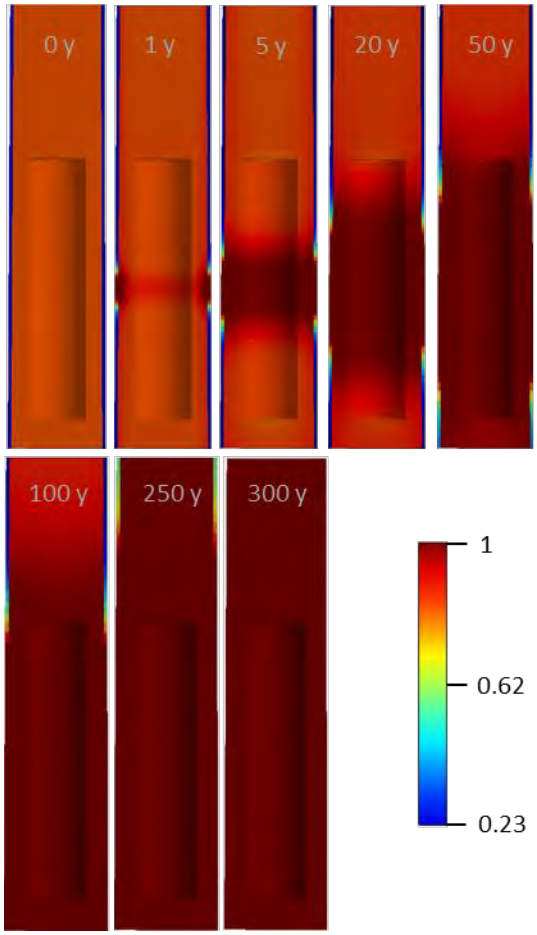

Figure 5-4: Water saturation of the bentonite blocks (red at t=0 y) and pellets (blue at t=0 y) through time for Case 0a.

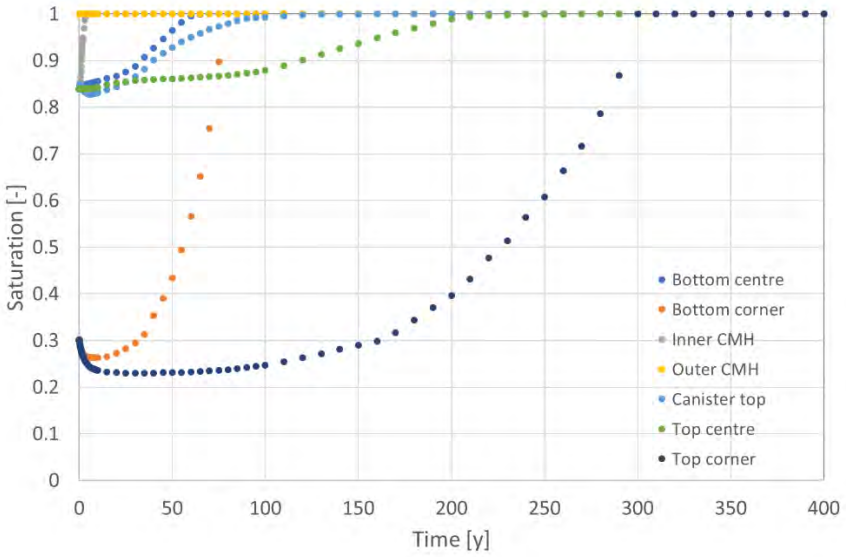

Figure 5-5: Water saturation through time at points indicated in Figure 2-10 for Case 0a.

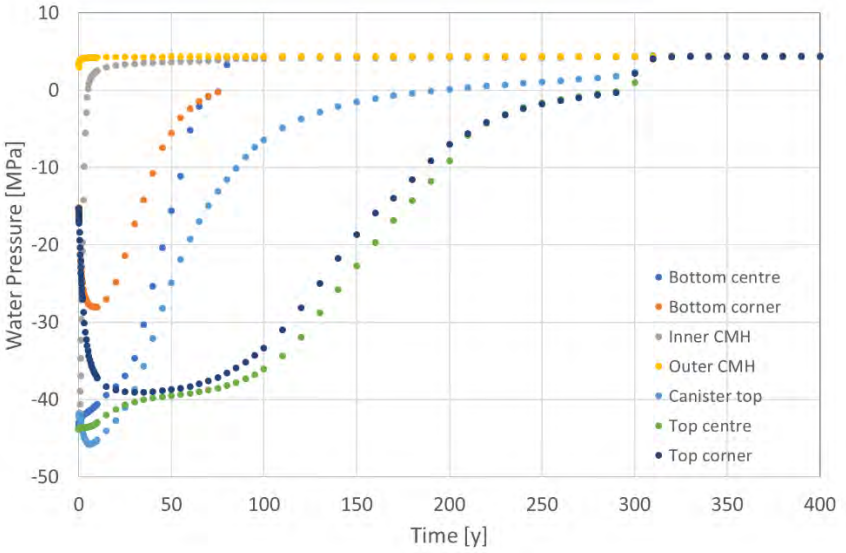

Figure 5-6: Water pressure (negative values indicate suction) through time at points indicated in Figure 2-10 for Case 0a.

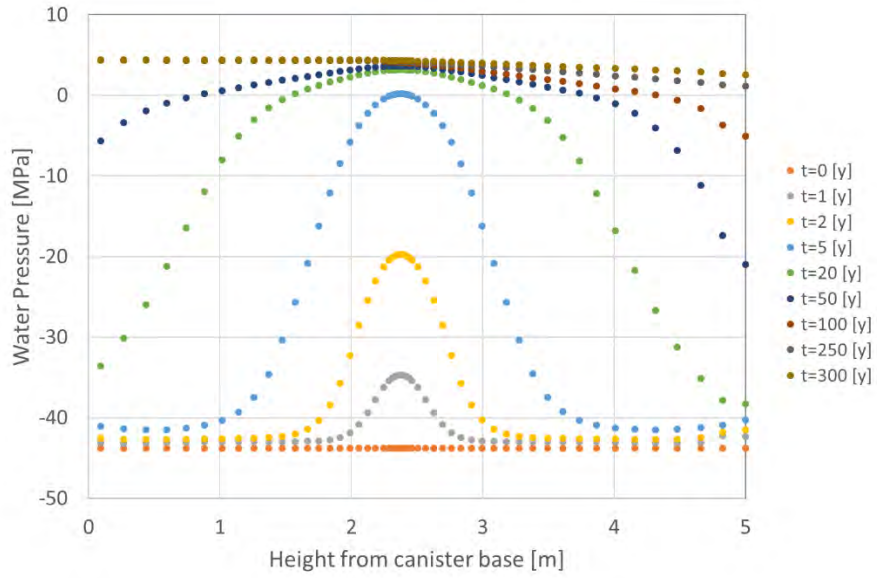

Figure 5-7: Variation through time of water pressure in 5cm of bentonite next to the canister along the length of the canister for Case 0a.

5.1.2. Case 0b – TH model without pellets

Removing the pellets from the model considerably simplifies the models and improves the run times (especially in THM cases), so this case is presented as a comparison to Case 0a to understand the implications of this simplification. Note in this case, the pellets were replaced with bentonite blocks and no averaging of the block and pellet porosity was used.

The peak temperatures in the bentonite close to the canister are approximately 2°C lower in Case 0b than Case 0a. This is because the pellets in Case 0a have been replaced by bentonite blocks in Case 0b, and the blocks have a higher saturation and a higher thermal conductivity. In Case 0b, the peak temperature is at canister mid height because the change in thermal conductivity around the fracture is less significant due to slower resaturation. The temporal change in temperature is similar to that shown in Figure 5-3.

Case 0b is much slower to resaturate than Case 0a, taking between 1 500 and 2 000 years for all compartments to saturate (Figure 5-8). This is because bentonite blocks have a lower permeability than pellets and hence flow into the deposition hole is slower in this case.

Because of the longer resaturation times, pressure gradients are present along the canister for longer than in Case 0a (Figure 5-9). However, the maximum gradients are lower as saturation and water pressure are more spatially uniform throughout the bentonite.

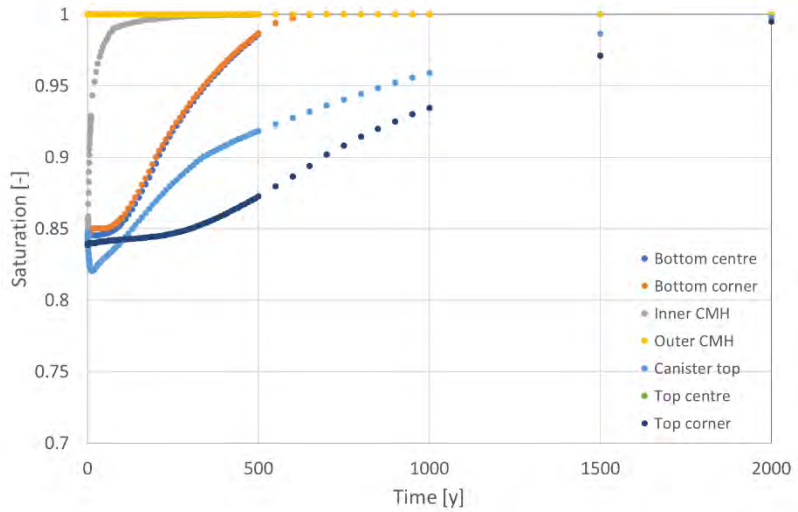

Figure 5-8: Water saturation through time at points indicated in Figure 2-10 for Case 0b.

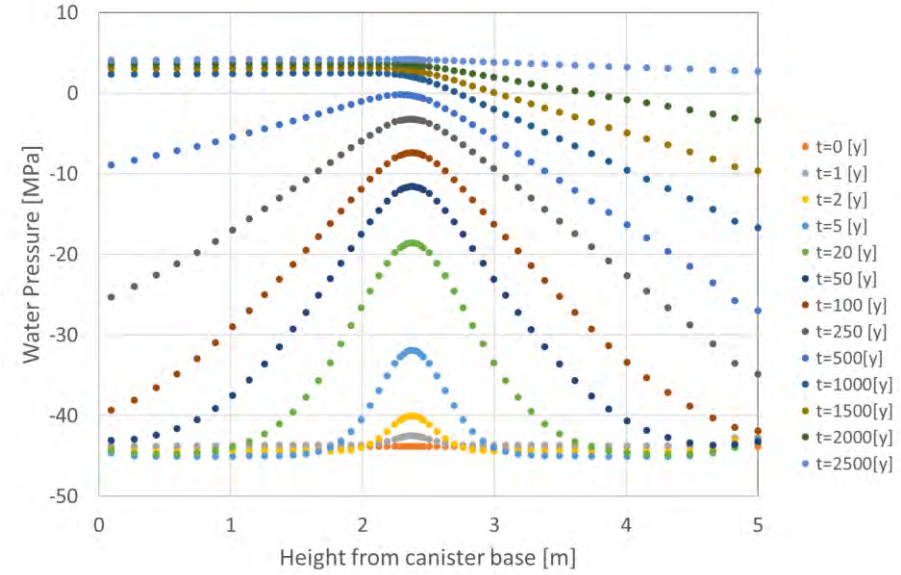

Figure 5-9: Variation through time of water pressure in 5cm of bentonite next to the canister along the length of the canister for Case 0b.

5.1.3. Case 0c – THM model without pellets

Case 0c is similar to Case 0b in that pellets are not represented, however, in order to represent sensible mechanical processes, the porosity of the bentonite blocks was increased to represent an average porosity of the blocks and pellets. Case 0c also couples the thermal and hydraulic problem to the mechanical problem which involves both calculating stresses and strains and coupling hydraulic properties such as capillary pressure to stress.

Peak temperature in Case 0c case is 5°C higher than in Case 0b but has a similar temporal and spatial pattern. The higher peak temperature is due to the lower water saturation in Case 0c which is a result of the higher initial porosity.

In Case 0c, the initial saturation is lower than in Case 0b because initial porosity is higher (Figure 5-10). As in Case 0b, the bentonite close to the fracture becomes saturated extremely quickly. In Case 0c, saturation next to the fracture slightly exceeds 1, which is permitted in the model since there is some experimental evidence for saturations greater than 1 in bentonite, associated with increased density of water (Jacinto 2012). The lower initial saturation in Case 0c also results in greater vapour diffusion away from the canister during the thermal period, which increases the initial drying closer to the canister (Figure 5-11). The time for resaturation is longer in Case 0c than in Case 0b; full saturation is not achieved in the 2 000 y of simulation, with locations at the canister top and bottom and corners of the buffer only achieving saturations of around 0.8 or less. An obvious reason for this is that Case 0c starts from a lower saturation, but resaturation is also slower because the suction in the bentonite has a different shaped curve (defined by the ILM) and is coupled to stress (Figure 5-12). As the bentonite gets closer to being saturated, the stress in the bentonite increases due to swelling and so the suction decreases which results in slower resaturation. The gradient of water pressure along the canister is similar to Case 0b (Figure 5-13).

Stresses build up in the bentonite as resaturation progresses (Figure 5-14). Initially the highest radial stress near the canister is at the canister mid height, as this is the first part of the bentonite that swells. As the resaturation of bentonite progresses away from the fracture, so the pattern of radial stress at the canister also widens and increases, but radial stress at the canister mid height does not increase and remains at a lower value than at other locations along the canister. This is because the initial rapid expansion of the bentonite close to the fracture gives rise to plastic failure and a significant reduction in the dry density of the bentonite close to the fracture (Figure 5-15). In the current model, there are no processes that could act to reverse this plastic deformation. Not accounting for the small scale effects at the canister mid height, there are some significant gradients in radial stress acting along the canister (up to 3 MPa/m) and at the canister mid height these stress gradients are higher.

Whilst the stress profile along the canister length is quite a bit more complex than the water pressure profile, the water pressure profile can be used to give an impression of what the stress profile may look like (ignoring effects around the fracture) and the timescales over which stress gradients exists for TH models where no stress results are available.

The dry density distribution (Figure 5-15) shows that dry density drops directly above the canister. This is due to swelling of bentonite around the outside of the canister pushing directly upwards and causing shear stress at the corners of the canister and resulting in expansion of the bentonite at the top of the canister.

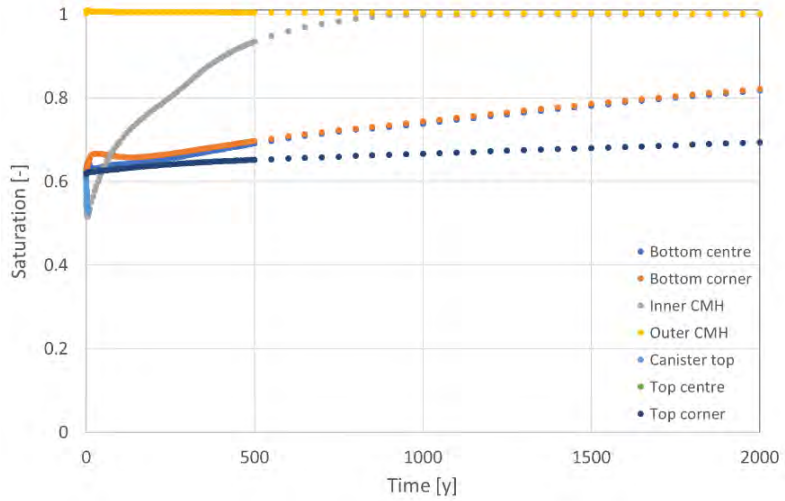

Figure 5-10: Water saturation through time at points indicated in Figure 2-10 for Case 0c.

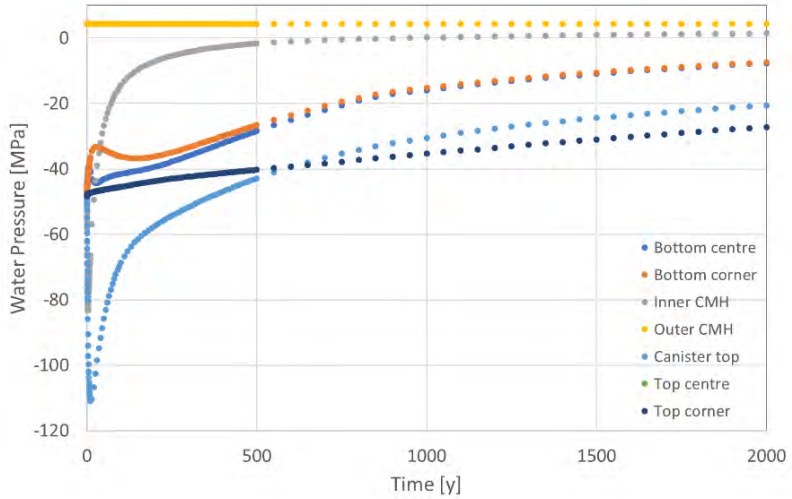

Figure 5-11: Water pressure (negative values indicate suction) through time at points indicated in Figure 2-10 for Case 0c.

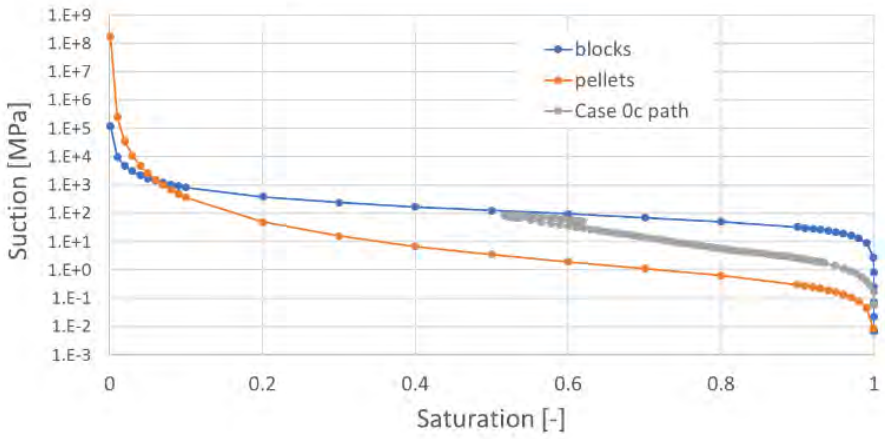

Figure 5-12: Capillary curves based on van Genuchten equations for blocks and pellets alongside the saturation-suction path followed by bentonite next to the canister at the canister mid height in Case 0c.

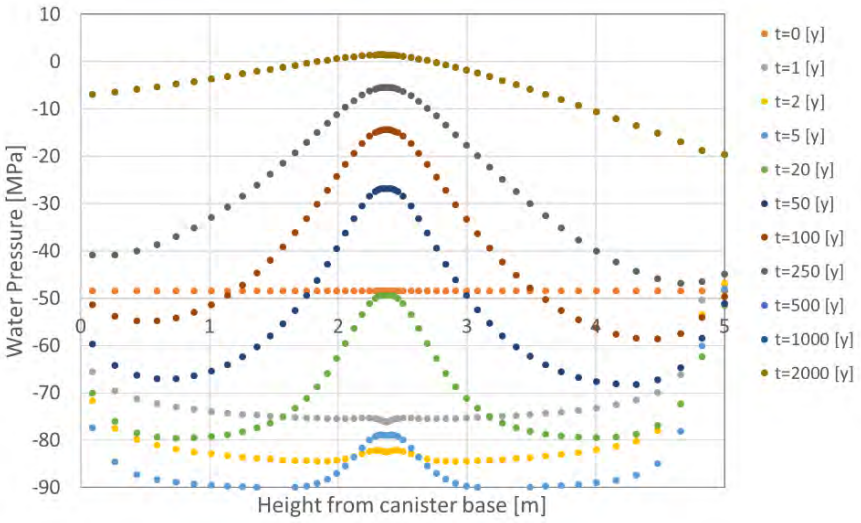

Figure 5-13: Variation through time of water pressure in 5cm of bentonite next to the canister along the length of the canister for Case 0c.

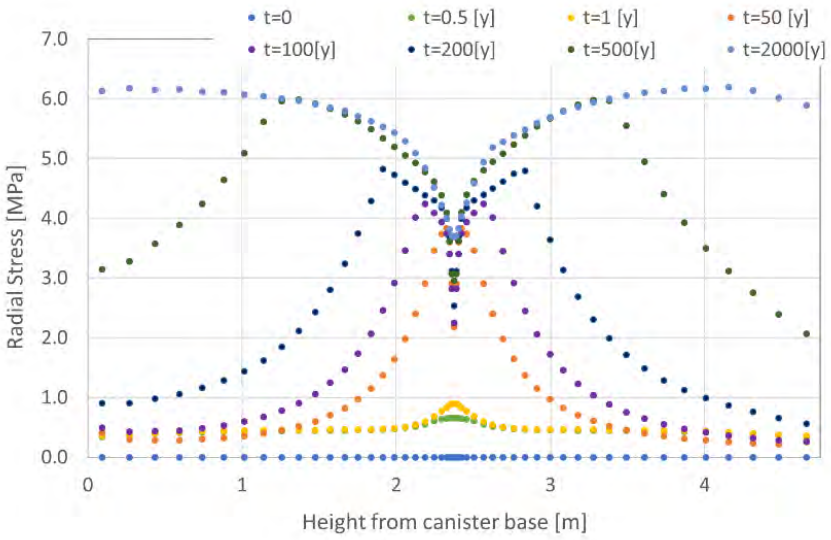

Figure 5-14: Variation through time of radial stress in 5cm of bentonite next to the canister along the length of the canister for Case 0c.

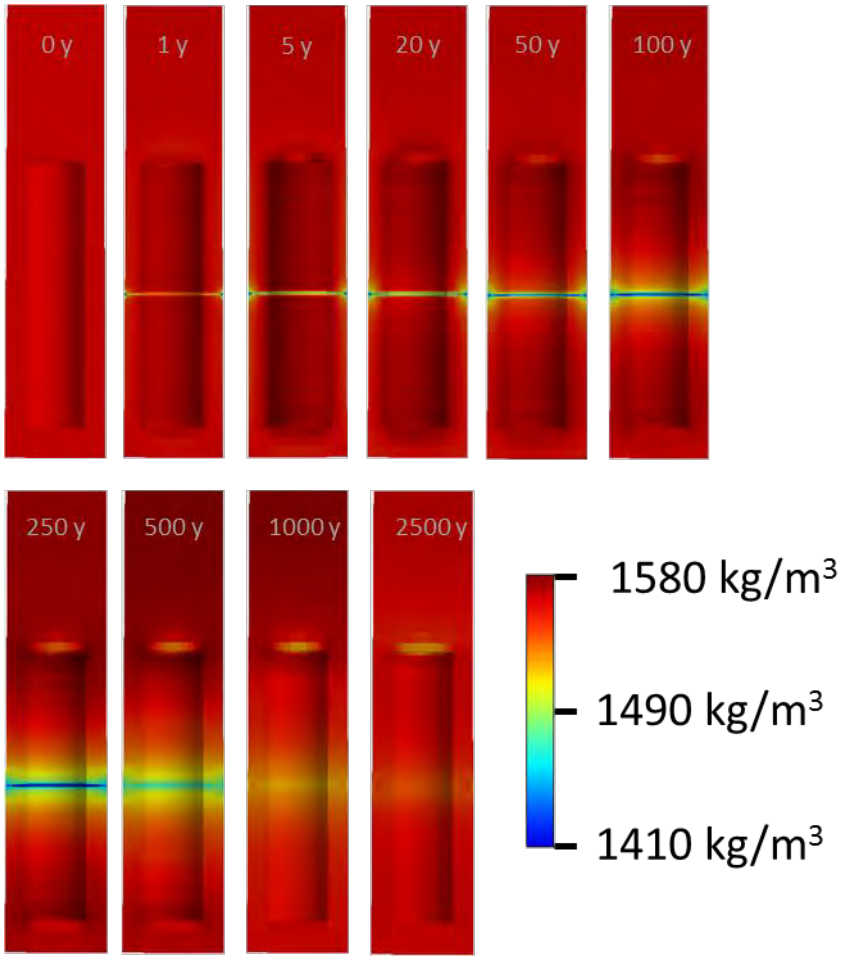

Figure 5-15: Dry density through time for Case 0c. Note initial dry density is 1560 kg/m^3 corresponding to the volume average of the block dry density and the pellet dry density.

5.2. Case 1 – Testing the impact of flow rate in the fracture

5.2.1. Case 1a – TH model with pellets

The peak temperatures in the bentonite are approximately 2°C higher than in Case 0a, since in this lower-inflow model the bentonite is drier close to the canister and hence has a lower thermal conductivity to transfer the heat away. However, the spatial and temporal patterns of heating are otherwise the same as those presented in Figure 5-1 and Figure 5-3.

The rate of resaturation is slower in Case 1a than in Case 0a, which is as expected given that the flow in the fracture is lower. The bentonite blocks far from the fracture take approximately 100 years longer to saturate, and the furthest pellets take approximately 200 years longer (Figure 5-16).

Because of the longer resaturation times, pressure gradients are present along the canister for longer than in Case 0a. However, the maximum gradients are

lower as saturation and water pressure are more spatially uniform throughout the bentonite.

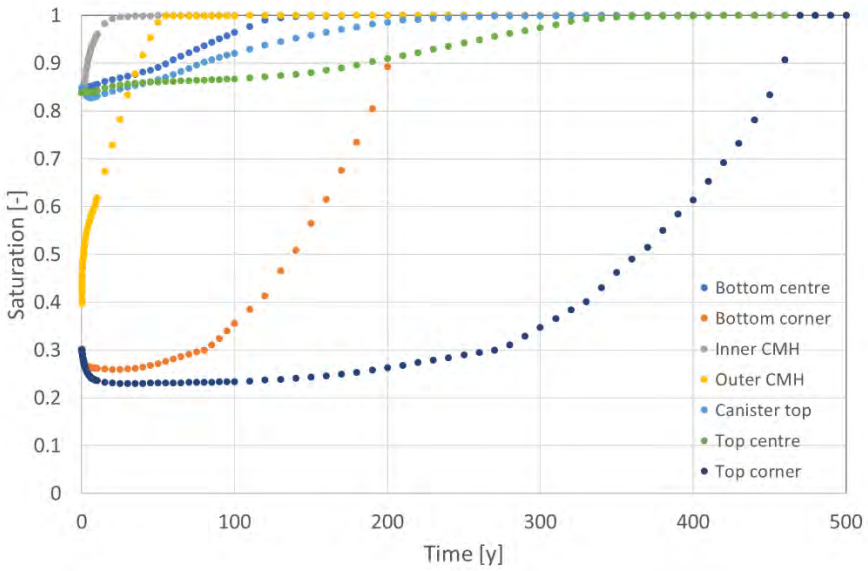

Figure 5-16: Water saturation through time at points indicated in Figure 2-10 for Case 1a.

5.2.2. Case 1b – THM model without pellets

The peak temperature and temperature change through time and space are similar to Case 0c.

The bentonite resaturation in Case 1b is only slightly slower than in Case 0c despite the flow in the fracture being 2 orders of magnitude lower. This is because the flow within the bentonite is limiting the uptake of water in the THM models without pellets, where as it is not limiting in the TH models with pellets. The permeability of bentonite next to the fracture is important in determining the flow into the deposition hole.

The general behaviour of stress build-up within the bentonite is similar to Case 0c (Figure 5-19).

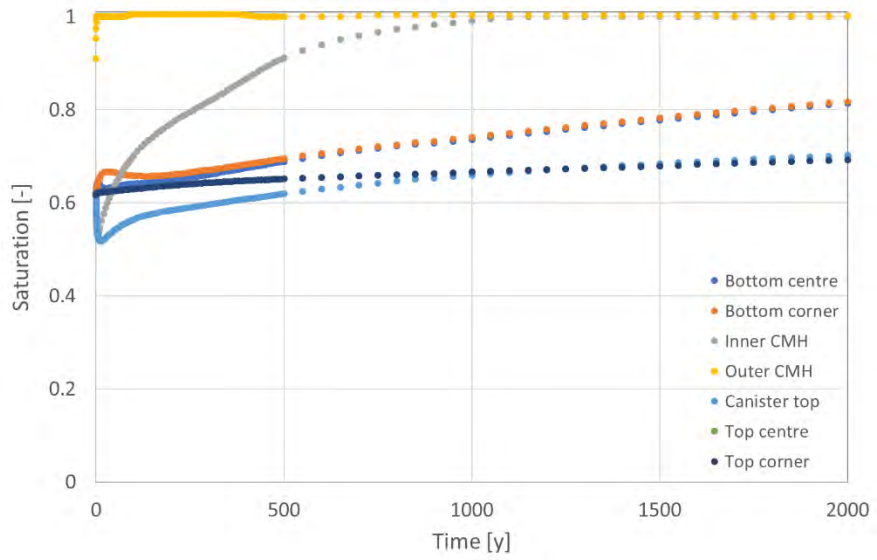

Figure 5-17: Water saturation through time at points indicated in Figure 2-10 for Case 1b.

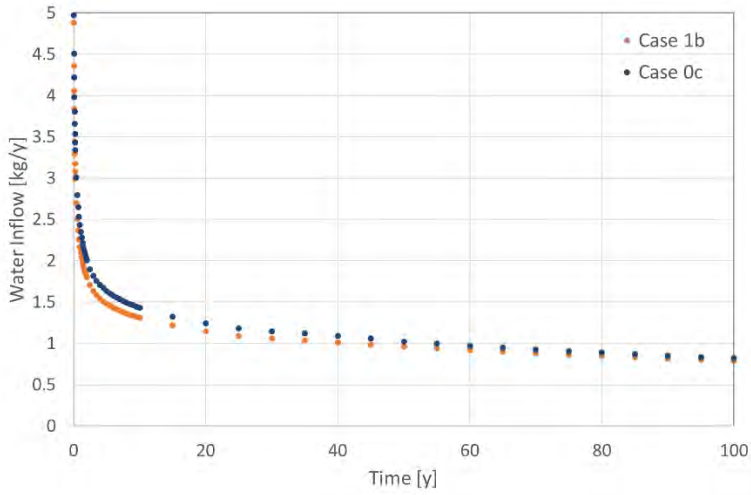

Figure 5-18: Comparison of water inflow to the bentonite from the fracture for Case 0c and Case 1b.

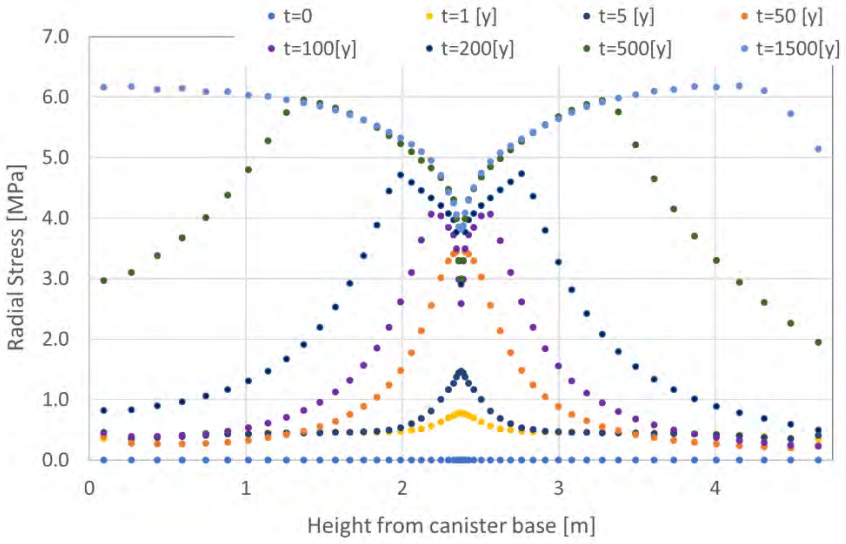

Figure 5-19: Variation through time of radial stress in 5cm of bentonite next to the canister along the length of the canister for Case 1b.

5.3. Case 2 – Testing the threshold gradient model

5.3.1. Case 2a – TH model with pellets

There are no significant differences in temperature between Case 2a and Case 0a.

Resaturation is slower in Case 2a than in Case 0a because the hydraulic gradients are lowered by the threshold model (Figure 5-20). Whereas full saturation is reached at 300 years in Case 0a, it takes between 3 000 and 3 500 years to resaturate all the bentonite in the model with the threshold model. Although resaturation is much slower, the water pressures next to the canister have a very similar pattern in Case 2a to Case 0a, with similar gradients, taking a longer time to reach equilibrium.

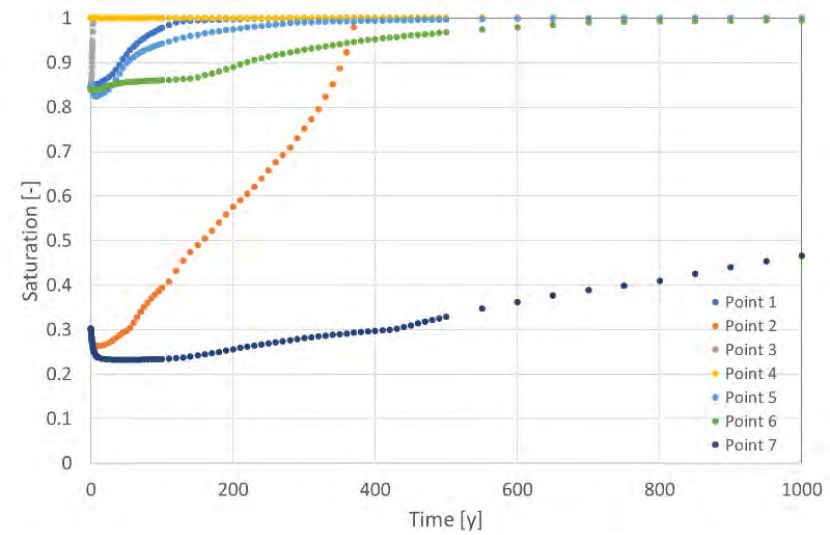

Figure 5-20: Water saturation through time at points indicated in Figure 2-10 for Case 2a.

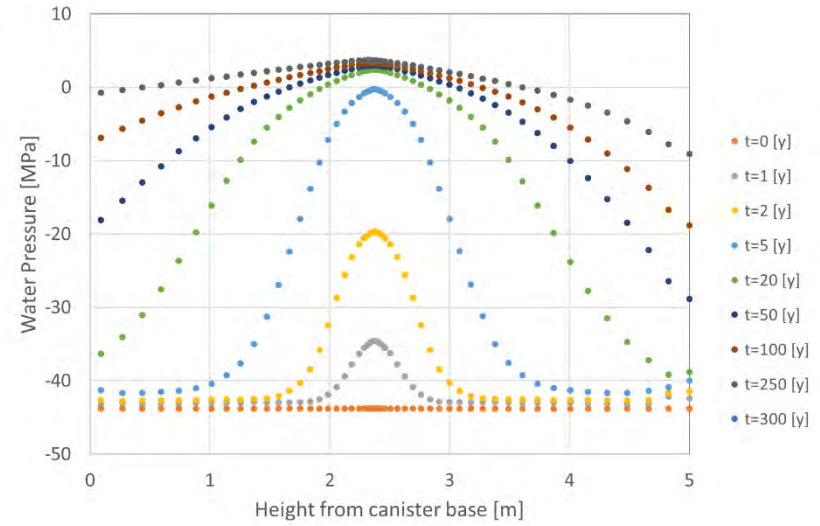

Figure 5-21: Variation through time of water pressure in 5cm of bentonite next to the canister along the length of the canister for Case 2a.

5.3.2. Case 2b – THM model without pellets

The peak temperature and temperature change through time and space are similar to Case 0c.

The rate of resaturation in Case 2b is very similar to Case 0c for the first 1 000 years, but then slows down. This is because the threshold gradient model causes flow to slow down and stop at low pressure gradients so the effect is most significant when the bentonite has become mostly saturated.

Stresses in the bentonite next to the canister change little between 1 000 and 3 000 years, indicating that bentonite in the ring around the canister is largely saturated by 1 000 years. The stresses are very similar in Case 2b to

Case 0a, so the threshold gradient model does not have a significant effect on stress.

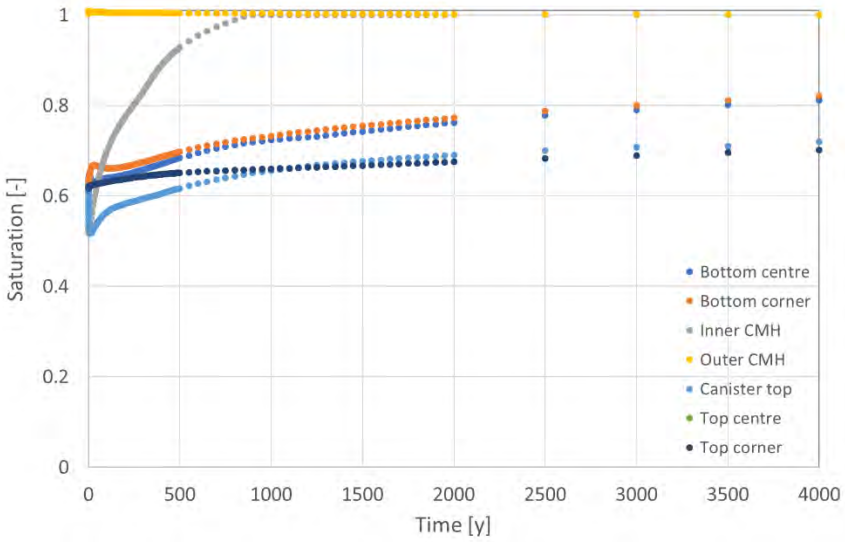

Figure 5-22: Water saturation through time at points indicated in Figure 2-10 for Case 2b.

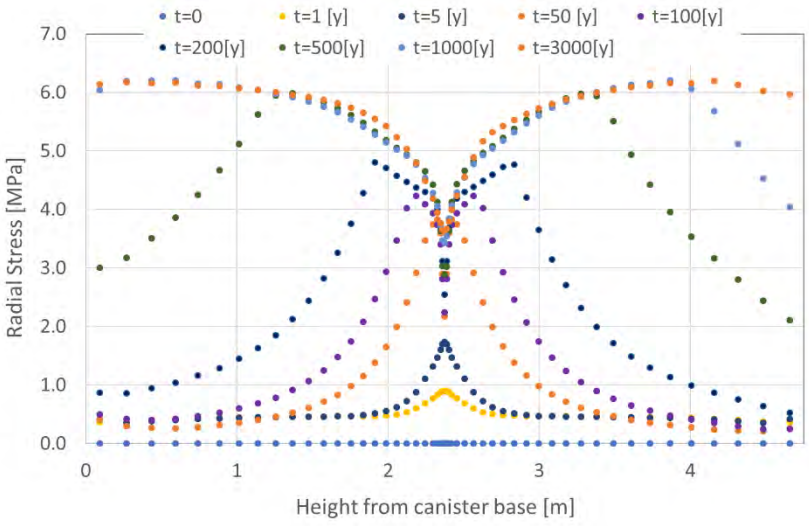

Figure 5-23: Variation through time of radial stress in 5cm of bentonite next to the canister along the length of the canister for Case 2b.

5.4. Case 3 – Testing the thermo-osmosis model

5.4.1. Case 3a – TH model with pellets

There are no significant differences in temperature between Case 3a and Case 0a.

Resaturation timings are very similar between Case 3a and Case 0a (Figure 5-24). The only visible changes are near the canister where there is more drying initially. This is consistent with the concept of the thermo-osmosis model as described in Section 4.3 (after Åkesson, 2013) whereby water flow is increased in the direction away from the heat source. The effect can be seen in water pressures along the canister, as they initially become more negative and are generally shifted to lower pressures (Figure 5-25).

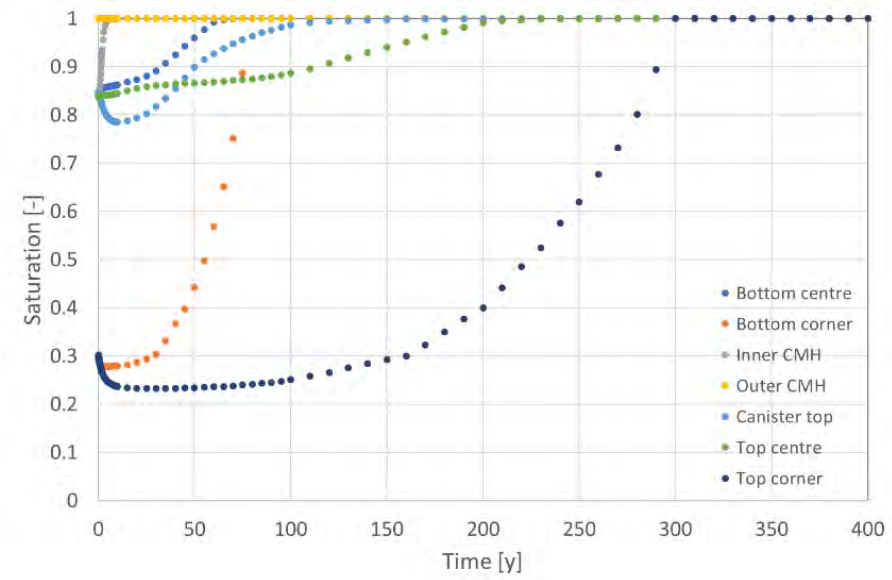

Figure 5-24: Water saturation through time at points indicated in Figure 2-10 for Case 3a.

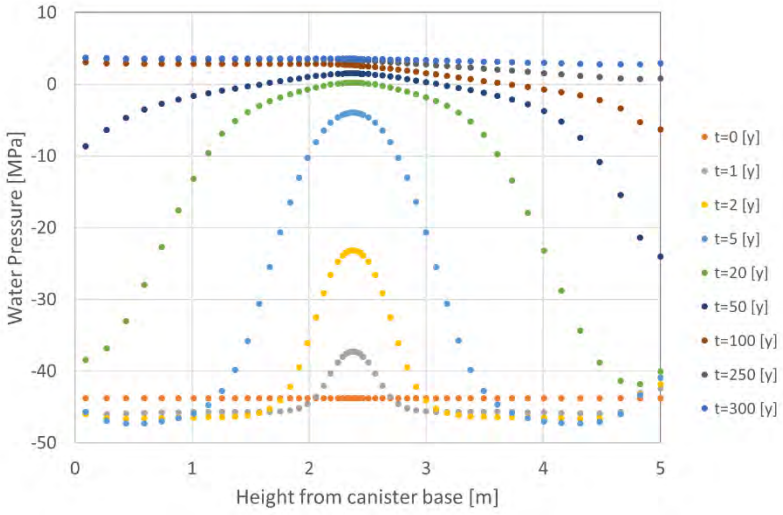

Figure 5-25: Variation through time of water pressure in 5cm of bentonite next to the canister along the length of the canister for Case 3a.

5.4.2. Case 3b – THM model without pellets

The peak temperature and temperature change through time and space are similar to Case 0c.

Both the rate of resaturation and the build-up of stress are similar to Case 0c.

5.5. Case 4 – Testing the micro-fabric evolution model

5.5.1. Case 4a – TH model with pellets

There are no significant differences in temperature between the micro-fabric evolution model (Case 4a) and the base case (Case 0a).

In the Case 4a, the bentonite blocks and pellets are much slower to saturate, except directly adjacent to the fracture, with the last pellet (Top Corner) taking almost 2 000 years to fully saturate (Figure 5-26). This is expected due to the reduced intrinsic permeability of the bentonite at high suctions. The water pressure next to the canister increases more slowly than in Case 0a and there are less steep gradients along the canister (Figure 5-27).

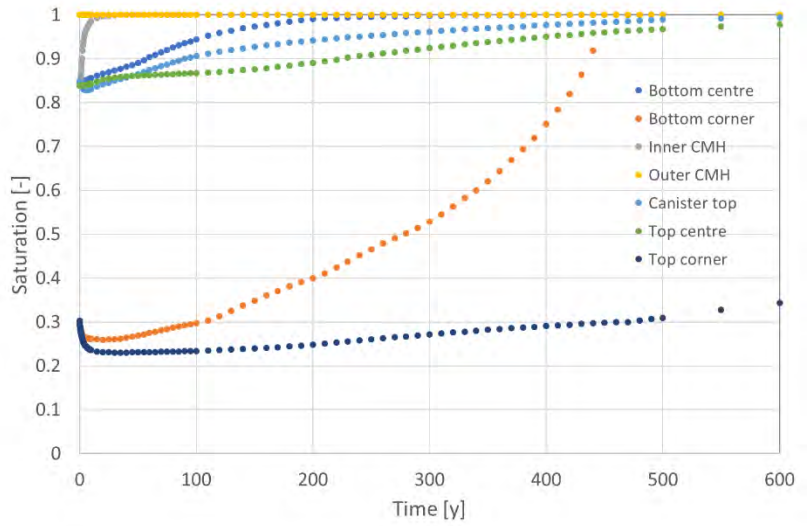

Figure 5-26 Water saturation through time at points indicated in Figure 2-10 for Case 4a.

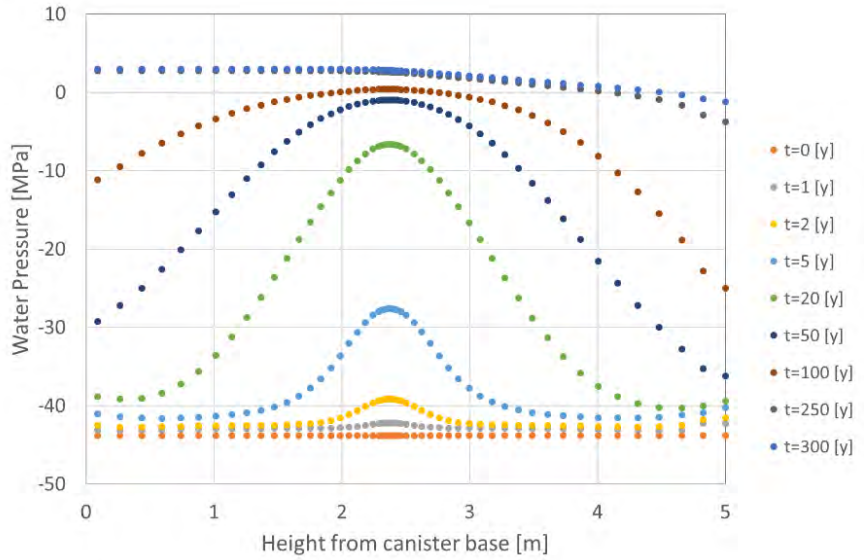

Figure 5-27: Variation through time of water pressure in 5cm of bentonite next to the canister along the length of the canister for Case 4a.

5.5.2. Case 4b – THM model without pellets

The peak temperature and temperature change through time and space are similar to Case 0c.

As with the TH model, the bentonite is much slower to saturate (Figure 5-29) in the micro-fabric evolution model (Case 4b), compared to the base case (Case 0c). The inflow rates are also lower, due to the reduced intrinsic permeability of the bentonite at high suctions, which limits its capacity to take up water from the fracture (Figure 5-28).

In this model, there are much lower stress gradients along the canister when compared with the base case (Figure 5-30). The slower resaturation leads to a more homogeneous pattern of resaturation and therefore lower stress gradients. It is particularly noticeable that the lower stress close to the fracture is much less significant a feature in this model, again due to slower more uniform resaturation.

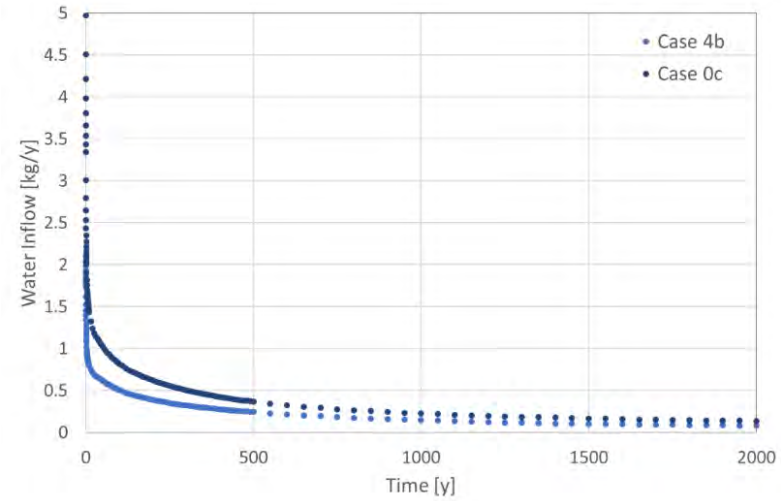

Figure 5-28: Comparison of water inflow to the bentonite from the fracture for Case 0c and Case 4b.

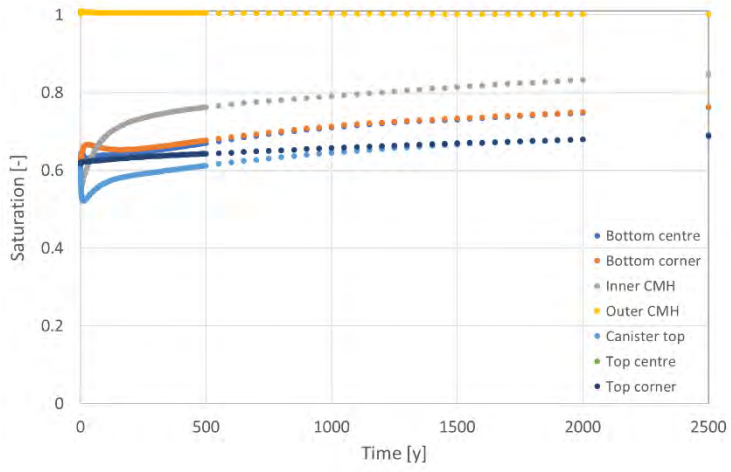

Figure 5-29: Water saturation through time at points indicated in Figure 2-10 for Case 4b.

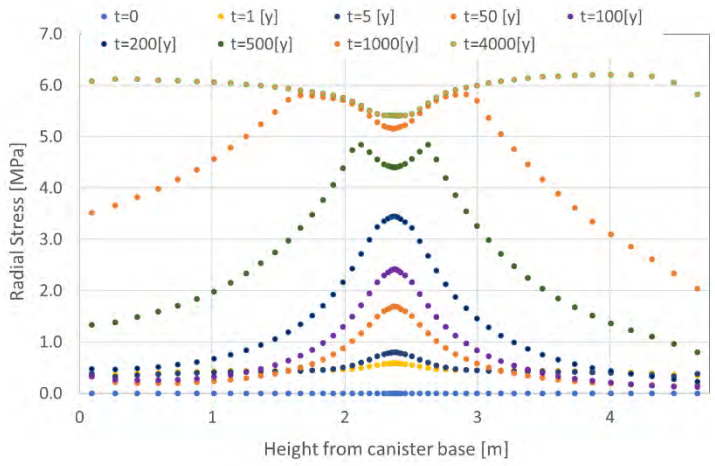

Figure 5-30: Variation through time of radial stress in 5cm of bentonite next to the canister along the length of the canister for Case 4b.

5.6. Case 5 – Testing flow from a disconnected channel fracture

5.6.1. Case 5a – TH model without pellets

The temperature in Case 5a is very similar to the temperature in Case 0b. The peak temperature in the direction of the fracture is 64.5°C and occurs at the canister mid height in the bentonite next to the canister (Figure 5-31). Temperatures at 90° to the fracture are 1°C higher.

Compared to the uniform fracture case (Case 0b), in Case 5a resaturation across most of the bentonite is much slower (Figure 5-32). The bentonite directly adjacent to the fracture (Outer CMH (right)) fully saturates in less than a year, but by 4 000 years the rest of the bentonite has not reached full saturation. Due to channelling of flow within the fracture, the total amount of water that is available to enter the disposition hole is the same order of magnitude in both the base case and this disconnected channel fracture case, yet the amount of flow entering the bentonite is a factor of ~20 lower in Case 5a (Figure 5-34). This indicates that flow within the bentonite is the limiting factor of the rate of resaturation. The much smaller intersection of the fracture with the deposition hole means that all the water entering the deposition hole must pass through a smaller area of bentonite, which limits inflow.

The resaturation is no longer axisymmetric near the fracture, but at the extremities of the model (Top and Bottom), the saturation doesn't change with angle (Figure 5-32 and Figure 5-33). In the bentonite around the canister mid height, there is angular variation in saturation and water pressure. Water pressure gradients along the canister close to the fracture are steeper than those along the far side of the canister (Figure 5-35). Water pressure gradients in this case are much less steep than in Case 0b.

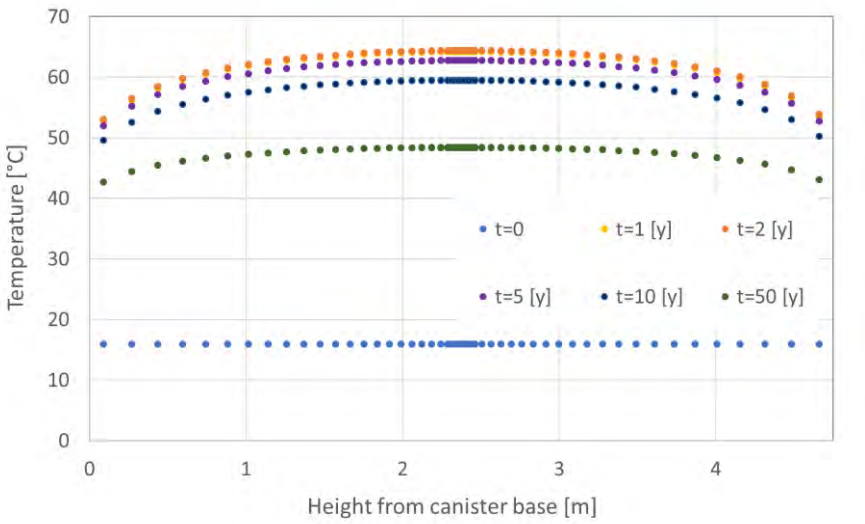

Figure 5-31: Temperature in the 5 cm of bentonite next to the canister in the direction of the fracture along the length of the canister at different times for Case 5a.

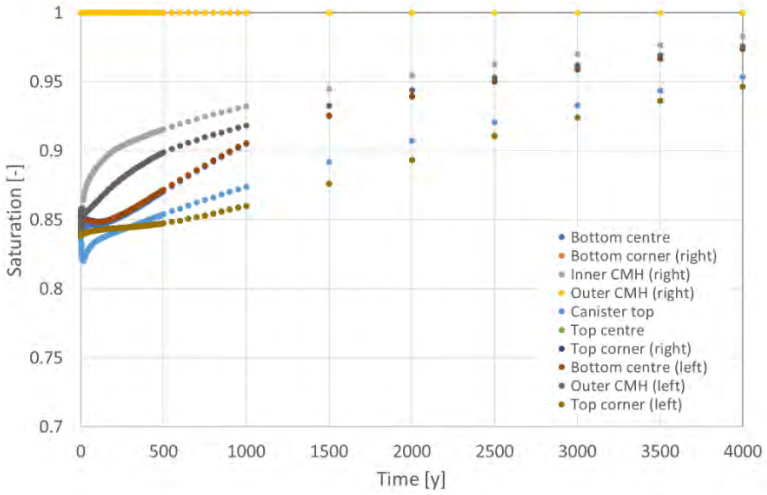

Figure 5-32: Water saturation through time at points indicated in Figure 2-10 for Case 0a.

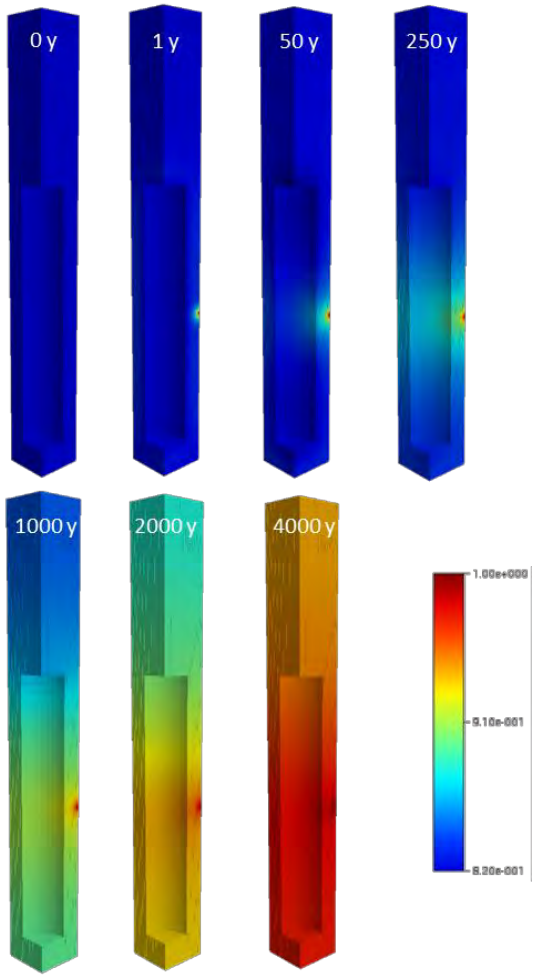

Figure 5-33: Water saturation of the bentonite through time for Case 5a.

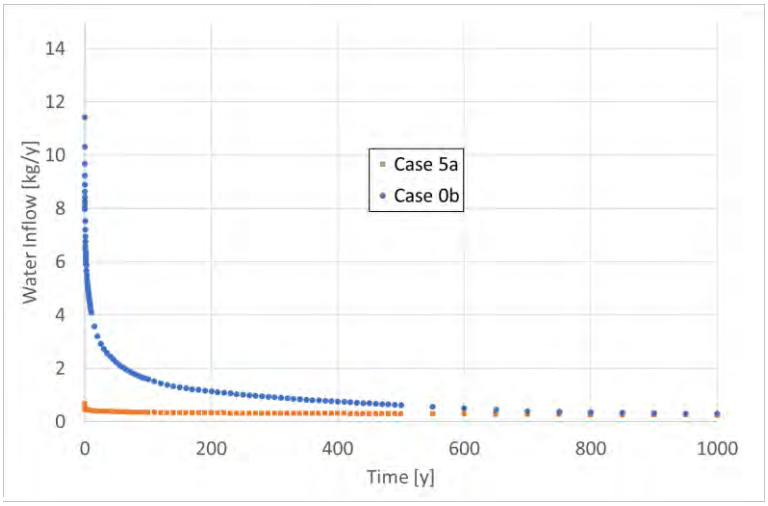

Figure 5-34: Comparison of water inflow to the bentonite from the fracture for Case 0b and Case 5a.

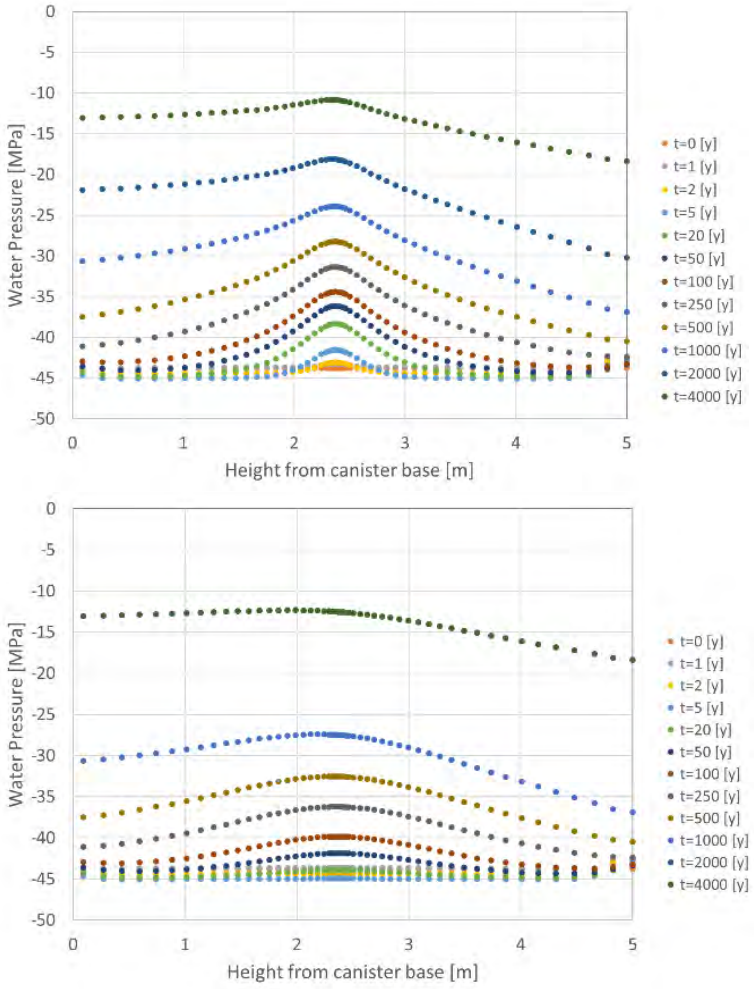

Figure 5-35: Variation through time of water pressure in 5cm of bentonite next to the canister along the length of the canister for Case 5a. (top) in the direction of the fracture, and (bottom) in the direction 90° away from the fracture.

5.7. Case 6 – Testing flow rate from a disconnected channel fracture

5.7.1. Case 6a – TH model without pellets

The spatial temperature patterns and changes through time are unchanged from Case 5a.

There is no significant difference in hydraulic behaviour between this case and the higher transmissivity case (Case 5). This is because although Case 5 uses a higher fracture transmissivity, in practice the inflow rate is controlled by the bentonite permeability. In both cases, the flow rate is high enough to saturate the bentonite adjacent to the fracture almost immediately, so the

transport of water through this region becomes the limiting factor. The inflow rate from the fracture is therefore almost identical in both cases (Figure 5-36).

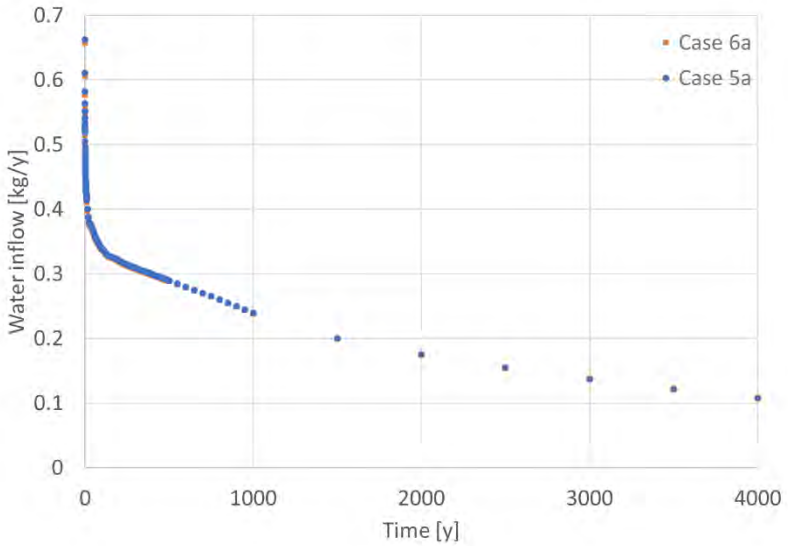

Figure 5-36: Comparison of water inflow to the bentonite from the fracture for Case 5a and Case 6a.

5.8. Case 7 – Testing flow from a glancing channel fracture

5.8.1. Case 7a – TH model without pellets, wide glancing channel intersection

The thermal behaviour of the wide glancing channel intersection model (Case 7a) is the same as that for Case 0b.

Resaturation is slower in Case 7a than in Case 6a because the fracture only intersects on one side of the deposition hole rather than both sides, so inflow is halved. The resaturation patterns through time are shown in Figure 5-37.

As with the disconnected channel fracture, although resaturation from the fracture is not angularly symmetric, the slow resaturation rates mean that saturation is almost homogeneous throughout the bentonite. The water pressure gradients are very shallow but do vary with angle (Figure 5-38).

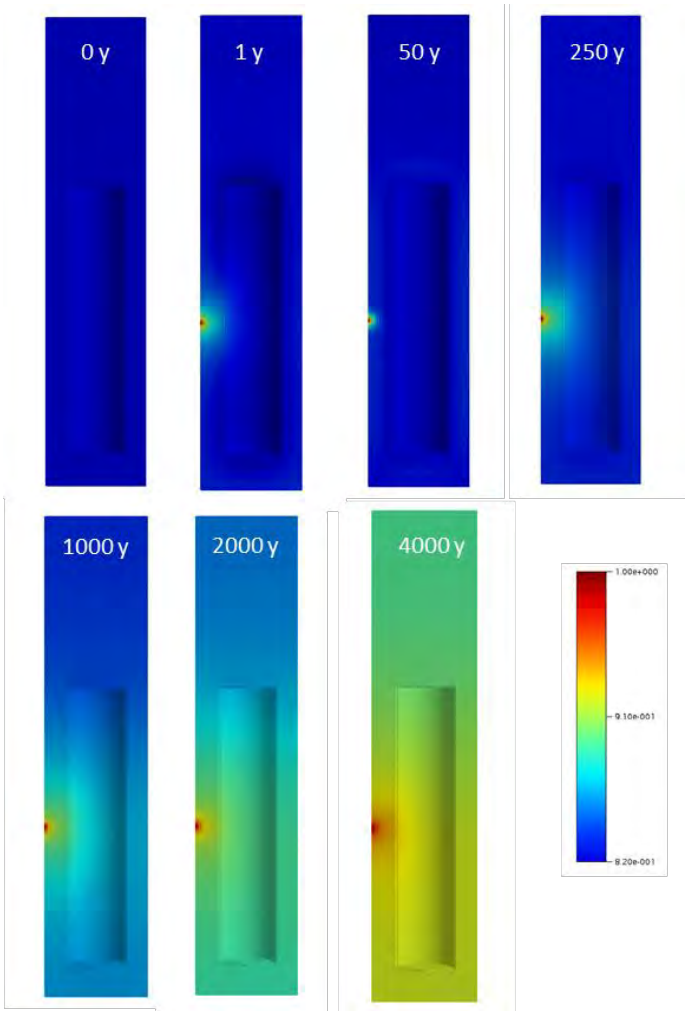

Figure 5-37: Water saturation of the bentonite through time for Case 7a.

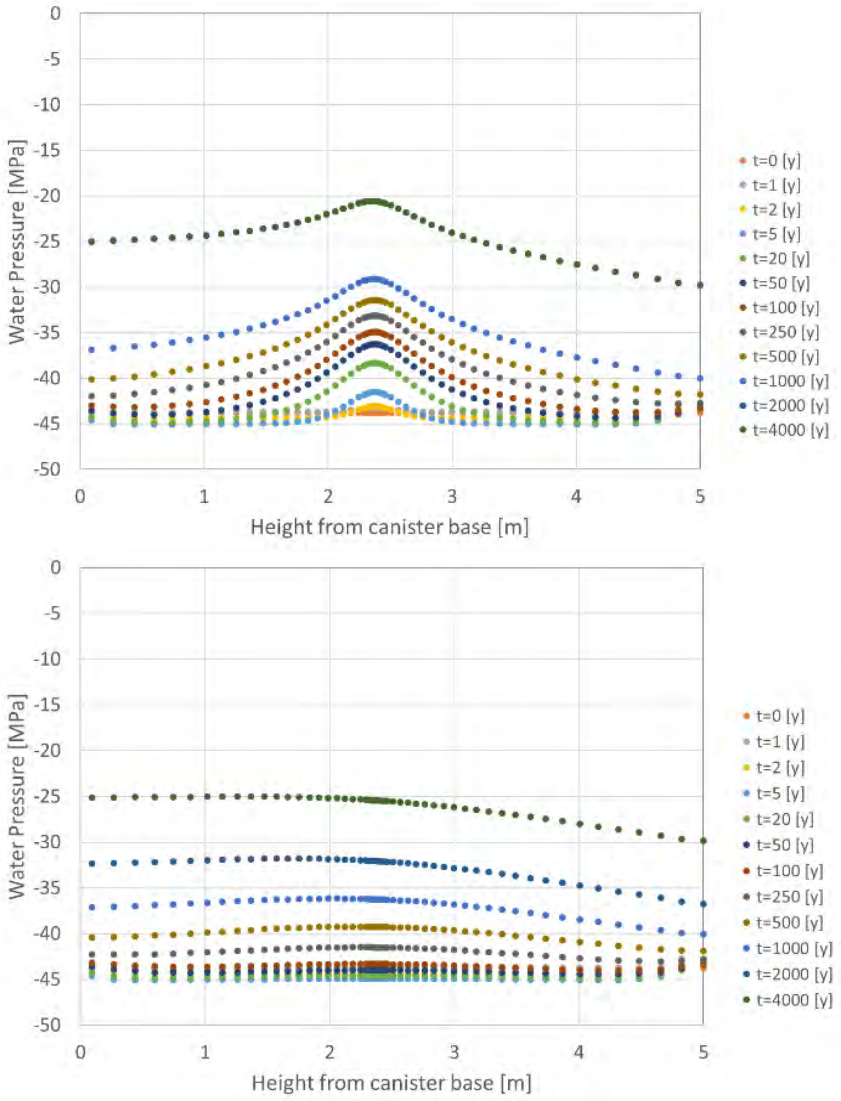

Figure 5-38: Variation through time of water pressure in 5cm of bentonite next to the canister along the length of the canister for Case 7a. (top) in the direction of the fracture (bottom) in the direction 180° away from the fracture.

5.8.2. Case 7b – TH model without pellets, narrow glancing channel intersection

There is no significant difference in temperature between Case 7a and Case 7b.

The resaturation is slightly slower for the point-like narrow intersection area case compared to the wider intersection area case, as the amount of water that can enter the bentonite through the small fracture aperture is further limited; the inflow rate is approximately half that of the wider intersection so resaturation rates are likely to be double those in Case 7a (i.e. over 8 000 years). The general hydraulic behaviour is otherwise similar.

5.9. Case 8 – Testing flow rate from a glancing channel fracture

5.9.1. Case 8a – TH model without pellets, wide glancing channel intersection

The spatial temperature patterns and changes through time are the same as in the higher transmissivity case (Case 7a).

There is no significant difference in hydraulic behaviour between this case and the higher transmissivity case (Case 7a). This is because the inflow rate is limited by the permeability of the bentonite rather than the fracture transmissivity. The inflow in each case is therefore very similar.

5.9.2. Case 8b – TH model without pellets, narrow glancing channel intersection

There is no significant difference in hydraulic behaviour between this case and the higher transmissivity case (Case 7b), due to limitation of the inflow rate.

5.10. Case 9 – Testing an alternative bentonite

5.10.1. Case 9a - TH model without pellets

The thermal behaviour of the FEBEX bentonite (Case 9a) is similar to the MX-80 bentonite (Case 0a), with two peaks in temperature either side of the canister centre. The peak temperature is slightly lower at 68°C (compared with 69°C for MX-80) but occurs at approximately the same time.

The FEBEX bentonite reaches total saturation faster than MX-80 bentonite, when comparing models without pellets (Figure 5-39). However, its initial rate of resaturation is slower - there is a greater initial drop in saturation at compartments close to the canister (but far from the fracture). This initial drop in saturation is likely to be higher because the vapour diffusivity is higher. The FEBEX bentonite also has a slightly lower initial saturation (69%) for the same initial water content.

The FEBEX bentonite also has more negative water pressures, and consequently higher pressure gradients along the canister (Figure 5-40), due to the higher initial drying at the canister.

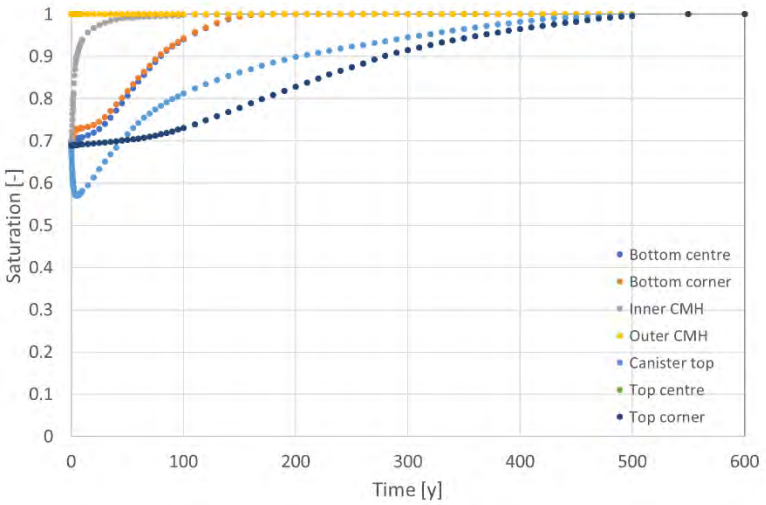

Figure 5-39: Water saturation through time at points indicated in Figure 2-10 for Case 9a.

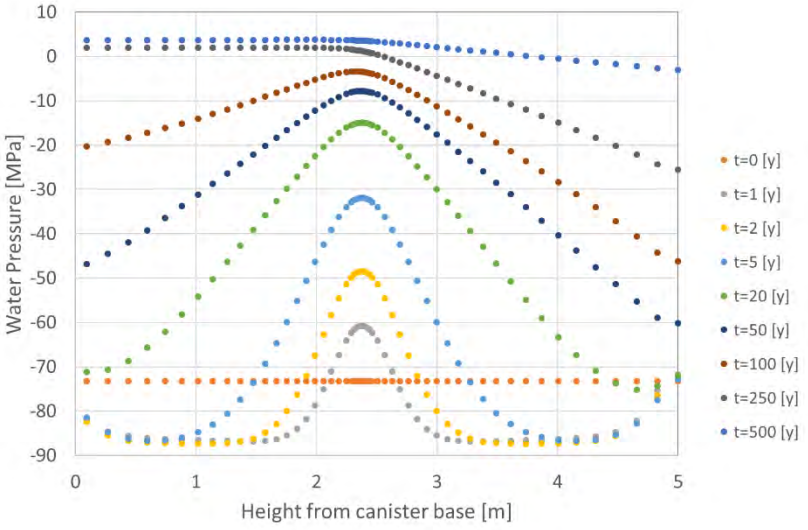

Figure 5-40: Water pressure gradient along the canister through time for Case 9a (alternative bentonite TH model without pellets).

5.10.2. Case 9b - THM model without pellets

Temperature is very similar to Case 9a, but around 1°C warmer at its peak.

As with the TH model, the FEBEX bentonite has a higher initial saturation than the MX-80 bentonite for the same water content, due to its lower initial porosity. It also saturates much faster than the MX-80 bentonite, although again there is a greater initial drop in saturation (Figure 5-41).

The general mechanical behaviour of the FEBEX bentonite is similar to the MX-80 bentonite, although much higher stresses are generated due to the higher bulk modulus of the FEBEX bentonite. In general, all the stresses are

approximately twice as high in Case 9b. This leads to correspondingly higher stress gradients along the canister (Figure 5-42).

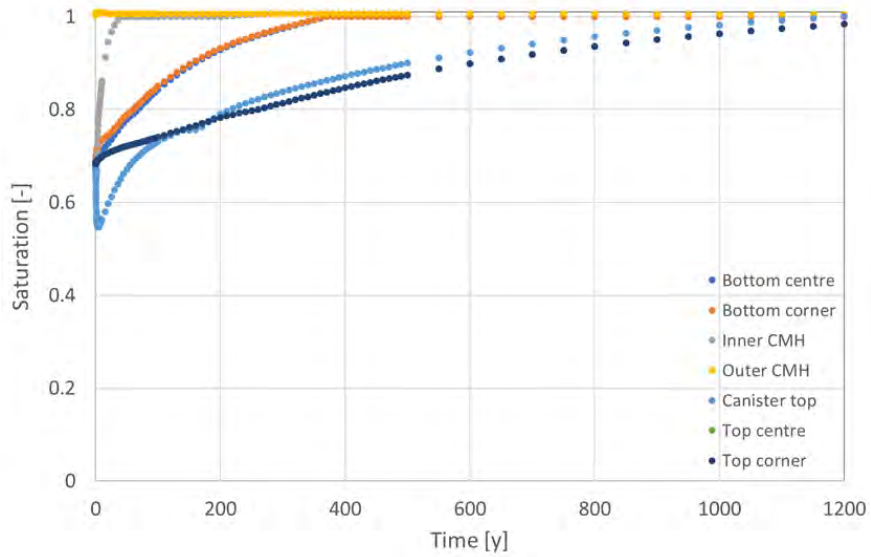

Figure 5-41: Water saturation through time at points indicated in Figure 2-10 for Case 9b.

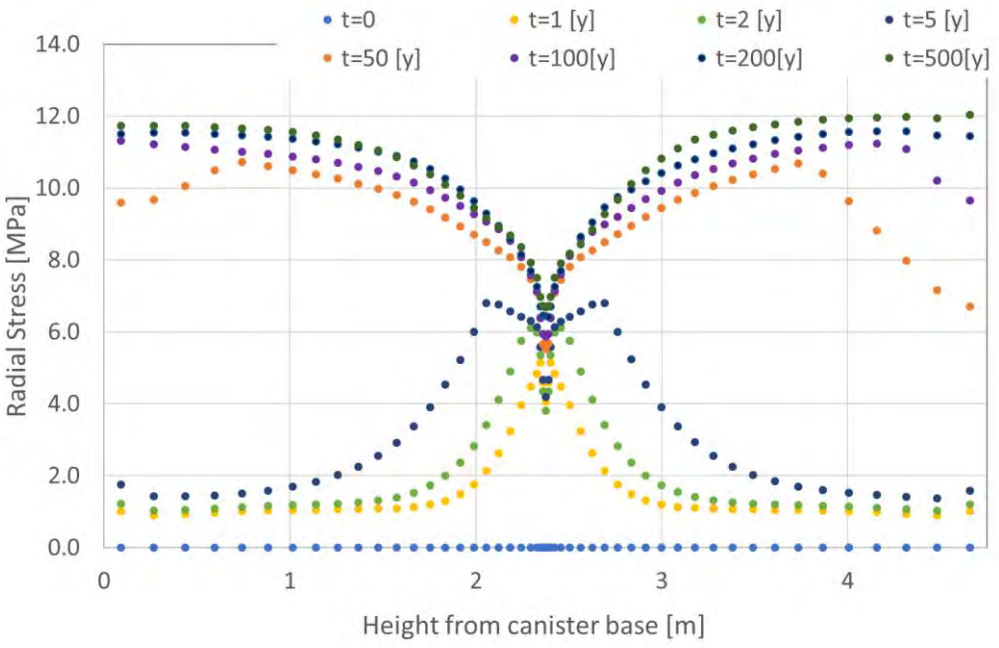

Figure 5-42: Variation through time of radial stress in 5cm of bentonite next to the canister along the length of the canister for Case 9b.

6. Discussion

Resaturation times reported in Åkesson et al. (2010) for canister mid height fractures range from 7 – 30 years for cases with pellets and from 20 – 40 years for cases with homogenised bentonite properties (i.e. no pellets but block properties updated to represent an average of blocks plus pellets). These times are all significantly shorter than the times reported in this report (Case 0a has resaturation time of 300 years, Case 0c of over 2 000 years). There are some differences between the models included in this report and those in Åkesson et al. (2010) which could account for this discrepancy:

- In this report, we assumed the rock around the deposition hole was impermeable, whereas Åkesson et al. (2010) assumed a range of permeabilities and showed that rock permeability can change resaturation time by an order of magnitude.
- Different representations of the fracture boundary have been used in this report and in Åkesson et al. (2010). In this work, a fixed pressure at a distance is prescribed with a constant transmissivity. In Åkesson et al. (2010) a constant flow rate into the deposition hole is prescribed.

We have not undertaken a thorough comparison of the differences between the models in this report and those of Åkesson et al. (2010), so it is difficult to say which report gives more realistic resaturation times. For the purposes of this report, we compare resaturation times to Case 0 times, to understand how different processes and representations of fractures affect resaturation.

In this report, three different initial conditions have been applied to the bentonite. In the TH models, bentonite blocks surrounded by an annulus of pellets have been represented as well as cases with no pellets and bentonite blocks filling the deposition hole. In the THM models, the bentonite has uniform initial properties, but the properties represent the volumetric average properties of the blocks and pellets. The implications of not including pellets and blocks separately in all models are:

- Resaturation times are significantly overestimated (e.g. by an order of magnitude) if pellets are not explicitly represented;
- Water pressure gradients at the canister are underestimated if pellets are not represented;
- Using an average porosity results in initial saturation being underestimated and enhanced vapour diffusion away from the canister, resulting in more drying next to the canister and longer resaturation times.

The reasons for using models without explicit representation of the pellets is that run times are much faster (for the 3D TH cases) enabling more runs to be undertaken. THM cases with explicit representation of pellets suffered convergence problems, hence relying on models without pellets. This is still a significant step forward as fully coupled THM modelling of bentonite is still an area of active research and Börgesson et al. (2013) reported that they were unable to achieve convergence for THM runs.

Rates of flow in the fracture have a limited effect on the modelling results because in many cases the inflow to the deposition hole is limited by the lower permeability of the more saturated bentonite adjacent to the fracture

rather than the availability of water in the fracture. This is true to some extent for all configurations of material properties, but when pellets are explicitly represented next to the fracture, flow into the deposition hole is less restricted by the bentonite, and there is a range of plausible transmissivities (2 orders of magnitude) over which resaturation timescales do depend on fracture properties.

The fully coupled THM models are useful in that they show the stresses that the canister may be subjected to during and after the resaturation period. Swelling pressure of bentonite is relatively well understood, so the magnitude of the stress is likely to be well represented by the models. The spatial distribution of the stress is dependent upon the rate of resaturation, which as discussed above, is less easy to constrain and over which there is significant uncertainty. The modelling shows that there could be significant gradients (several MPa per m) in compressive stress acting along the length of the canister. The gradients are highest when resaturation is fastest. Undertaking modelling of the effect of these stress gradients on the copper canisters is not in the scope of this work, but it would be interesting to understand whether such gradients could have an effect on the shape and durability of the copper overpack, and in particular whether there would be any effect on copper creep. The modelling indicates that significant gradients in stress could persist for 10s or even 100s of years.

There are particularly high stress gradients at the canister mid height, caused by the rapid resaturation and early swelling of bentonite near the fracture. It is perhaps not unrealistic that bentonite close to the fracture could swell significantly and maintain different properties compared to bentonite further from the fracture. However, this effect has not been demonstrated in laboratories and whilst a representation of plastic deformation is included in the model, this has only been tested on experimental data over several years and does not include processes that may be important on longer time scales, such as creep.

An additional feature of the mechanics that develops during resaturation is that shear stresses develop at the corners of the canister. This can be understood because the bentonite surrounding the canister is swelling and creating vertical stresses in an annulus outside of the canister. Directly above and below the canister, the bentonite does not see this vertical stress, so there is a significant vertical stress gradient with radial distance above and below the canister. This gives rise to shear stresses and to volumetric expansion directly above the canister.

Testing the implications of different flow regimes within a fracture (channels of different geometries and widths) shows that, despite flow rates in channels being higher than in whole fractures (to maintain overall fracture transmissivity), resaturation from the channels is slower because uptake of water into the bentonite is limited by flow in the bentonite and because the length of the intersection between the channel and the bentonite is much shorter than if the whole fracture is flowing. These models did not represent pellets next to the fracture and it is possible that much higher inflow could be seen

if the inflow was into higher permeability pellets. However, there is significant uncertainty in how best to represent the hydraulic properties of bentonite pellets.

The threshold gradient model gave slower resaturation, but otherwise didn't change the spatial distribution of stress. The thermal osmosis model also had little effect on the results other than an increase in drying around the canister at early times. The micro-fabric evolution model significantly increased resaturation times but the stress gradients along the canister were lower. It would be an interesting exercise to understand the implications of lower gradients for a longer time on the copper canisters.

The modelling results show sensitivity to the type of bentonite used in the buffer, but this does not change any conclusions about the processes that occur. Different types of bentonite have different hydraulic properties and swelling properties depending on their chemistry so the timings of resaturation and magnitudes of stresses can be expected to change with the type of bentonite.

7. Conclusions

The safety functions that the EBS system are required to fulfil in SKB's KBS-3 repository concept are:

- Buff1: Limit advective transport;
- Buff2: Reduce microbial activity;
- Buff4: Resist transformation; and
- Buff6: Limit pressure on canister and rock.

Fulfilling these safety functions requires that the buffer emplaced within deposition holes resaturates and swells, causing the initial contrast in dry density between bentonite blocks and pellets to homogenise. For this reason, there is interest in how quickly the buffer resaturates which may indicate the timescales on which the bentonite homogenises.

During the period over which the buffer resaturates, additional spatial differences in bentonite density will develop due to parts of the buffer that are close to water sources resaturating and swelling whilst parts further from water sources do not swell and may even compact. The modelling in this report demonstrates that when resaturation is fast, high gradients in suction and stress are present along the length of the canister during the resaturation process. When resaturation is slow, shallower gradients in suction and stress are present along the length of the canister, but they last for longer. The implications of these two scenarios for potential deformation of canisters has not been assessed in this work, but it could be useful to understand whether either of these scenarios could deform the canisters.

The pattern of flow within a fracture plane affects the spatial pattern of resaturation and stress development within the buffer. For the case of a uniformly flowing fracture, resaturation is axially symmetric. The intersection of the flowing fracture and the deposition hole is a full ring around the circumference of the hole leading to faster resaturation times but also to high stress gradients on the canister. Where flow is channelled within the fracture plane, the intersection of the flowing channel with the deposition hole is a small portion of the hole's circumference. This results in saturation and stress gradients around the circumference of the canister as well as along the length. Despite assuming flow in the fracture is focussed into the channel and hence the channel transmissivity being greater than the fracture transmissivity in the uniform flowing case, resaturation is slower in the channel cases because inflow to the deposition hole is limited by the flow in the bentonite, not the flow in the fracture. The slower resaturation corresponds to lower gradients of suction and stress on the canister.

The rate of resaturation is dependent upon the flow rate within the fractures to some degree, although the rate of flow into the deposition hole is also limited by the rate at which water can flow from the fracture into the buffer. In models with pellets explicitly represented, changes in fracture flow rate of two orders of magnitude did affect resaturation times, but when pellets were not explicitly represented, flow into the buffer was controlled by the properties of the bentonite blocks. Further work is required to both improve the

representation of resaturation of the pellets (such as the EBS Task Force project) and also to enable a good representation of the mechanics of pellets (such as in the BEACON project), so the results given here should be taken as indicative rather than definitive.

There remain uncertainties as to the process models for hydraulics and mechanics of bentonite, especially over timescales longer than those used in experiments to date. These uncertainties have led to different proposed models of the hydraulics. This work has found that both the threshold gradient and thermo-osmosis models have little effect on resaturation times but the microfabric evolution model significantly increases resaturation times and reduces stress gradients.

Fully coupled thermal-hydraulic-mechanical modelling of bentonite resaturation remains a challenging prospect, but the work in this report has considered some alternative approaches to process representation and boundary conditions on the deposition holes to improve understanding of both rates of resaturation and development of stress around canisters within deposition holes.

8. References

Alonso E, Gens A, Josa A (1990) A constitutive model for partially saturated soils. Géotechnique 40(3):405–430.

Benbow S, Metcalfe R, Watson C and Bond A (2012), SR-Site Independent Modelling of Engineered Barrier Evolution and Coupled THMC: Contribution to the Initial Review Phase. SSM Technical Note 2012:18. Swedish Radiation Safety Authority.

Black J H (2012), Selective review of the hydrogeological aspects of SR-Site. SSM Technical Note 2012:37. Swedish Radiation Safety Authority.

Börgesson L, Åkesson M and Hernelind J (2013). Analysis of risks and consequences of uneven wetting in a dry deposition hole. SKB document ID 1415878. Swedish Nuclear Fuel and Waste Management Co.

Claesson J and Sällfors G (2004). Drying and resaturation of the bentonite barrier. New tools for modelling and analysis. SKI Workshop. EBS – Long-term Stability of Buffer and Backfill, Lund, Sweden, Nov. 2004.

Dueck A (2005). Hydro-mechanical properties of a water unsaturated sodium bentonite, Laboratory study and theoretical interpretation, Doctoral Dissertation, Division of Soil Mechanics and Foundation Engineering, Lund Institute of Technology, Lund University, Sweden.

Geier J (2014), Assessment of flows to deposition holes: Main Review Phase. SSM Technical Note 2014:05. Swedish Radiation Safety Authority.

Geier J (2018), Hydrogeology: Modelling of resaturation processes. Part I of this report.

Howell P, Kozyreff G and Ockenden J (2009). Applied Solid Mechanics. Cambridge University Press.

Jacinto AC, Villar M, Ledesma A (2012) Influence of water density on the water retention curve of expansive clays. Geotechnique 62(8):657–667.

Quintessa (2013). QPAC: Quintessa's General Purpose Modelling Code (General Overview). QRS-QPAC-11.

Roscoe KH, Burland JB (1968) On the generalised stress-strain behaviour of 'wet clay'. In: Heyman J, Leckie FA (eds) Engineering plasticity. Cambridge University Press, pp 535–609

Segle P (2015), Review of SKB's creep model, its implementation into ABAQUS and an evaluation of SKB's analyses of the copper canister. SSM Technical Note 2015:52. Swedish Radiation Safety Authority.

SKB (2011), Long-term safety for the final repository for spent nuclear fuel at Forsmark: Main report of the SR-Site project (3 volumes). SKB Technical Report TR-11-01. Swedish Nuclear Fuel and Waste Management Co.

Tang A-M, Cui Y-J and Barnel N (2008) Thermo-mechanical behaviour of a compacted swelling clay. Geotechnique, 58, 45-54.

Thatcher KE, Bond AE, Robinson P, McDermott C, Fraser Harris AP and Norris S, (2016). A new hydro-mechanical model for bentonite resaturation

applied to the SEALEX experiments. Environmental Earth Sciences, 75:1-17. DOI 10.1007/s12665-016-5741-z

Thatcher KE (2017). FEBEX-DP: THM modelling. Quintessa report to RWM. QRS-1713A-R2.

Villar MV (2005). MX-80 bentonite. Thermo-hydro-mechanical characterisation performed at CIEMAT in the context of the Prototype Project. CIEMAT/DIAE/54540/2/04. http://www.iaea.org/inis/collection/NCLCollectionStore/_Public/36/083/36083408.pdf

Åkesson M (2013), Conceptual uncertainties and their influence on bentonite hydration. SKB Document ID 1415874. Swedish Nuclear Fuel and Waste Management Co.

Åkesson M, Kristensson O, Börgesson L, Dueck A, Hernelind J (2010), THM modelling of buffer, backfill and other system components critical processes and scenarios. SKB Technical Report TR-10-11. Swedish Nuclear Fuel and Waste Management Co.

Author: Benoît Dessirier
(Dept. of Earth Sciences, Uppsala University, Sweden)

3

Research on Resaturation of Bentonite Buffer – Coupling between Bentonite and Rock

Project number: 3030045-40
Registration number: SSM2017-3021
Contact person at SSM: Jinsong Liu

Abstract

The KBS-3 method, proposed by SKB for disposal of long-lived high-level radioactive waste is a multi-barrier design for a geological repository in crystalline bedrock. Waste canisters would be embedded in a buffer material of unsaturated compacted bentonite and buried in deposition holes in deep tunnels. As the buffer takes up groundwater from the surrounding rock mass, it would swell, sealing any potential gap and forming a low permeability barrier. Bentonite swelling is a complex hydro-mechanical process that would in this case depend on the highly heterogeneous water delivery from naturally occurring rock fractures or through the primary pore system of the host rock. This report presents estimations of buffer saturation times under KBS-3 repository conditions. It assesses more specifically the uncertainty introduced by common modeling assumptions used to represent the bentonite/rock interface of a deposition hole, namely for (i) the degree of flow channeling and its representation in a fracture intersecting a deposition hole and for (ii) the representation of the hydraulic behavior of the bentonite pellet filling used to plug the outer gap between central compacted bentonite blocks and the rock wall. A short synthesis of the lessons learned about in situ saturation of bentonite from two field experiments: the Prototype Repository and BRIE, and the associated numerical modeling is introduced first.

A new numerical modeling study is then presented to estimate the uncertainty on buffer saturation time implied by some modeling assumptions about the bentonite/rock interface. The impact of background intact rock permeability on saturation is estimated with a simple radial model. Saturation via inflow from a single fracture into the buffer is estimated by 3-dimensional models with three different cases: (i) a homogeneous parallel plate fracture, (ii) a rough but fully connected fracture and (iii) a rough fracture including impermeable contact zones. Each modeling case is run alternatively for a fully homogenized equivalent buffer material and for the initial state of the buffer comprising blocks and a pellet-filled outer slot. The pressure on the outer part of the fracture or the rock matrix is simulated at two different reference levels representing respectively the repository construction phase and the longer-term conditions.

One identified behavior is that the pellet-filled slot acts as a fast pathway to distribute the water intake from the fracture onto the outer surface of the inner bentonite blocks until it homogenizes with the nearby blocks, thus amplifying the water intake from the fracture compared to the homogenized bentonite case. A rough but fully connected fracture yields the same buffer saturation estimate as a homogeneous parallel plate. Flow channeling in the fracture near the deposition hole can however affect the buffer saturation time significantly if it strictly constricts the area of the fracture inflow zone on the deposition hole wall. Buffer saturation via matrix flow is likely a viable scenario if the closest mapped inflow point on the deposition hole wall is located more than a meter away. Finally, recommendations are formulated for future work on modeling the water uptake at the bentonite/rock interface of a deposition hole.

Contents

1. Introduction

The KBS-3 method, proposed by SKB for disposal of long-lived high-level radioactive waste such as spent nuclear fuel, is a multi-barrier design for a deep geological repository. The spent fuel assemblies would be packaged into copper canisters to be embedded in a compacted bentonite buffer and put in place in vertical deposition holes in a deep crystalline formation. Compacted bentonite blocks and rings would directly surround the canisters and the interstitial gap between the blocks and the rock wall would be filled with bentonite pellets right before the deposition tunnel is backfilled (SKB, 2010).

A potential candidate for this buffer material is MX-80 bentonite, which is a sodium clay with a high content of montmorillonite that grants it an expansive/swelling behavior as it hydrates. In a confined volume such as a deposition hole or tunnel, this behavior would first seal any potential gaps and then result in the development of a swelling pressure that depends, among other factors, on the dry density of the compacted buffer (Karnland et al., 2006). The time evolution of the buffer saturation and swelling would be highly dependent on the groundwater flow from the host rock to the deposition hole. Making predictions on the buffer saturation process is a complex task that requires detailed knowledge of unsaturated flow in both the rock mass surrounding a deposition hole and in the buffer itself. The challenges arise both from the natural variability of the natural host rock and from the coupling of thermo-hydro-mechanical processes in the buffer.

The interface between the rock and the buffer is a zone of particular complexity. On the bentonite side, one can wonder about the actual time required for the pellet filling of the outer slot to homogenize with the bentonite blocks and about its hydraulic impact until then. It is not immediately clear what the final density distribution in the buffer will be especially with potential deviations from the nominal alignment and centering, and from the targeted initial density for the loose pellet filling. The high initial suction of unsaturated bentonite can cause a temporary desaturation of the pore space of the adjacent rock matrix or intersecting rock fractures. The distribution of inflow points or zones across the deposition hole wall and the associated inflow rates is not easy to determine and can have a very significant impact on the final saturation time (Dessirier et al., 2016).

Understanding the saturation time for the bentonite buffer can inform on correct buffer design and on suitability criteria for potential deposition holes to guarantee adequate levels of safety, which has motivated several in situ experiments to observe the saturation of compacted bentonite in contact with fractured crystalline rock. Parallel modeling efforts have tried to identify and quantify the sources of uncertainty on the buffer saturation time. One recent endeavor that deserves a specific mention is the Bentonite Rock Interaction Experiment (BRIE) that took place at the Äspö Hard Rock Laboratory and was led in conjunction with a common modeling task (#8) for the SKB Task Forces on Engineered Barrier Systems and on Modeling of Groundwater Flow and Transport of Solutes (Fransson et al., 2017; Vidstrand et al., 2017).

The current report will start by a short review of the lessons learned from the BRIE project and from another relevant experiment on buffer saturation in the context of the KBS-3V method, the Prototype Repository. It will then describe a new analysis

undertaken to identify the level of uncertainty on the estimation of the buffer saturation time implied by common modeling assumptions used to simplify the treatment of the bentonite/rock interface. This modeling study consists of two parallel parts: (i) a simplified quantification of the expected saturation time for a deposition hole in the absence of significantly flowing fracture, and (ii) an estimation of the saturation time for a deposition hole intersected by a single fracture. The latter part focuses on identifying the impact of different degrees of channeling in the fracture near the deposition hole and the impact the homogenization time of the pellet-filled outer slot near the interface.

2. Review of two experiments with in situ saturation of compacted bentonite

2.1. Prototype repository

The prototype repository at the Äspö Hard Rock Laboratory is a full-scale experiment designed to illustrate the performance of the KBS-3V concept and support the license application for a final repository. A 64 m-long deposition tunnel with six deposition holes was built at an average depth of 450 m and filled with artificially heated canister replicas, a buffer of compacted MX-80 bentonite and a tunnel backfill consisting of crushed rock and bentonite all sealed with two concrete plugs in order to separate two different sections of the experiment (Figure 1). The inner section of the tunnel with four deposition holes was designed to remain in field conditions for 20 years and started operating in 2001. The outer section of the tunnel with two deposition holes was designed for a shorter exposure to repository conditions, put in place in 2003 and dismantled after approximately seven years (Svemar et al., 2016).

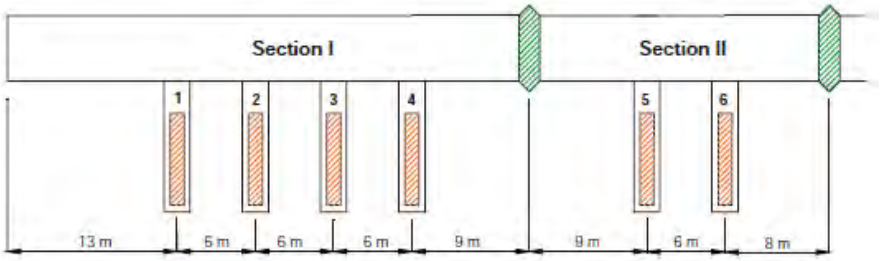

Figure 1. schematic layout of the prototype repository (Figure 5-2 reproduced from Svemar et al., 2016).

While the backfill was essentially fully saturated and there was strong indications that the buffer had started to saturate from the top, large parts of the lower sections of the buffer were still dry when the outer section was dismantled (Figure 2; Svemar et al., 2016; Johannesson, 2014). Many retrieved blocks show a lower water content near the center, which is consistent with a water delivery at the rock wall. The models calibrated on deposition hole inflow with a conceptual model relying on homogeneous inflow through a homogeneous background rock were shown to systematically predict a buffer near full saturation which was not consistent with the field observations. Models need to consider more discretely distributed sources of inflow at the deposition hole wall to match observed saturation patterns. The summary report on the work on the outer section of the prototype repository has the following quote regarding the hydrogeological modeling associated with the hydrogeological modeling:

> *"Remaining work of scientific interest is the development of discrete images of the hydraulic properties in the rock that can fit better the measured and*

observed variation of buffer saturation in the two deposition holes respectively." (Svemar et al., 2016, page 4)

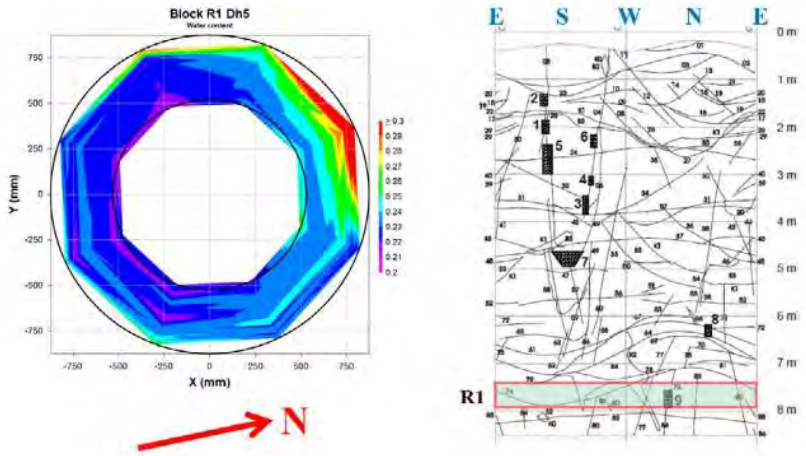

Figure 2. Example of water content at dismantling of the outer section of the prototype (Figure 5-3 reproduced from Johannesson, 2014). For reference the blocks are installed with an initial water content of 0.17.

2.2. Bentonite Rock Interaction Experiment (BRIE)

BRIE was a small scale in situ experiment led from 2010 to 2016 at the Äspö Hard Rock Laboratory. It started by a site selection and characterization phase prior to drilling two 3 m-long deposition holes of 30 cm in diameter to be filled with bentonite blocks left to saturate naturally for a period of approximately two years. The intent was to design a simplified experiment, without thermal processes or pellet gap, to test the understanding and predictions of models against observations of the early onset of buffer saturation. The rock characterization phase consisted, among other tests, of hydraulic tests in exploratory boreholes (76 mm in diameter), weir and sorbing mat measurements of tunnel inflows as well as laboratory measurements on rock cores and inflow mapping over the expanded selected deposition hole walls, the so-called "nappy test" by means of a novel equipment (Fransson et al., 2017). One objective was to test the feasibility and usefulness of different types on characterization data to perform buffer saturation time predictions.

The bentonite saturation process was monitored by embedded relative humidity, total and pore pressure sensors. The two bentonite columns were later extracted along with the outer rock wall and an extensive set of samples was analyzed in the laboratory for density and water content. A large part of the bentonite columns could be retrieved without significant damage to their outer surface which allowed a detailed photo-documentation of the bentonite surface (the so-called "bentographs", Figure 3). The photos clearly show the presence of known as well as uncharted intersecting fractures that led the onset of buffer saturation, and the darkness level of the photos seemed to correlate positively with water content which made a detailed reconstruction of the water content near the bentonite surface possible (Figure 3 and Dessirier et al., 2017a). The irregularity of the darkness patterns along the fracture traces seems to indicate a significant level of flow channeling in the intersecting fractures. Relative humidity measurements could also be performed in the dismantled rock

wall, which allowed the identification of a persistent desaturation of the latter near the interface, beyond the first year of contact between the rock and the bentonite.

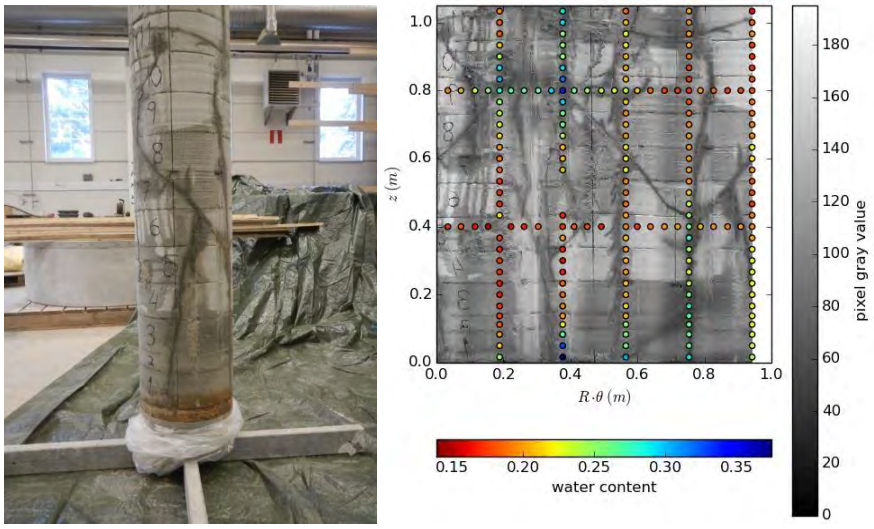

Figure 3. (left) Post-mortem photo-documentation of the bottom of the bentonite column retrieved from BRIE-hole 18 and (right) overlay of the assembled photo grey tones and the surface bentonite samples analyzed for final water content (Illustrations reproduced from Dessirier et al., 2017a, Photo credits: Mattias Åkesson).

The modeling work in the Äspö Task Forces associated with BRIE, consisted of several subtasks (Vidstrand et al., 2017): (i) scoping calculations for bentonite saturation time, (ii) modeling of the tunnel inflows at the experimental site, (iii) predictive modeling of deposition hole inflow and bentonite saturation with limited and later (iv) with more detailed structural information near the deposition hole walls, and finally (v) a limited inverse modeling task once the sensor and post-mortem data were made available. Several teams attempted this modeling exercise with different conceptual models for the rock mass ranging from pure DFN approaches to continuum representations (e.g Dessirier et al, 2017b). The conclusions from this modeling exercise were the following:

- the permeability near the rock wall had to be set near 10^{-20} m^2 in models including a continuous representation of the near rock domain in order to avoid over-predictions of the water content,
- no tested rock matrix model could convincingly sustain the rock wall desaturation that was observed post-mortem in BRIE without calibration,
- detailed identification of the positions of intersecting flowing fractures was necessary to reproduce sensor data series,
- structural information near the rock wall had a higher positive impact on the quality of the predictions than detailed hydraulic characterization of the fractures.

3. Scenario analysis of buffer saturation times

3.1. Rationale and Objectives

Experiments on flow and transport in fractured rock masses have shown indications of a strong channeling effect taking place on different scales (e.g. Tsang and Neretnieks, 1998; Black et al., 2017). At the scale of a single fracture, the variations of the fracture aperture generally determine a handful of pathways of least resistance, which tend to concentrate the vast majority of the flow. On a larger scale with a network of fractures, the larger fractures form dominant long-ranging hydraulic connections that also tend to produce strong channeling. It is striking that none of the models that have been reported for groundwater flow and buffer saturation at the Prototype repository and BRIE had a particular focus on flow channeling. The examples of fractures intersecting deposition holes are systematically introduced as parallel plates, or thin homogeneous volumetric domains, despite signs in the bentographs, for example, that different points along the trace of an intersecting fracture may have seen great variations in water delivery from the rock to the bentonite (Figure 3).

This report presents a new modeling analysis that focuses on a real-size canister deposition hole and on the time required for the ring-shaped blocks of the buffer mass to reach near full saturation. The objective is to assess the impact on the predicted buffer saturation times of commonly applied modeling assumptions (see e.g. Åkesson et al., 2010) near the bentonite/rock interface, regarding the degree and representation of flow channeling near a deposition hole intersection with a flowing fracture and the homogenization state of the outer slot that is filled with bentonite pellets.

3.2. Model development, interface features and processes

In order to quantify the impact of modeling assumptions on predicted saturation times, this study distinguishes two different saturation modes:

- Mode I: buffer saturation from rock matrix flow only and
- Mode II: buffer saturation solely based on inflow from a single intersecting fracture.

The complex Thermo-Hydro-Mechanical (THM) processes governing buffer saturation are simplified in this study as a purely hydraulic process in order to obtain preliminary estimates and an understanding of the system through a relatively simple model. Thermal and mechanical processes including deformations in the buffer could be incorporated for future studies.

Regardless of the saturation mode, flow in both unsaturated bentonite and rock matrix or fracture is represented by Richards' equation:

$$n\frac{\partial S_l \rho_l}{\partial t} = \nabla \cdot \left(\frac{k_{sat} k_r(S_l) \rho_l}{\mu_l} \nabla [P_c(S_l) + P_{atm}] \right)$$

where n is the material porosity, S_l is the liquid saturation, k_{sat} is the saturated permeability, k_r is the relative permeability, μ_l the fluid viscosity, P_c the capillary pressure and P_{atm} the atmospheric pressure. This flow equation of flow has been shown to give similar predictions to a set of coupled two-phase liquid and gas mass-balance equations for predictions up to saturation levels of 0.9 (Dessirier et al., 2014).

Saturated flow is handled by switching the variable to the liquid pressure P_l and by solving the classical Laplacian equation for saturated groundwater flow. The implementation in TOUGH2 – equation of state 9 was used to obtain the flow solutions (Pruess et al., 1999). The pre- and post-processing was done using the PyTOUGH scripting library (Croucher, 2011).

The van Genuchten parameterization is used for the relative permeability function (van Genuchten, 1980):

$$k_r(S_l) = \sqrt{S_l} \left[1 - \left(1 - S_l^{1/\lambda} \right)^{\lambda} \right]^2$$

and for the retention curve (van Genuchten, 1980):

$$P_c(S_l) = -P_0 \left(S_l^{-1/\lambda} - 1 \right)^{1-\lambda}$$

The values used for the equation parameters are summarized in Table 1 for all the material considered in this study and the associated reference curves are plotted in Figures 4 and 5.

Each modeling case is considered in two versions:

- One where the bentonite is inserted and remains as two different materials, pellets and blocks, throughout the whole simulation, denoted as “pellets and blocks” or “p&b”,
- One where the homogenization is considered to happen rapidly and the bentonite is inserted as a single homogenized material directly at the installation time, denoted as “homogenized” or short-handed as “hom” in some figure legends.

These two simplified scenarios are intended to illustrate the uncertainty on water uptake at the bentonite/rock interface induced by the treatment of the swelling and homogenization of the bentonite near the interface. Defined as two extremes these two versions can give a prediction interval for the actual expected buffer saturation time.

The parameter values described in Table 1 are based on the nominal buffer design for bentonite ring blocks, pellet filling and installed homogenized properties described in SKB (2010). For reference, the parameter values used for the BRIE experiment are also indicated (Fransson et al., 2017).

For the rock matrix a reference value is indicated in Table 1 that corresponds to typical fitted values for the background rock near the deposition holes used in modeling the BRIE experiment (Dessirier et al., 2016) and that correspond to the low range of

permeability measurements obtained on rock cores from the BRIE boreholes (Fransson et al., 2017). The saturated permeability of the rock is then systematically varied to obtain the corresponding buffer saturation time by matrix flow (see upcoming specific Mode I section). When the value for the saturated permeability of the rock is changed from its reference value, the entry pressure P_0 is scaled by the following relationship (Leverett, 1941):

$$P_0(k_{sat}) = P_{0,ref}\sqrt{k_{sat,ref}/k_{sat}}$$

It is interesting to note that Richards' equation can be expressed in the form a diffusion equation where the diffusion coefficient D is dependent on saturation that is the unknown in this case and is expressed as a combination of material's permeability and the derivative of the capillary pressure curve (Vidstrand et al., 2017):

$$D(S_l) = \frac{k_{sat}k_r(S_l)}{n\,\mu}\frac{\partial P_c}{\partial S_l}$$

The corresponding apparent diffusivity is represented in Figure 6 as a function of saturation for the different considered materials. One can interpret the apparent diffusivity as a ranking of the propensity of each material to homogenize its liquid saturation. One can for example state that its larger permeability dominates the loss in capillarity in the fracture resulting in an overall higher capacity to transport moisture, whereas the relatively strong capillary forces in the rock matrix do not compensate the decrease in relative permeability, resulting in a net loss of apparent moisture diffusivity as saturation goes down. It is also noteworthy that the adopted representation for the bentonite pellet filling has a higher moisture diffusivity that the compacted blocks, which qualitatively implies that the pellet filling of the outer slot will likely distribute the water delivery from the fracture trace onto a larger surface of the bentonite blocks until it homogenizes.

Table 3. Reference values for hydraulic parameters.

Material	Poro-sity n	Saturated perm. k_{sat} [m^2]	Rel. perm. k_r	Dry density ρ_d [kg/m^3]	Initial sat. $S_{l,i}$	vG parame-ter λ	Entry pres-sure P_0
KBS-3 bentonite ring block	0.36[2]	3e-21[3]	S_l^4 [c]	1779[a]	0.79	0.28[c]	1.46e7
KBS-3 bentonite pellets	0.68[a]	3e-19[b]	S_l^4 [c]	884[a]	0.22	0.28[c]	1.46e6
KBS-3 homoge-nized ring block	0.438[a]	6.4e-21[c]	S_l^4 [c]	1577[a]	0.6	0.28[c]	1.0e7[c]
BRIE bentonite blocks	0.438[4]	6.4e-21[c]	S_l^4 [c]	1562[c]	0.42	0.28[c]	1.0e7[c]
BRIE Rock ma-trix	0.009[c]	3.0e-21[c]	vG[c]	-	from pre-run	0.24[c]	6.0e5[c]
Rock fracture	0.005[5]	1.e-14[d]	vG[d]	-	from pre-run	0.56[d]	8.8e3[d]

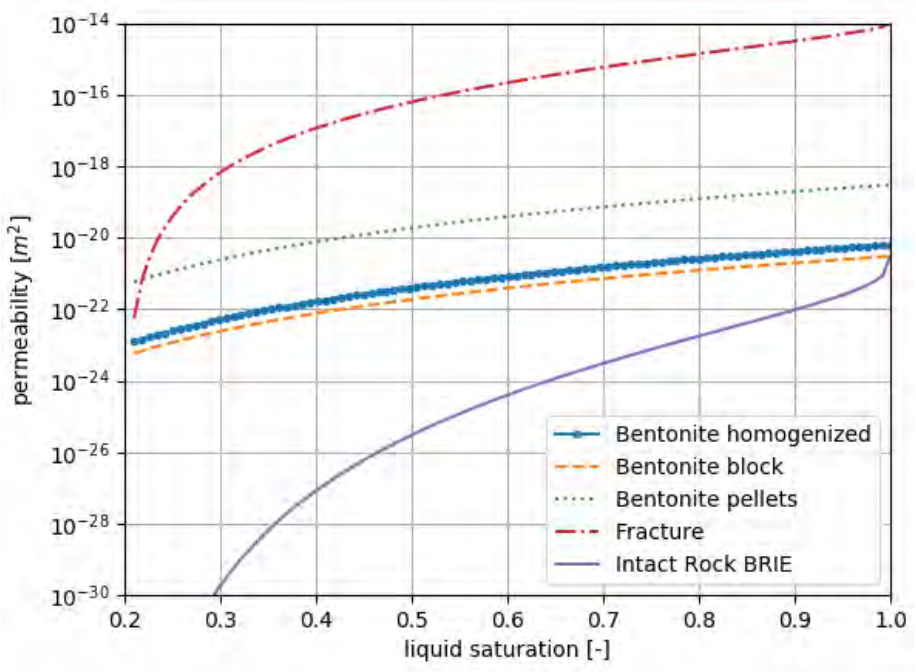

Figure 4. Reference absolute permeability curves.

[2] SKB (2010)
[3] Karnland et al. (2006)
[4] Fransson et al. (2017)
[5] Jarsjö et al. (2017)

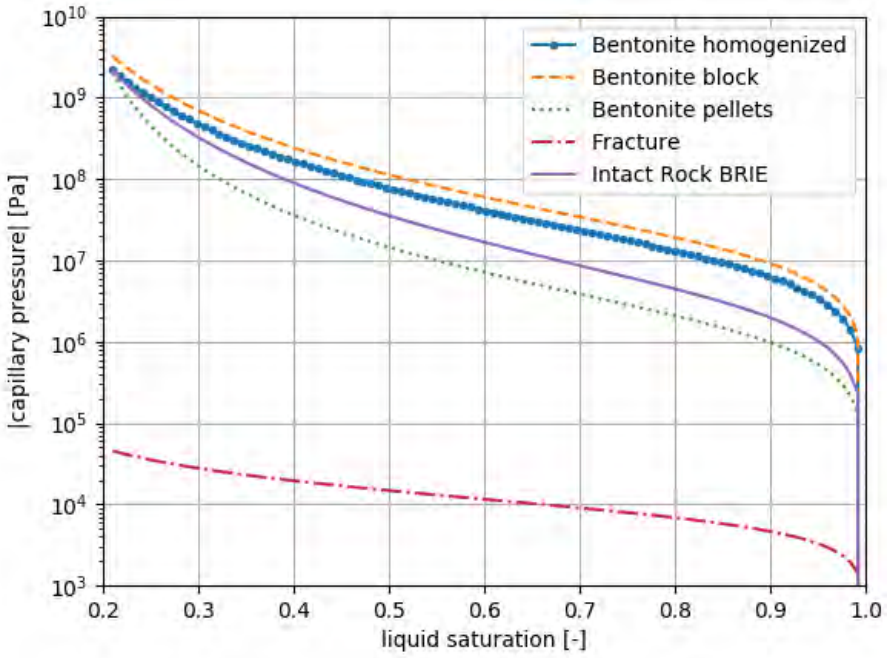

Figure 5. Reference retention curves.

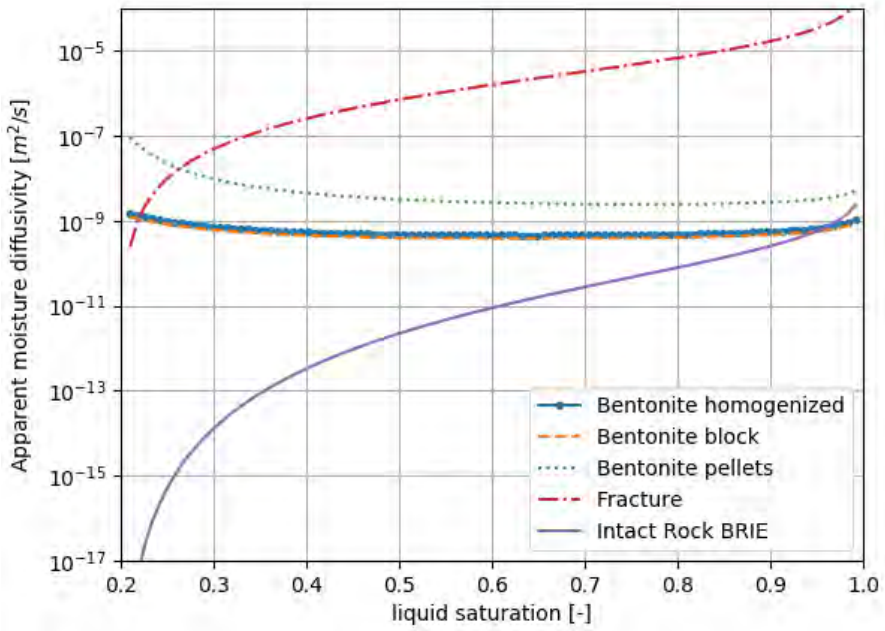

Figure 6. Reference apparent moisture diffusivity curves.

3.3. Saturation mode I: matrix flow

The first mode of saturation is through the intact rock matrix only, which could be relevant for a dry zone of a deposition hole that is not intersected by any local flowing fractures. In this case, the flow domain is restricted to the ring-shaped buffer domain surrounding the canisters and conceptualized as a radial model with cells representing the bentonite blocks between radii of 0.535 and 0.825 m, the pellet filling between radii of 0.825 and 0.875 m and a homogeneous rock matrix between 0.875 and 3.0 m.

The far boundary at r=3.0 m is set to full saturation with a constant pressure. The idea is that this far boundary is where the intact rock connects with a branch of a fracture network that has good connectivity and can act as a stable source that delivers with constant pressure. A working value of 1 MPa (100 m of head above borehole pressure) is adopted as it lies within the range of observation borehole pressures at the BRIE site (Dessirier et al., 2016; Fransson et al., 2017). This represents the case where the fracture network is still affected by neighboring tunnels that have not yet been backfilled. An alternative version of each modeling scenario is also carried out with an outer pressure of 5 MPa which corresponds to the natural hydrostatic pressure at 500 m depth, which is the approximate depth envisioned for a repository. This case corresponds to the situation of a part of the repository that has recovered its natural pressure level. The underlying idea is to apply both boundary conditions in the same way to Mode I and Mode II in order to compare the expected saturation times under both scenarios. A pre-simulation is run to obtain initial conditions for the rock domain (see example in Figure 7). For this initial run, the bentonite cells are set to conditions representing an open ventilated deposition hole, i.e. unsaturated conditions with a capillary pressure of approximately -1 MPa which is in the middle of the range of equivalent suctions used by Dessirier et al. (2015). The pre-run is ended when a steady state is reached. The applied suction at the deposition hole wall generates a desaturation of the rock wall over a few decimeters (Figure 5).

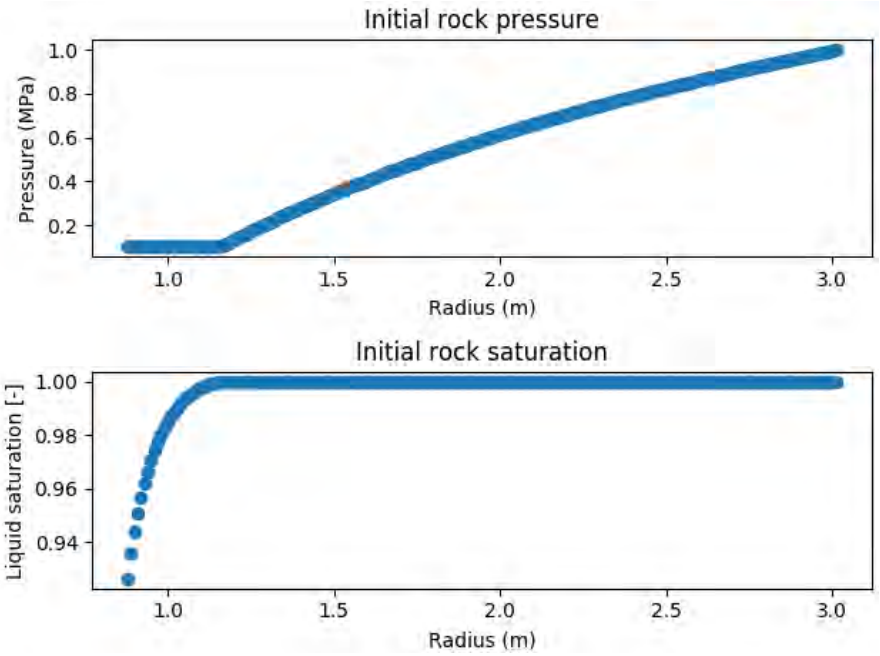

Figure 7. Initial state calculated by the pre-run for the reference rock matrix parameter values (Table 1).

After the pre-run, the bentonite saturation process is initialized by setting the bentonite cells either to the blocks and pellets material properties or to the radially homogenized equivalent properties and initial saturation (see Table 1). The simulation is conducted until the last cell in the buffer reaches a saturation level of 0.9.

By systematically varying the saturated rock permeability in the model from 10^{-21} to 10^{-18} m^2 one can estimate the expected saturation time purely through matrix flow (Figure 8). One can, first of all, notice that the assumptions of the homogenization time of the bentonite plays a minor role in determining the time to near saturation by

matrix inflow. As we look at the time to saturate the innermost buffer cell and that the radial nature of the model preempts any axial or lateral redistribution of the flow, the mass of water ending up in at the innermost cell will have to flow the same distance through pellets and blocks or through a homogenized equivalent material. It is thus not surprising that segregated and homogenized model perform similarly for a radial flow prediction. It is worth commenting on the investigated range of intact rock permeabilities in light of the experience from the BRIE project. Initial permeameter measurements on de-stressed rock cores from BRIE exploratory boreholes (oriented vertically) were reported to range from $6 \cdot 10^{-21}$ to $5 \cdot 10^{-19}$, with a median value around $2 \cdot 10^{-20}$ m^2. Later tests on samples taken in the direction normal to the rock/bentonite interface yielded significantly lower values from $2 \cdot 10^{-22}$ to $5 \cdot 10^{-20}$ with a median at $4 \cdot 10^{-21}$ m^2. Assuming these values are representative of potential conditions at a future repository and according to this simple radial model, the range of saturation times from pure matrix flow could range from a half a decade to several centuries.

These predicted ranges are relatively similar to the ranges reported by Åkesson et al. (2010) for unfractured deposition holes despite the absence of thermal processes in the present model (a feature included in their work), minor differences between the adopted hydraulic parameters and the fact that their predictions are expressed for a target saturation of 0.99 and for a whole set of ring and cylinder blocks.

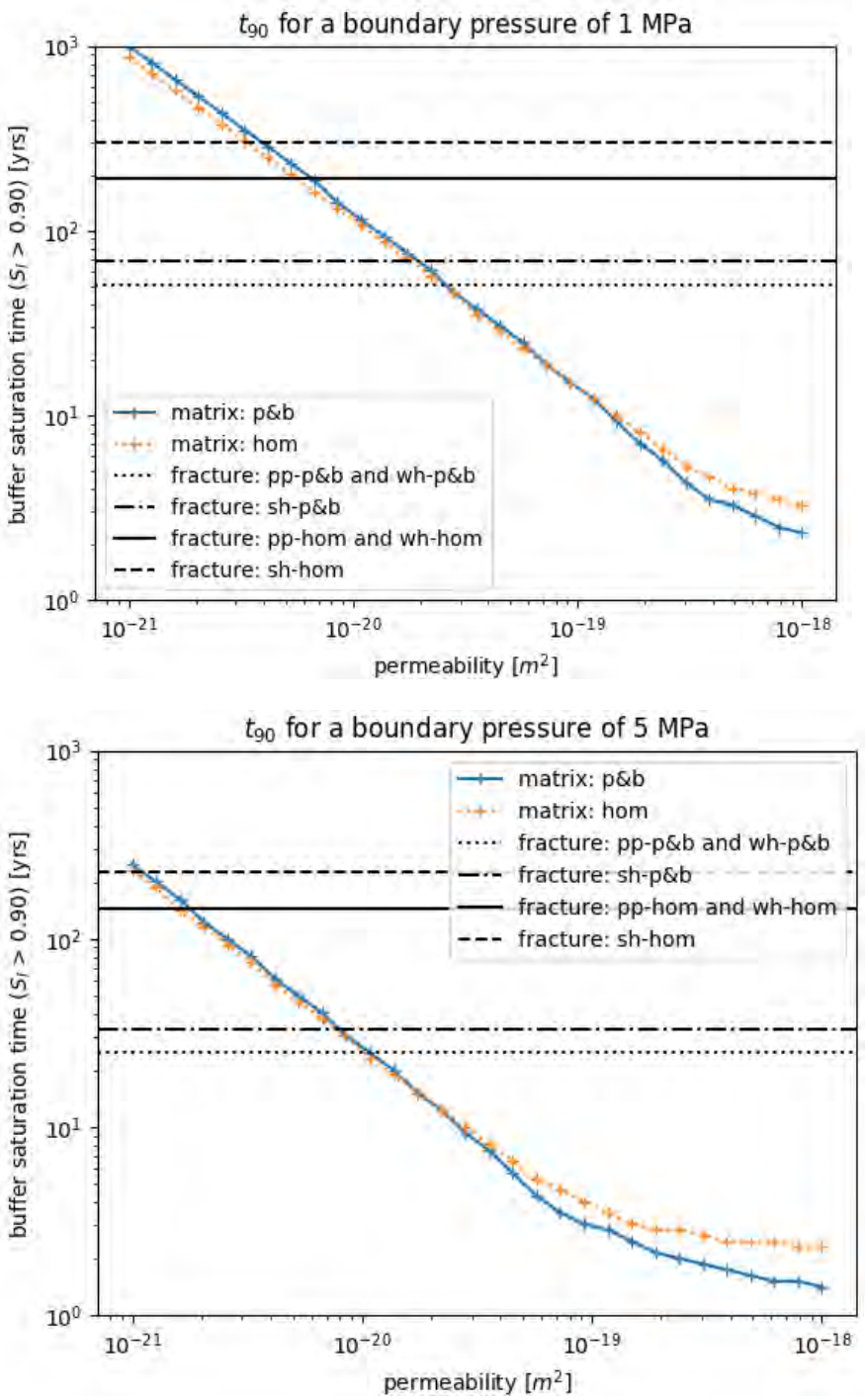

Figure 8. Buffer saturation time as a function of the intact rock matrix permeability and several scenarios of fracture flow for a boundary pressure of 1 MPa (top) and 5 MPa (bottom).

3.4. Saturation mode II: inflow from intersecting fracture

The second mode neglects any rock matrix flow and is based solely on water delivery through a single intersecting fracture. The selected fracture for these simulations

have a transmissivity of 10^{-10} m^2/s, which would be likely to pass the tentative suitability criteria for a deposition hole based on a maximum inflow of 0.1 liter/min for example. It has an arbitrarily chosen dip angle of 45°.

The flow in the fracture is described by Richards' equation as presented for Mode I and also numerically solved with the TOUGH2 code. Unsaturated equivalent parameters for the van Genuchten curves are estimated according to the methodology of Jarsjö et al. (2017) assuming a hydraulic parallel plate mean aperture of 5 µm which was estimated to correspond to an approximate mean logarithmic mechanical aperture $\mu_{ln\,a}$ of -5 (a expressed in mm) and a standard deviation $\sigma_{ln\,a}$ of 0.8, which yielded the reference values of $\lambda = 0.56$ and $P_0 = 8{,}8 \cdot 10^3$ Pa presented in Table 1. The programs GMSH (Geuzaine and Remacle, 2009) and voro++ (Rycroft, 2009) were used to mesh the fracture with a typical element size of 0.1 m near the deposition hole and 0.7 m near the outer boundary, and to build the TOUGH2 meshes. The fracture elements are represented by 1 mm plates with an average porosity value of 0.005.

This second mode is divided into three alternative cases whereby the fracture is described as:

- a fully connected, homogeneous parallel plate, denoted "parallel-plate" or "pp" (Figure 9)
- a fully connected plate with variable aperture denoted as "weak heterogeneity" or "wh", implemented here uncorrelated lognormally distributed apertures (a single realization is considered that is displayed in Figure 10) and
- a plane with the same variable aperture as the previous case but with additional contact areas that are considered fully closed accounting for 40% of all the fracture cells, denoted as "strong heterogeneity" or "sh" (Figure 11).

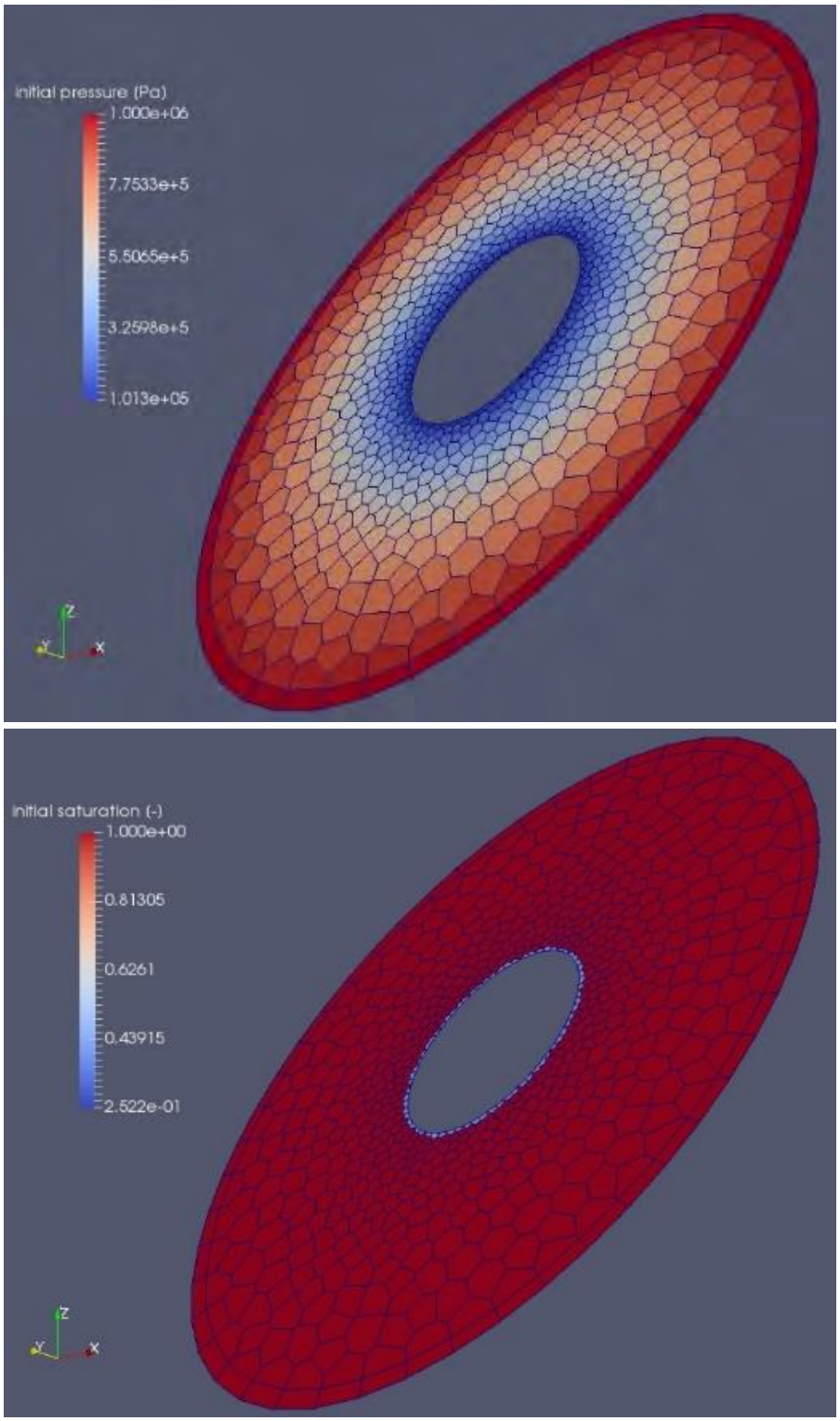

Figure 9. Initial pressure (top) and saturation field (bottom) and in the fracture under case “parallel plate”.

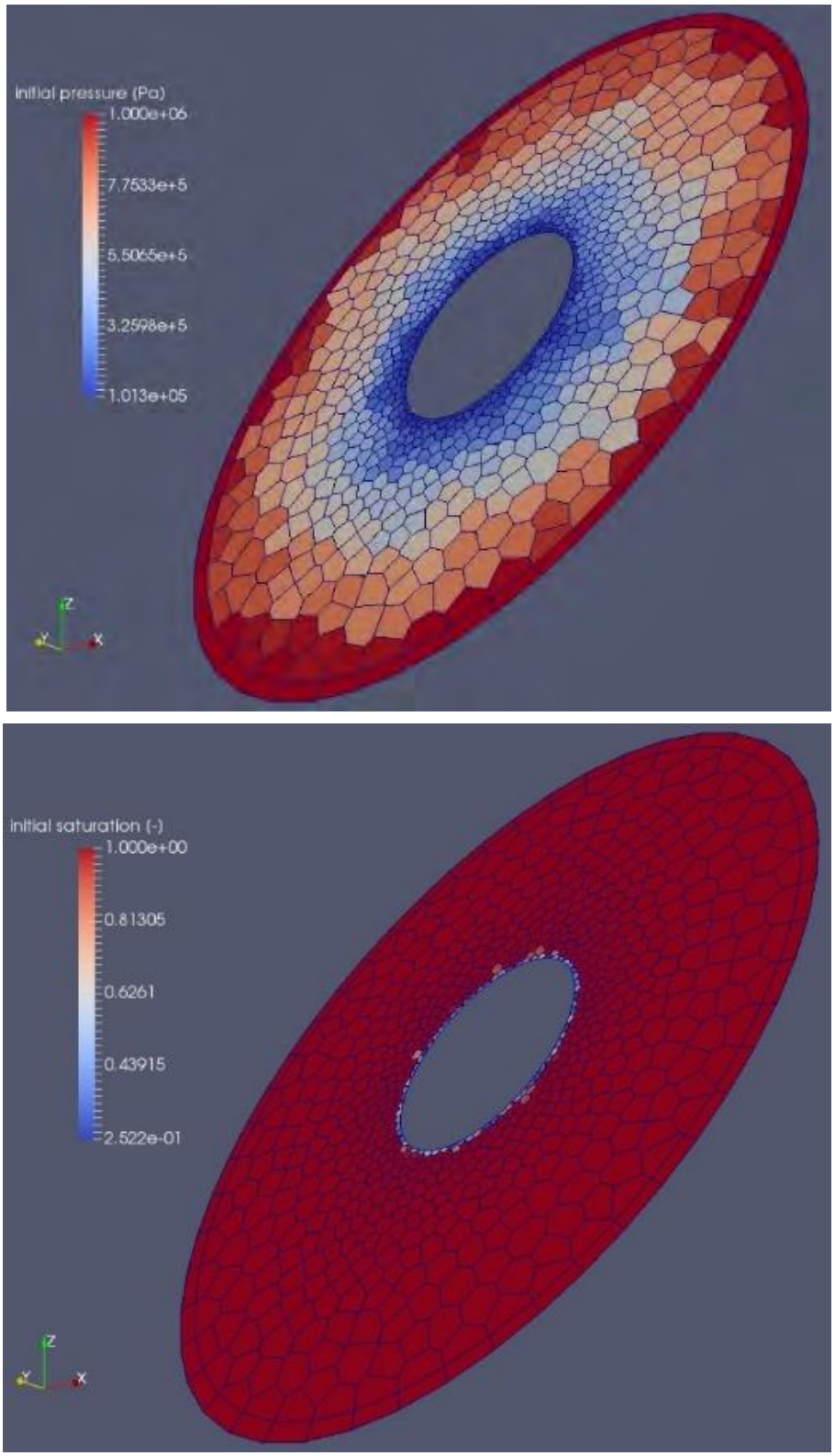

Figure 10. Initial pressure (top) and saturation field (bottom) in the fracture under case “weak heterogeneity”.

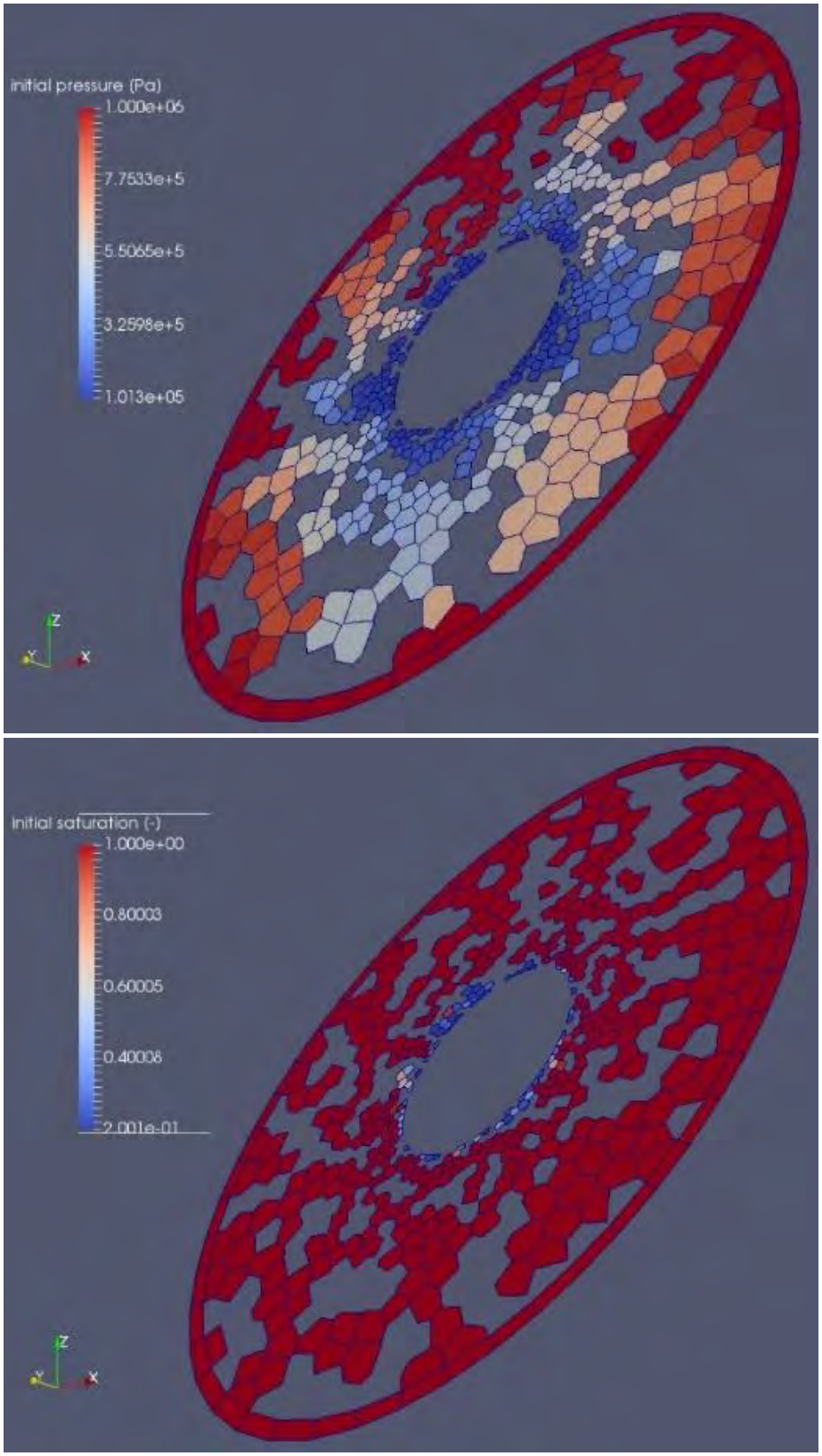

Figure 11. Initial pressure (top) and saturation field (bottom) for case “strong heterogeneity”.

Similarly to Mode I, the outer boundary cells are set at a saturated pressure of 1 MPa (or alternatively 5 MPa), signifying that they are well connected to a wider fracture network and act as a stable pressure water source. The inner cells representing the open deposition hole are set to a capillary pressure of -1 MPa to represent the equivalent suction of a ventilated deposition hole and tunnel before bentonite installation. The corresponding pressure and saturation fields obtained after the pre-run are shown in Figures 9, 10 and 11 and act as initial conditions for the following bentonite saturation runs.

(It was verified that the numerical flow solution gave the same inflow as the Thiem well equation for a horizontal parallel plate fracture and an inner boundary conditions representing saturated liquid phase at atmospheric pressure.)

In the case of a parallel plate fracture of transmissivity 10^{-10} m^2/s with a dip angle of 45°, the fracture flow rate into the open hole was calculated at $4.73 \cdot 10^{-8}$ m^3/s for an outer pressure of 1 MPa (respectively $2.54 \cdot 10^{-7}$ m^3/s for an outer pressure of 5 MPa). For the two heterogeneous cases the geometric mean of the element transmissivities was calibrated to yield the same deposition hole inflow rate as the parallel plate case to make the cases directly comparable. The distribution of non-zero cell inflow rates along the fracture intersection with the borehole is shown in Figure 12. One can observe that the inflow is almost perfectly evenly distributed in the parallel plate case and that the median remains the same with little dispersion in the weak heterogeneity case. On the contrary, in the strong heterogeneity case, a single cell is responsible for more than 25% of the total inflow, and the top three inflow cells together account for approximately 50% of the total inflow (Figure 12).

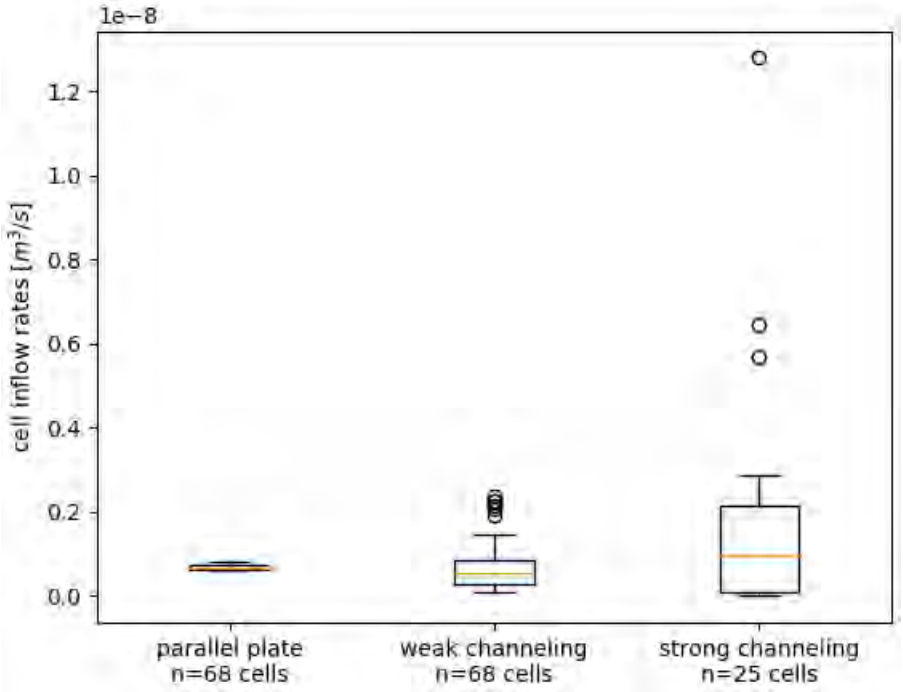

Figure 12. Distribution of deposition hole inflow rate per cell in the three different fracture cases for a boundary pressure of 1 MPa.

The mesh is then extended to represent the bentonite buffer for a total height of 5 m and between radii of 0.875 and 0.535 m (SKB, 2010). The new mesh is cylindrical with a cell size of 0.2 m in the vertical and tangential direction to the bentonite rock

interface on the outer surface, and from 0.01 m radially near the interface up to 0.07 m at the innermost part near the canister. The mesh is also refined in the lateral direction to 0.1 m to conform with the fracture mesh near the interface.

The bentonite saturation predictions are then calculated by combining the three fracture cases: parallel plate, weak heterogeneity and strong heterogeneity (visualized from top to bottom in Figures 13, 14 and 15) with the two previously defined bentonite installation versions: homogenized vs. pellets and blocks (visualized from left to right in Figures 13, 14 and 15).

All six modeling cases are carried out until the last buffer cell has reached a target saturation of 0.9 considered as near-full saturation. The corresponding times denoted t_{90} are summarized for all scenarios (and boundary pressures) in Table 2 and also represented in Figure 8 for comparison with the buffer saturation times via matrix flow.

Table 4. Time to reach a saturation level of 0.9 in the last cell in each modeling scenario for an outer pressure of 1 MPa (resp. 5 MPa).

t_{90} (yrs) for a boundary pressure of 1 MPa (resp. 5 MPa)	Homogenized	Pellets & Blocks
Parallel plate	191 (145)	51 (25)
Weak heterogeneity	191 (145)	51 (25)
Strong heterogeneity	300 (228)	69 (33)

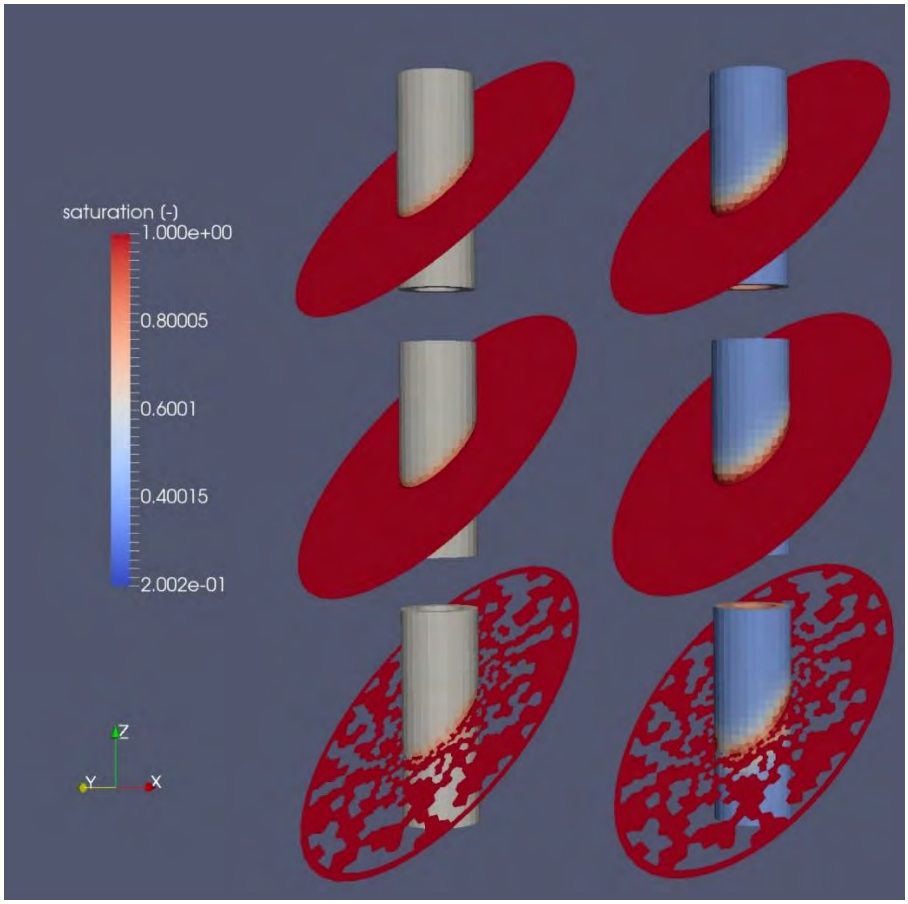

Figure 13. Saturation one year after installation in the six reference cases with an outer pressure of 1 MPa (from left to right: hom vs p&b; from top to bottom: pp, wh, sh).

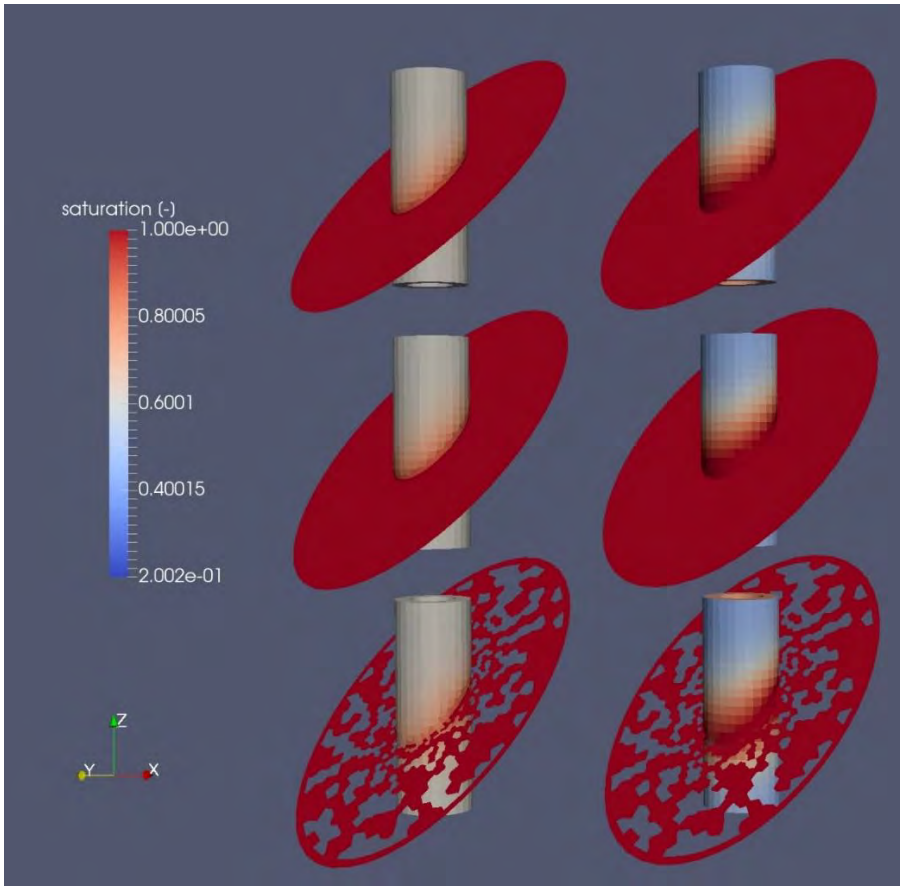

Figure 434. Saturation 12 years after installation in the six reference cases with an outer pressure of 1 MPa (from left to right: hom vs p&b; from top to bottom: pp, wh, sh).

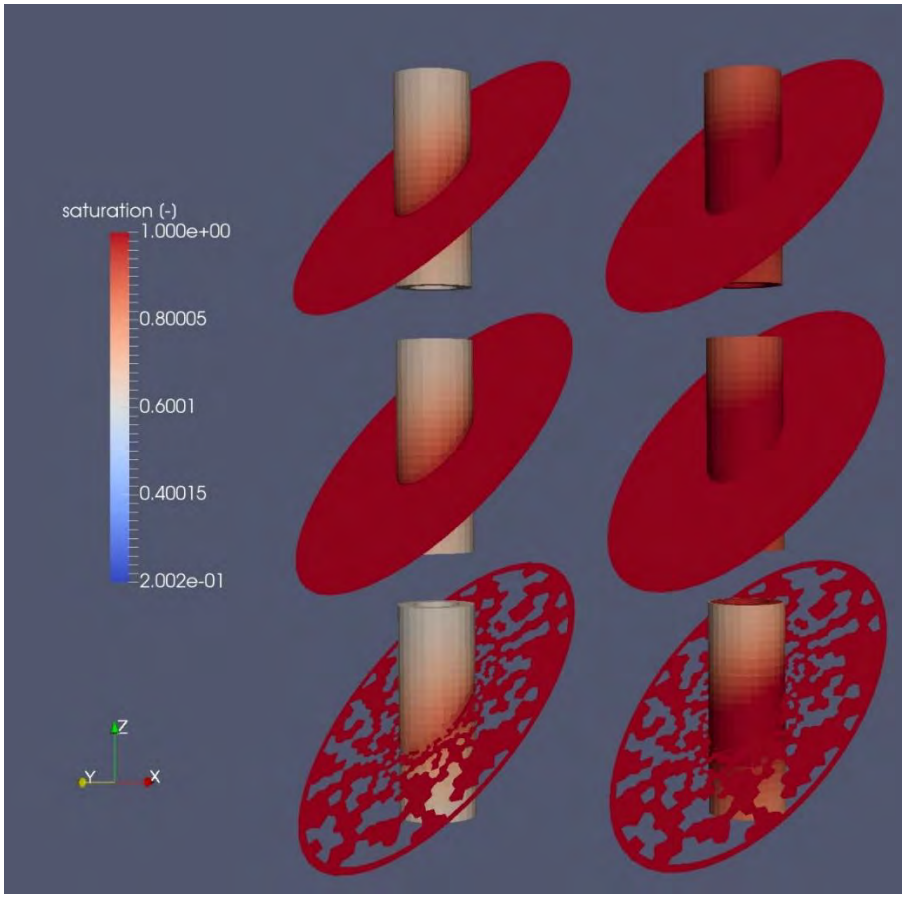

Figure 15. Saturation 50 years after installation in the six reference cases with an outer pressure of 1 MPa (from left to right: hom vs p&b; from top to bottom: pp, wh, sh).

One can see by comparing the saturation times for both boundary cases that the outer boundary pressure has a clear effect on the water uptake at the bentonite but that the relationship is not proportional: the time to near saturation is decreased by approximately half for the cases with pellets and blocks and by approximately 25% for the homogenized cases for an increase in boundary pressure by a factor five. It can also be observed that the fracture quickly recovers from the initial desaturation, as could be conjectured from the comparison of the apparent moisture diffusivities in the fracture and the bentonite (Figure 6). It then rapidly reaches an average pressure very close to the value applied at the outer boundary and almost all the head drop is concentrated across the bentonite. In other words, the water uptake seems for a large part driven by the buffer's capacity for water uptake and for a lesser part on the ambient pressure conditions of the natural fracture system.

Another direct observation is that the parallel plate case and the weak heterogeneity case produce outcomes that are virtually indistinguishable in terms of buffer saturation times. This can again be understood if one considers that the water uptake at the interface is not limited in this case by the fracture properties but by the uptake capacity of the bentonite. The contrasts in pressure in the fracture are overshadowed by the hydraulic gradient in the saturated bentonite region directly near the fracture inlet. What can have an effect however is a reduced interface area between the fracture and the bentonite as is the case in the strong heterogeneity scenario. One can see in Figure 12 that the number of flowing cells and thus the contact area between the

fracture and the bentonite is reduced by half by considering contact areas in the fracture that are impermeable for flow. This creates a constriction effect at the interface that has a significant impact on the saturation time of the buffer mass.

The last point to comment on from these results is the difference between the homogenized cases and the cases with pellets and blocks. The difference of the saturation time is nearly a factor 4 between the two sets of scenarios. This can be explained by comparing the apparent moisture diffusivities of the pellet filling and the homogenized material (Figure 6). The pellet slot as parametrized in this study has a much higher apparent moisture diffusivity than the homogenized material and therefore distributes the fracture inflow onto a wider area of the bentonite blocks. The water uptake bottleneck is relocated from the fracture trace to the pellet/block interface with a much larger cross-sectional area, which can explain the speed-up of the saturation process for all fracture scenarios. This phenomenon would counteract the previously described constriction effect possibly caused by closed contact areas of the fracture. This has also been described by Åkesson et al. (2010). This observation has to be nuanced though in light of the simplistic approach used to represent pellets and blocks without explicit treatment the mechanical deformations and the swelling that would occur as soon as the pellet slot would start saturating. It sends however, a strong signal for need of further investigation of the amplification effect of the pellet slot on the estimation of the effective area of inflow zones across the bentonite/rock interface, which seems to play an important role in the saturation process of the whole buffer mass.

4. Discussion

The comparison of Mode I and Mode II makes it possible to discuss the likelihood of deposition holes saturating via fracture inflow or inflow through relatively intact rock. The comparisons of all scenarios in Figure 8 show that even deposition holes intersected by a fracture with a transmissivity of the order of 10^{-10} m^2/s would likely see a non-negligible part of the saturation coming from the relatively intact rock where the nearest fracture inflow point is a couple of meters away. One is then looking at saturation times nearing a couple of centuries.

One can elaborate on the fact that the weak heterogeneity and strong heterogeneity cases were explored with a single realization of the fracture permeability distribution, which limits the reach of systematic conclusions from this analysis. (It is noteworthy to state that the two cases presented in this report share the exact same mesh and permeability field prior to the removal of the contact areas in the case of the strong heterogeneity scenario). Nevertheless, this rapid exploration of alternative conceptual representations of the fracture allowed to hint at the fact that the global time needed to saturate a mass of buffer seems to rely on the total cross-sectional area of hydraulic connections between rock fractures and bentonite, possibly amplified by the pellet-filled slot. A strong model of heterogeneity with closed segments along a fracture trace displays a very significant constriction effect on the bentonite water uptake whereas the same permeability distribution produces negligible differences with a homogeneous parallel plate model if contact areas are not explicitly impermeable.

What was not tested in this analysis, was the role of the rock matrix near the fracture intersection with the deposition hole which could potentially form a parallel saturation mode. The two simplified modes of buffer saturation presented in this report were actually intended to be treated as a single combined model including the bentonite buffer, a single fracture and the surrounding rock matrix (Figure 16). This combined model was not pursued further as it became apparent that it would require a very tangible step up to high-performance computing routines and resources that were deemed outside the reach of the defined project but could be envisaged in the future. Efforts in this direction could allow for evaluating the potential of the intact rock to form a parallel pathway from the fracture trace to further location on the bentonite/rock interface once the fracture has gained significant fluid pressure and the saturated bentonite near the fracture mouth starts acting as the bottleneck. This combined fracture-matrix path could explain the longer times predicted in this study compared to the values reported by Åkesson et al. (2010) on the order of 10 - 30 years for a deposition hole intersected by a fracture at mid-height. Their 2D radial setup considers a horizontal parallel plate fracture and the rock matrix below and above it.

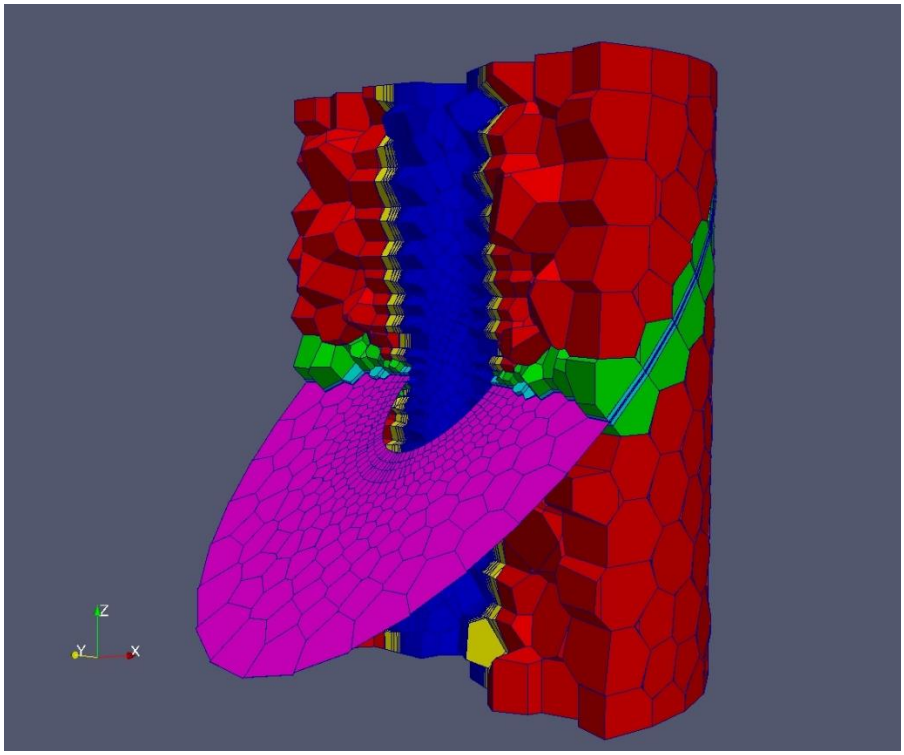

Figure 16. Attempt at a single model including bentonite (blue), fracture (purple), a fracture alteration zone (cyan) and intact rock (red, yellow and green).

Finally, the main limitation to the results discussed here is the purely hydraulic nature of the model when the flow processes, primarily in the buffer but also in the rock mass, can be intricately coupled with thermal and mechanical processes. The most natural extension to strengthen the confidence in the model presented here would be to use the functionality of the TOUGH2 code to handle heat transport and use a coupling scheme with a mechanical model such a FLAC3D (Rutqvist et al., 2011) or Code_Aster (Loschetter et al., 2012) that include a suitable constitutive model for expansive clays such as the Barcelona Basic Model (Alonso et al., 1990).

5. Conclusions and recommendations

This report presented a synthesis of the lessons learned in two past experiments and the associated numerical modeling: the Prototype Repository and BRIE, aimed at investigating the in situ saturation process of a compacted bentonite buffer under repository conditions as envisaged with the KBS-3 method for disposal of spent nuclear fuel. The dismantling of the outer section of the Prototype Repository after seven years in situ revealed fully saturated sections of the buffer near intersections with flowing fractures or from the tunnel backfill at the top of the deposition holes as well as very dry buffer sections where the rock in contact with the buffer had a lower permeability. Modeling and predicting the saturation time for a deposition hole is a complex task and requires detailed knowledge of the distribution of inflow points into the deposition hole. Structural information and location of the inflow spots on the bentonite/rock interface is paramount to get a correct estimation of the saturation time. Models that fit background effective rock permeability against aggregated open deposition hole inflow only have very poor predictive capabilities. Bentonite columns from the BRIE project show uneven water delivery along intersecting fracture traces after approximately two years in situ. Flow models for the BRIE experiments that explicitly represent the intact rock matrix between charted fractures had to adopt rock permeability values in line with the low range of permeameter measurements on rock cores for the intact rock mass near the deposition hole wall to avoid overestimating the speed of the buffer saturation process. Relative humidity sampling of the dismantled rock walls from the BRIE deposition holes showed a de-saturated zone in the rock reaching a couple of decimeters in.

A new analysis is introduced to assess the impact of some common modeling assumptions for features near the bentonite/rock interface on the prediction of buffer saturation time, regarding the background intact rock permeability, the degree and representation of flow channeling in an intersecting fracture and the homogenization time for the pellet filling of the outer slot of the deposition hole. The impact of background intact rock permeability on saturation is estimated with a simple radial model that represents both the initially unsaturated buffer, a de-saturated zone in the rock and the saturated zone of the rock until it is assumed to meet a fracture that is well-connected to a wider network. Saturation via inflow from a single fracture into the buffer is estimated by 3-dimensional models for three different cases: (i) a homogeneous parallel plate fracture, (ii) a rough but fully connected fracture and (iii) a rough fracture including impermeable contact zones. Each modeling case is run alternatively for a fully homogenized equivalent buffer material and for a juxtaposition of two materials representing the properties of the pellets and the blocks as they are installed. The pressure on the outer part of the fracture or the rock matrix is simulated at two different reference levels: 1 MPa, to represent initial repository conditions when neighboring tunnels might still be under construction, and 5 MPa which is more representative of the long term expected value after backfilling and closure of all repository sections.

This simplified study identified the following interface features and processes as causes of significant uncertainty on the saturation time prediction:

- the hydraulic role of the pellet slot during the bentonite homogenization time,

- the flow channeling effect near the fracture intersection, if it is considered that it can reduce the fraction of the fracture trace that can deliver groundwater flow to the bentonite (inflow zone area on the deposition hole wall).

A potential behavior is that the pellet slot acts as a fast pathway to distribute the water intake from the fracture onto the outer surface of the bentonite blocks until it homogenizes with the same nearby blocks.

Buffer saturation via matrix flow is likely a viable scenario if the closest mapped inflow point on the deposition hole wall is located more than a meter away.

Based on these considerations, the author would recommend to:

- consider scenarios with a strict constriction of the fracture trace lengths that can lead to water uptake if the range of potentially longest buffer saturation times is a concern,
- investigate the potential for the pellet slot to act as a redistribution layer for fracture inflow points, a minima with a fully coupled continuum THM model for the bentonite buffer, and even possibly with a discrete element model representing the saturation and homogenization of the pellet filling to reach a better understanding of its hydro-mechanical behavior,
- investigate the potential for secondary flow pathways to form from the pressurized fracture to the deposition hole via the rock matrix.

Acknowledgements

This work was funded by the Swedish Radiation Safety Authority (SSM) under project SSM2017-3021.

References

Alonso E. E., Gens,A., Josa A. (1990). A constitutive model for partially saturated soils. Géotechnique, 40(3), pp. 405-430.

Black J. H., Woodman N. D., Barker J. A. (2017). Groundwater flow into underground openings in fractured crystalline rocks: an interpretation based on long channels. Hydrogeology Journal, 25(2), pp. 445-463.

Croucher A. (2011, November). PyTOUGH: a Python scripting library for automating TOUGH2 simulations. In Proceedings of the New Zealand Geothermal Workshop (Vol. 21, pp. 1-6).

Dessirier B., Jarsjö J., Frampton A. (2014). Modeling two-phase-flow interactions across a bentonite clay and fractured rock interface. Nuclear Technology, 187(2), pp. 147-157.

Dessirier B., Frampton A., Jarsjö J. (2015). A global sensitivity analysis of two-phase flow between fractured crystalline rock and bentonite with application to spent nuclear fuel disposal. Journal of contaminant hydrology, 182, pp. 25-35.

Dessirier B., Frampton A., Fransson Å., Jarsjö J. (2016). Modeling early in situ wetting of a compacted bentonite buffer installed in low permeable crystalline bedrock. Water resources research, 52(8), pp. 6207-6221.

Dessirier B., Åkesson M., Lanyon B., Frampton A., Jarsjö, J. (2017a). Reconstruction of the water content at an interface between compacted bentonite blocks and fractured crystalline bedrock. Applied Clay Science, 142, pp. 145-152.

Dessirier B., Frampton A., Jarsjö J. (2017b) Two-phase flows during re-saturation of sparsely fractured bedrock and bentonite around canisters for deep storage of spent nuclear fuel. Modelling Task 8 of SKB Task Forces GWFTS and EBS. SKB P-17-02. Swedish Nuclear Fuel and Management Co.

Fransson Å., Åkesson M., Andersson L. (2017). Bentonite Rock Interaction Experiment. Characterisation of rock and installation, hydration and dismantling of bentonite parcels. SKB R-14-11. Swedish Nuclear Fuel and Management Co.

Gueuzaine C., Remacle J. F. (2009). Gmsh: a three-dimensional finite element mesh generator with built-in pre-and post-processing facilities. International Journal for Numerical Methods in Engineering, 79(11), pp. 1309-1331.

Jarsjö J., Prieto C., Destouni G. (2017). Estimation of characteristic relations for unsaturated flow through rock fractures in the Forsmark area. SKB P-15-17. Swedish Nuclear Fuel and Management Co.

Johannesson L.-E. (2014). Prototype Repository. Measurements of water content and density of the retrieved buffer material from deposition hole 5 and 6 and the backfill in the outer section of the Prototype Repository. SKB P-13-14. Swedish Nuclear Fuel and Management Co.

Karnland O., Olsson S., Nilsson U. (2006). Mineralogy and sealing properties of various bentonites and smectite-rich clay materials. SKB TR-06-30. Swedish Nuclear Fuel and Management Co.

Leverett M. (1941). Capillary behavior in porous solids. Transactions of the AIME, 142(01), pp. 152-169.

Loschetter A., Smaï F., Sy S., Burnol A., Leynet A., Lafortune S., Thoraval A. (2012, September). Simulation of CO_2 storage in coal seams: Coupling of TOUGH2 with the solver for mechanics CODE_ASTER®. In: TOUGH symposium 2012 (pp. Session-IX).

Pruess K., Oldenburg C. M., Moridis G. J. (1999). TOUGH2 user's guide version 2 (No. LBNL--43134). Ernest Orlando Lawrence Berkeley National Laboratory, Berkeley, CA (US).

Rutqvist J., Ijiri Y., Yamamoto H. (2011). Implementation of the Barcelona Basic Model into TOUGH–FLAC for simulations of the geomechanical behavior of unsaturated soils. Computers & Geosciences, 37(6), pp. 751-762.

Rycroft C. (2009). Voro++: A three-dimensional Voronoi cell library in C++.

SKB (2010). Design, production and initial state of the buffer. Updated 2013-01. SKB TR-10-15. Swedish Nuclear Fuel and Waste Management Co.

Svemar C., Johannesson L.-E., Grahm P., Svensson D., Kristensson O., Lönnqvist M., Nilsson U. (2016). Prototype Repository. Opening and retrieval of outer section of Prototype Repository at Äspö Hard Rock Laboratory. Summary report. SKB TR-13-22. Swedish Nuclear Fuel and Management Co.

Tsang C. F., Neretnieks I. (1998). Flow channeling in heterogeneous fractured rocks. Reviews of Geophysics, 36(2), pp. 275-298.

Vidstrand P., Stigsson M., Åkesson M., Fransson Å. (2017). SKB Task Forces EBS and GWFTS. Modelling the interaction between engineered and natural barriers. A compilation of Task 8 descriptions. SKB P-16-05. Swedish Nuclear Fuel and Management Co.

van Genuchten M. T. (1980). A closed-form equation for predicting the hydraulic conductivity of unsaturated soils 1. Soil science society of America journal, 44(5), pp. 892-898.

Åkesson M., Kristensson O., Börgesson L., Dueck A., Hernelind J. (2010). THM modelling of buffer, backfill and other system components. Critical processes and scenarios. Updated 2015-08. SKB TR-10-11. Swedish Nuclear Fuel and Management Co.

2018:21

The Swedish Radiation Safety Authority has a comprehensive responsibility to ensure that society is safe from the effects of radiation. The Authority works to achieve radiation safety in a number of areas: nuclear power, medical care as well as commercial products and services. The Authority also works to achieve protection from natural radiation and to increase the level of radiation safety internationally.

The Swedish Radiation Safety Authority works proactively and preventively to protect people and the environment from the harmful effects of radiation, now and in the future. The Authority issues regulations and supervises compliance, while also supporting research, providing training and information, and issuing advice. Often, activities involving radiation require licences issued by the Authority. The Swedish Radiation Safety Authority maintains emergency preparedness around the clock with the aim of limiting the aftermath of radiation accidents and the unintentional spreading of radioactive substances. The Authority participates in international co-operation in order to promote radiation safety and finances projects aiming to raise the level of radiation safety in certain Eastern European countries.

The Authority reports to the Ministry of the Environment and has around 300 employees with competencies in the fields of engineering, natural and behavioural sciences, law, economics and communications. We have received quality, environmental and working environment certification.

Strålsäkerhetsmyndigheten
Swedish Radiation Safety Authority

SE-171 16 Stockholm
Solna strandväg 96

Tel: +46 8 799 40 00
Fax: +46 8 799 40 10

E-mail: registrator@ssm.se
Web: stralsakerhetsmyndigheten.se

Ale Tryckteam AB, Bohus, 2018